

16. SITE 728¹

Shipboard Scientific Party²

HOLE 728A

Date occupied: 25 September 1987
Date departed: 26 September 1987
Time on hole: 1 day, 13 hr, 30 min
Position: 17°40.790'N, 57°49.553'E
Water depth (sea level; corrected m, echo-sounding): 1427.8
Water depth (rig floor; corrected m, echo-sounding): 1438.3
Bottom felt (m, drill pipe): 1433.4
Penetration (m): 346.40
Number of cores: 36
Total length of cored section (m): 346.40
Total core recovered (m): 343.72
Core recovery (%): 99.2
Oldest sediment cored
Depth sub-bottom (m): 346.40
Nature: foraminifer nannofossil chalk
Age: late Miocene
Measured velocity (km/s): 1.55–1.66

HOLE 728B

Date occupied: 26 September 1987
Date departed: 28 September 1987
Time on hole: 1 day, 3 hr, 30 min
Position: 17°40.790'N, 57°49.553'E
Water depth (sea level; corrected m, echo-sounding): 1427.8
Water depth (rig floor; corrected m, echo-sounding): 1438.3
Bottom felt (m, drill pipe): 1435.8
Penetration (m): 347.70
Number of cores: 37
Total length of cored section (m): 347.70
Total core recovered (m): 349.50
Core recovery (%): 100.5
Oldest sediment cored
Depth sub-bottom (m): 347.70
Nature: foraminifer nannofossil chalk
Age: late Miocene
Measured velocity (km/s): 1.56
Principal results: Site 728 is located on the Oman margin at a water depth where the lower part of the oxygen-minimum zone intersects the continental slope. The purpose of drilling at Site 728 was to trace the evolution and fluctuation of the oxygen-minimum zone through

time. A second intention was to investigate tectonic movements of basement by comparing the sediments in two adjacent slope basins.

Major findings at Site 728 include:

1. An expanded Pliocene section, which is well constrained by paleomagnetic data;
2. Common occurrence of opaline microfossils in the Miocene and Pliocene intervals; and
3. Indication for rapid vertical movement of the site from upper bathyal depths in the late Miocene, rising to neritic depths in the early Pliocene, and subsiding to middle bathyal depths in the late Pliocene and Pleistocene, as indicated by benthic foraminifers.

A zone of high organic-carbon concentrations that was encountered at 80 to 110 mbsf may reflect the movement of Site 728 through the oxygen-minimum zone during the late Pliocene. This zone, high in organic carbon, coincides with maxima in alkalinity of interstitial waters and in uranium concentrations from logs, as well as with the depletion of interstitial sulfate. The elevated organic carbon concentrations (up to 5.5%) appear to foster significant bacterial activity at this depth.

BACKGROUND AND OBJECTIVES

Site 728 is located at 17°40.790'N and 57°49.553'E, on the continental margin of Oman in a water depth of 1428 m, near the center of the deeper of two slope basins (Fig. 1). The location of Site 728 is shown in Figure 2, and its structural and depositional setting is shown in Figure 3. At this location, the deeper slope basin is about 8 km wide and is much smaller in extent than the adjacent basin upslope, where Sites 723, 724, and 727 are located. This deeper basin is bounded on the west by the faulted block that forms the seaward edge of the upper basin. On the east, the basin is bounded by a basement peak that has substantial sediment cover and an eastern scarp that descends to about 2500 m. Both basement features are thought to be ophiolitic. The seismic-reflection profiles of the basin sediments show numerous reflective layers that both onlap onto and are deformed by the adjacent basement structures. The surface layer and shallow reflectors dip seaward from the upper basin toward the lower constraining basement peak. The sediments are thickest in the center of the basin and form a syncline-shaped deposit (Fig. 3); these thin significantly by pinching out and onlapping to both east and west. This deeper basin is not a linear feature like the upper basin, and extends only about 15 km along the trend (northeast-southwest) of the basement ridges. Average accumulation rates at Site 728 were expected to be between 50 and 60 m/m.y. on the basis of preliminary stratigraphy of piston cores taken during the site survey cruise (RC2704). The site was expected to provide a high-resolution sedimentary record that is more pelagic than the other margin sites, but that still reflects the proximal variations of monsoonal upwelling and the oxygen-minimum zone during the Pliocene-Pleistocene. Specific objectives for drilling at Site 728 were as follows:

1. To obtain a high-resolution record of the sediments associated with the proximal zone of the monsoonal upwelling system to establish changes in timing and intensity of the monsoon.

¹ Prell, W. L., Niitsuma, N., et al., 1989. *Proc. ODP, Init. Repts.*, 117: College Station, TX (Ocean Drilling Program).

² Shipboard Scientific Party is as given in list of Participants preceding the contents.

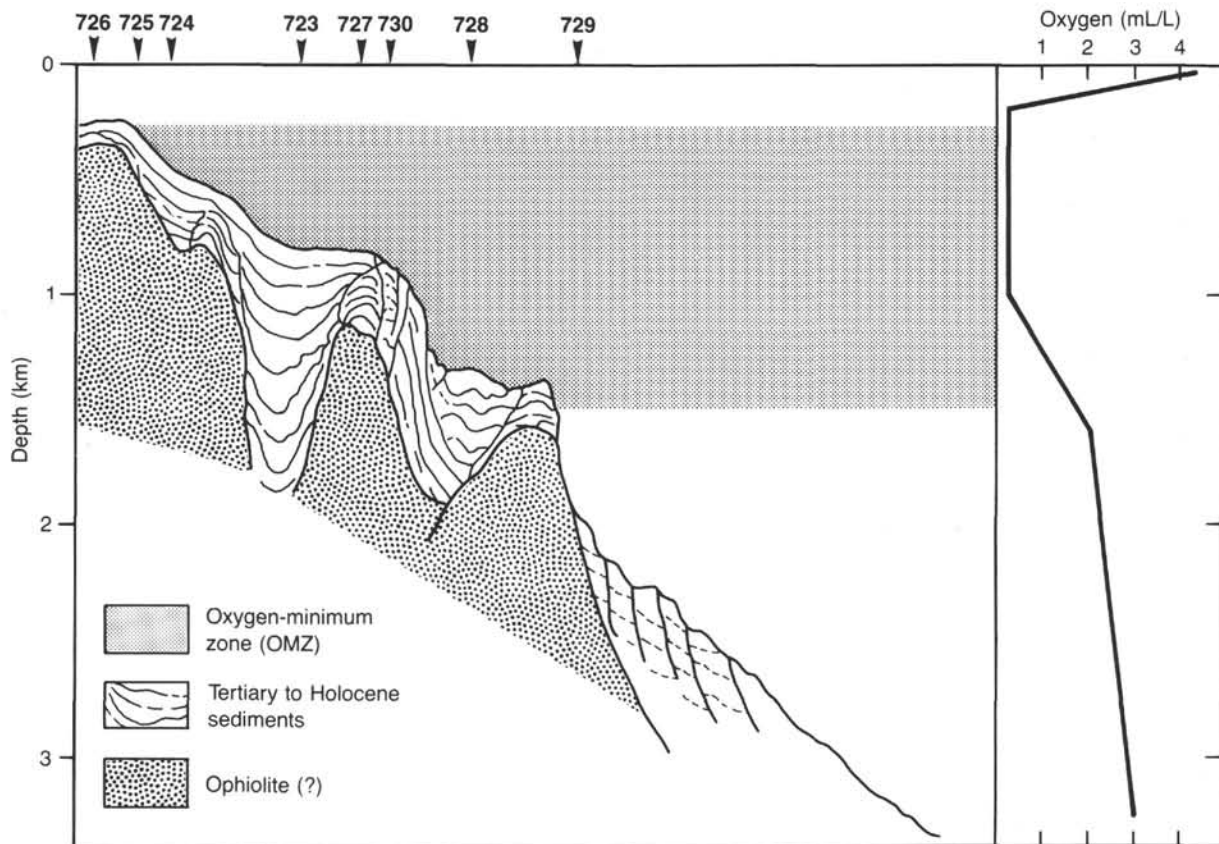


Figure 1. Structure of the Oman margin and the oxygen-minimum zone. The schematic profile shows the series of basement ophiolite blocks and the sedimentary basins between them. The concentration of oxygen in the water column (RC2704, unpubl. data) defines the depth range of the oxygen and where it impinges on the margin.

2. To provide the deepwater end-member of a depth transect that will be used to examine the organic-rich sedimentary facies of the margin to establish their diagenetic history and their relationship to the oxygen-minimum zone and its spatial variation through time.

3. To search for evidence of changes in the structure of the intermediate water masses of the Arabian Sea during the Pliocene-Pleistocene.

OPERATIONS

Site 728 was surveyed jointly with Site 729 on 25 September 1987, after drilling operations at Site 727 had terminated. The ship left Site 727 at 0600 hr with the seismic gear deployed, crossed the future Site 728, and continued to Site 729, where a beacon was dropped at 0900 hr. The *JOIDES Resolution* then returned to Site 728 and dropped a beacon at 1130 hr in a water depth of 1427.8 m. The ship's track line is plotted in Figure 4 according to global positioning system (GPS) navigation fixes. The position of Site 728 was assessed as 17°40.790'N and 59°49.553'E. Seismic gear was retrieved, and the ship positioned by 1230 hr. The mudline of Hole 727A was shot at 1500 hr on 25 September.

Nine APC cores recovered 103% of the sediments from the interval 0 to 85.7 mbsf, after which an overpull of 80,000 lb necessitated a switch to extended-core barrel (XCB) coring mode. Hole 728A was terminated at 0745 hr on 26 September, at a total depth of 346.4 mbsf (Core 117-728A-36X) with an overall recovery as high as 99% owing to cutting shoe modification and favorable sediments (Table 1). The hole was conditioned, swept with mud, displaced with polymer, and prepared for logging.

After the lockable flapper valve had been opened and a wiper trip, the bit was positioned at 80 mbsf.

Two logging strings were successfully run in Hole 728A. String 1 consisted of a combination of resistivity (DIT), sonic (BHC), gamma ray (GR), and caliper (CAL) logs, while string 2 ran a combination of gamma spectrometry (GST), neutron porosity (CNT), and spectral gamma ray (NGT) logs. At 2315 hr, logging tools were rigged down, the string was pulled out of Hole 728A, the ship moved 10 m northwest, and Hole 728B was spudded at 0100 hr on 26 September. Nine advanced corer (APC) cores were followed by XCB coring to Core 117-728A-37X, a total depth of 347.7 mbsf. The *in-situ* pore-water sampler was deployed after Cores 117-728B-6H, -12X, -17X, and -25X. Overall recovery again averaged 100% for the entire hole, with 104% for the interval from 0 to 77.3 mbsf cored in APC mode. The performance of the XCB system was extraordinary at this site.

Hole 728B was displaced with heavy mud, the string cleared the mudline, and at 2400 hr on 27 September, the ship was under way to Site 729 in dynamic positioning mode.

LITHOSTRATIGRAPHY

Lithologic Units

The two holes drilled at Site 728 are located in a water depth of 1428 m near the center of a lower slope basin. Hole 728B is 10 m northwest of Hole 728A. APC recovery was almost perfect in these holes, and the top of Hole 728B recovered the mudline. The age range of the sedimentary sequence is Pleistocene to late Miocene, the longest continuous section recovered on the Oman margin. The sediments are mostly marly nannofossil ooze and

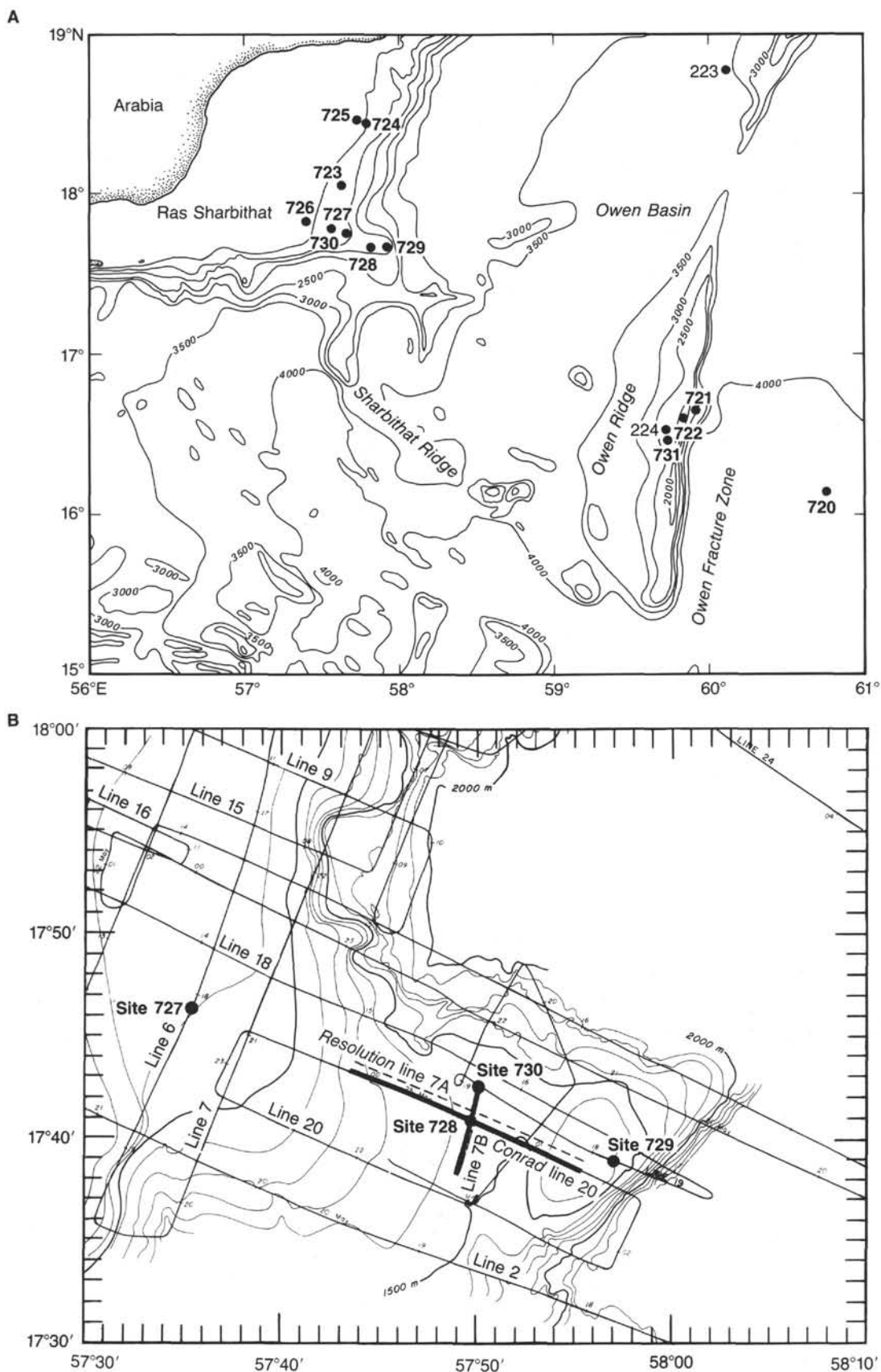


Figure 2. **A.** Bathymetry of the Oman margin and the location of Site 728. **B.** The detailed location of Site 728 and the seismic profiles shown in Figure 3. Bathymetry data are from the site survey (RC2704, 1986).

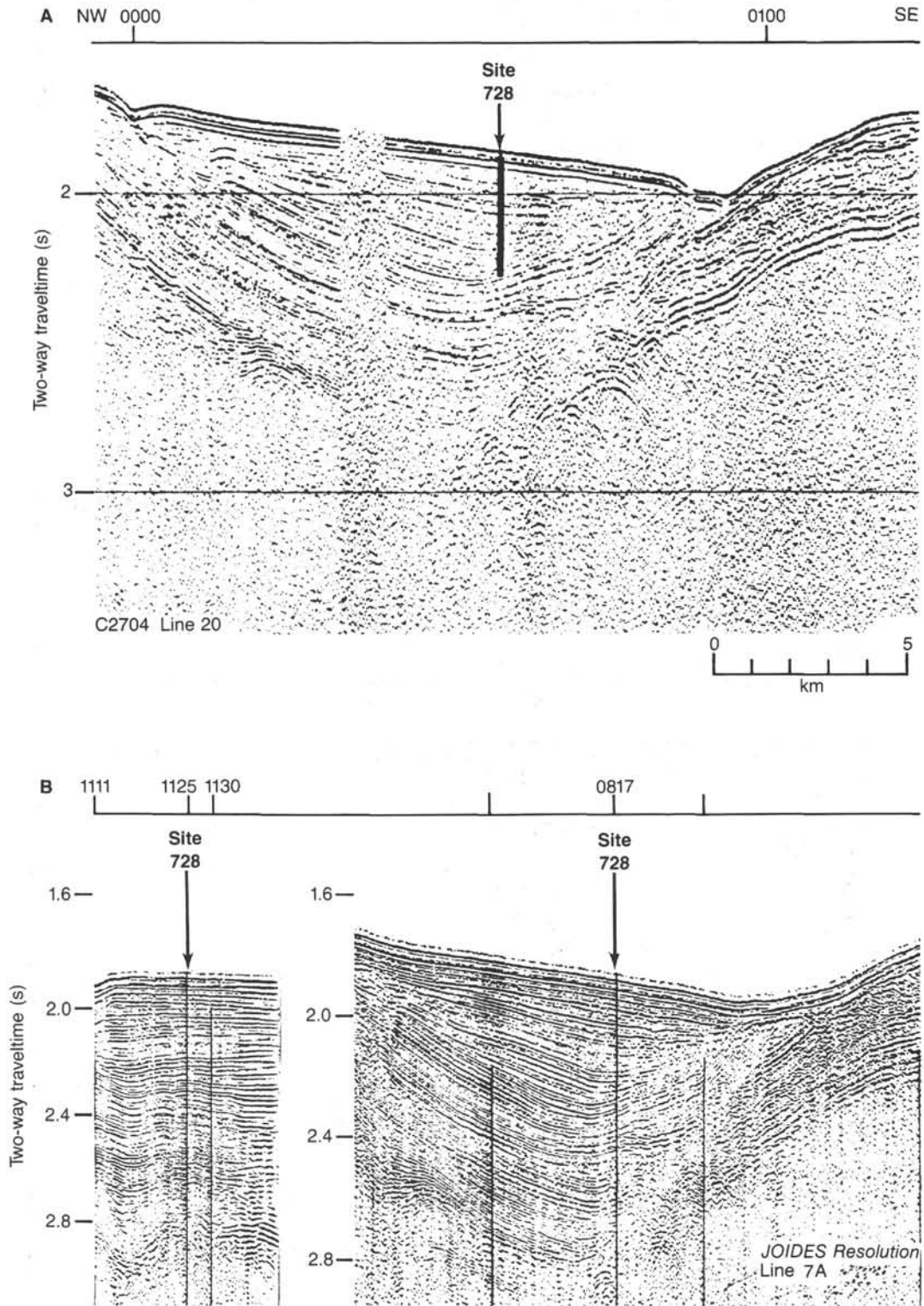


Figure 3. A. Single-channel seismic (SCS) reflection profiles showing the structural and depositional setting of Site 728. RC2704 Line 20 and *JOIDES Resolution* Line 7A are perpendicular to the trend of the basin and shows the bounding basement blocks and the synclinal-shaped sediment fill. B. *JOIDES Resolution* Line 7B is along the strike of the basement ridges and shows the relatively uniform sediment thickness and horizontal reflectors at Site 728. (All times are local time.)

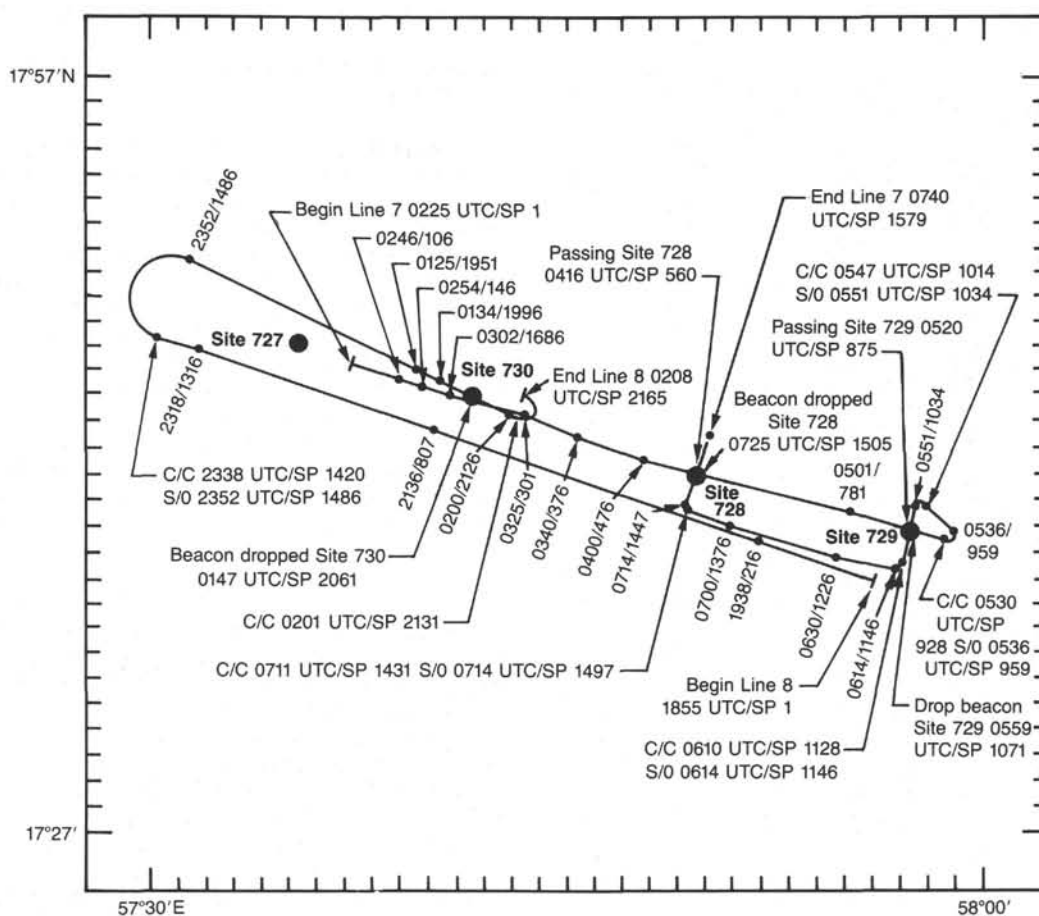


Figure 4. Ship's track during survey and approach to Sites 728 and 729.

are considered as one lithologic unit. We subdivided lithologic Unit I into three subunits, based on carbonate and organic carbon contents and the presence of minor biogenic components (Fig. 5 and Table 2). The upper subunit (IA) is rich in foraminifers. The middle subunit (IB) grades downward from a foraminifer-bearing, marly nannofossil ooze to marly nannofossil and nannofossil oozes. The upper part is dark and more uniform in color, whereas the lower part contains pronounced light and dark cycles that are heavily mottled (bioturbated). Siliceous microfossils are present throughout. Subunit IC is siliceous-bearing, marly nannofossil ooze, often with more than 10% diatoms.

Subunit IA (Depth: 0–58 mbsf; Age: Holocene to early Pleistocene)

Cores 117-728A-1H through -6H and 117-728B-1H through 117-728B-7H.

Subunit IA consists of marly foraminifer-nannofossil ooze and foraminifer-bearing, marly nannofossil ooze. The upper two cores contain abundant foraminifers (more than 10% in smear slides). Foraminifers decrease in abundance within this unit and are only present in minor amounts throughout the hole below 58 mbsf. Smear-slide analysis indicates 20%–50% nannofossils and a variable terrigenous component dominated by clay, and clay and silt-sized detrital calcite (often 20% or more). Calcium carbonate determined coulometrically varies between 50% and 60% (Fig. 6 and Table 2). Subunit IA is similar to the upper sequence observed at other margin sites, although the carbonate

content is greater, and the sedimentation rate is significantly slower (34 m/m.y. vs. 80–175 m/m.y.). Variable-thickness, light and dark intervals are olive (5Y 4/2, 4/3) and light olive gray (5Y 5/2, 5/3), mottled throughout, with pyrite flecks visible in the lighter intervals.

Subunit IB (Depth: 58–320 mbsf; Age: early Pleistocene to Miocene)

Cores 117-728A-7H through -33X and 117-728B-8H through 117-728B-34X.

Subunit IB consists mostly of foraminifer-bearing, marly nannofossil ooze with alternating dark beds, olive (5Y 4/4, 4/3), olive gray (5Y 4/2), dark olive gray (5Y 3/2); and lighter beds, olive gray (5Y 5/2) and olive (5Y 5/3). In the lower part, these become lighter in color and more nannofossil rich; light olive gray (5Y 6/2), olive gray (5Y 5/2), and olive (5Y 5/3) nannofossil ooze, containing approximately 70% nannofossils; mottling (bioturbation) is more pronounced. Siliceous microfossils are present throughout this unit. Within the unit, organic carbon gradually decreases in content (Fig. 6), which corresponds to the presence of the lighter, more nannofossil-rich beds.

The abundance of detrital calcite (clay and silt-sized) decreases downward within this unit, from 15% to 25% to less than 10% below 120 mbsf. Thus, in the upper Pleistocene (Subunit IA and upper Subunit IB), detrital calcite is a major component, and in older sediments its abundance is reduced. Quartz is generally present in low abundance (less than 10%) in the up-

Table 1. Coring summary for Site 728.

Core no.	Date (Sept. 1987)	Time (Local)	Depth (mbsf)	Cored (m)	Recovered (m)	Recovery (%)
117-728A-1H	25	1550	0-9.6	9.6	9.63	100.0
2H	25	1615	9.6-19.1	9.5	9.72	102.0
3H	25	1635	19.1-28.5	9.4	9.78	104.0
4H	25	1700	28.5-38.0	9.5	9.83	103.0
5H	25	1740	38.0-47.5	9.5	9.69	102.0
6H	25	1805	47.5-57.0	9.5	10.03	105.6
7H	25	1825	57.0-66.5	9.5	9.86	104.0
8H	25	1845	66.5-76.1	9.6	9.90	103.0
9H	25	1910	76.1-85.7	9.6	9.85	102.0
10X	25	1945	85.7-95.3	9.6	9.18	95.6
11X	25	2010	95.3-104.9	9.6	8.87	92.4
12X	25	2035	104.9-114.5	9.6	5.34	55.6
13X	25	2055	114.5-124.2	9.7	8.52	87.8
14X	25	2115	124.2-133.9	9.7	9.61	99.1
15X	25	2140	133.9-143.5	9.6	9.10	94.8
16X	25	2200	143.5-153.1	9.6	9.05	94.3
17X	25	2225	153.1-162.8	9.7	9.66	99.6
18X	25	2245	162.8-172.5	9.7	8.52	87.8
19X	25	2305	172.5-182.2	9.7	9.81	101.0
20X	25	2325	182.2-191.8	9.6	9.59	99.9
21X	25	2355	191.8-201.5	9.7	9.91	102.0
22X	26	0030	201.5-211.1	9.6	9.93	103.0
23X	26	0100	211.1-220.8	9.7	9.34	96.3
24X	26	0130	220.8-230.5	9.7	9.88	102.0
25X	26	0200	230.5-240.1	9.6	9.91	103.0
26X	26	0235	240.1-249.8	9.7	10.18	104.9
27X	26	0305	249.8-259.5	9.7	9.93	102.0
28X	26	0340	259.5-269.1	9.6	9.96	104.0
29X	26	0405	269.1-278.8	9.7	9.70	100.0
30X	26	0435	278.8-288.5	9.7	10.00	103.1
31X	26	0505	288.5-298.1	9.6	9.99	104.0
32X	26	0530	298.1-307.8	9.7	10.02	103.3
33X	26	0600	307.8-317.5	9.7	9.96	102.0
34X	26	0630	317.5-327.2	9.7	9.83	101.0
35X	26	0655	327.2-336.8	9.6	9.87	103.0
36X	26	0730	336.8-346.4	9.6	9.77	102.0
117-728B-1H	27	0115	0-1.2	1.2	1.24	103.0
2H	27	0220	1.2-10.7	9.5	10.02	105.5
3H	27	0245	10.7-20.1	9.4	10.02	106.6
4H	27	0310	20.1-29.6	9.5	9.98	105.0
5H	27	0345	29.6-29.1	9.5	9.88	104.0
6H	27	0420	39.1-48.6	9.5	9.84	103.0
7H	27	0615	48.6-58.1	9.5	10.09	106.2
8H	27	0650	58.1-67.7	9.6	10.01	104.3
9H	27	0725	67.7-77.3	9.6	10.02	104.4
10X	27	0825	77.3-86.9	9.6	9.68	101.0
11X	27	0855	86.9-96.5	9.6	9.43	98.2
12X	27	0925	96.5-106.1	9.6	9.55	99.5
13X	27	1050	106.1-115.8	9.7	9.65	99.5
14X	27	1125	115.8-125.5	9.7	9.77	101.0
15X	27	1145	125.5-135.1	9.6	9.73	101.0
16X	27	1205	135.1-144.7	9.6	9.13	95.1
17X	27	1235	144.7-154.4	9.7	8.38	86.4
18X	27	1415	154.4-164.1	9.7	9.46	97.5
19X	27	1440	164.1-173.8	9.7	9.75	100.0
20X	27	1505	173.8-183.5	9.7	9.47	97.6
21X	27	1535	183.5-193.2	9.7	9.65	99.5
22X	27	1600	193.2-202.8	9.6	9.82	102.0
23X	27	1625	202.8-212.5	9.7	10.02	103.3
24X	27	1650	212.5-222.2	9.7	9.74	100.0
25X	27	1720	222.2-231.8	9.6	9.96	104.0
26X	27	1900	231.8-241.5	9.7	6.83	70.4
27X	27	1925	241.5-251.2	9.7	9.94	102.0
28X	27	1950	251.2-260.8	9.6	9.76	101.0
29X	27	2015	260.8-270.5	9.7	9.90	102.0
30X	27	2040	270.5-280.2	9.7	10.04	103.5
31X	27	2105	280.2-289.8	9.6	9.68	101.0
32X	27	2125	289.8-299.5	9.7	9.90	102.0
33X	27	2150	299.5-309.2	9.7	9.98	103.0
34X	27	2215	309.2-318.8	9.6	10.06	104.8
35X	27	2240	318.8-328.5	9.7	9.40	96.9
36X	27	2305	328.5-338.1	9.6	9.86	103.0
37X	27	2330	338.1-347.7	9.6	9.86	103.0

per section of Site 728 and at other margin sites (723, 724, and 727). Below 250 mbsf (lower Subunits IB and IC) at Site 728, quartz grains can be found in greater abundance (up to 30% in isolated samples).

Subunit IC (Depth: 320-349 mbsf; Age: late Miocene)

Cores 117-728A-34X through -36X and 117-728B-35X through 117-728B-37X.

Subunit IC is similar to lower Subunit IB described above, but contains a greater abundance of siliceous microfossils. The siliceous assemblage is composed primarily of diatoms (10%-35%), with silicoflagellates, sponge spicules, and radiolarians present in minor abundances. The sediments are diatom-bearing nanofossil, marly nanofossil, and nanofossil oozes and are intensely bioturbated. Generally, the darker layers contain more silica. Color is similar to that in the base of Subunit IB (olive 5Y 4/3, 4/2, 3/2 and light olive gray 5Y 6/2, 5/3, 5/2). Calcium carbonate is 10% lower in the dark intervals within Subunit IC relative to the dark intervals in Subunits IA and IB. Calcium carbonate decreases from a maximum at 250 mbsf to low and variable concentrations observed in Subunit IC (Table 2 and Fig. 6). An increase in quartz abundance below 250 mbsf is obvious in this unit.

Discussion

Subunit IA, foraminifer-rich marly nanofossil ooze, is represented at all margin sites. The proportion of biogenic to terrigenous sediment is highest at Site 728 (more than 50%), which is consistent with its position on the outer margin in a more pelagic setting. Clay and detrital calcite, presumably of eolian origin, dominate the terrigenous component in the modern environment. Foraminifers are an abundant component of the smear-slide assemblage in upper Pleistocene sediments.

Lower Pleistocene and upper Pliocene sediments (upper Subunit IB) are more organic carbon-rich, and trace amounts of siliceous microfossils are preserved. The sediments are marly nanofossil ooze, uniformly olive (5Y 4/3), with few foraminifers. The upper section of Subunit IB correlates with an interval of organic carbon and silica preservation found at margin Sites 723, 724, and 726. At shallower depths and nearer the center of the oxygen-minimum zone (i.e., Site 723), organic carbon values increase to more than 8%; at Site 728, the maximum value is 5% (Table 2 and Fig. 6). During this depositional period, silica preservation is enhanced at shallow sites, and occasionally forms laminated diatomite at Sites 723, 724, and 726; however, no laminae were observed at Site 728. Detrital calcite is abundant within this interval of Subunit IB (often greater than 20%). Thus, Site 728 contains a facies that is correlative with the laminated zone at other margin sites, but the variations in sedimentary facies are not as pronounced.

Lithologic changes in minor components occur within Subunit IB between the upper Miocene and the upper Pliocene. Upper Miocene sediments have more pronounced cycles of light olive nanofossil ooze and darker marly nanofossil ooze and, as a rule, are intensely bioturbated. Mean organic carbon content is about 1%, and detrital calcite is a minor component. Organic carbon increases gradually during the Pliocene to maximum values in the upper Pliocene. The sediment becomes a darker and more uniform marly nanofossil ooze. Detrital calcite, interpreted as an eolian component, increases in Cores 117-728A-14X and 117-728B-15X in the upper Pliocene. These changes suggest that the deposition of the organic carbon-rich interval observed at the other margin sites began in the early Pliocene.

In the upper Miocene (below 320 mbsf) silica is preserved (up to 30%) in marly nanofossil ooze that is intensely bioturbated and shows pronounced light and dark cycles. Preliminary stratigraphy indicates this may be correlated with a Miocene interval of silica preservation that was observed on the Owen Ridge

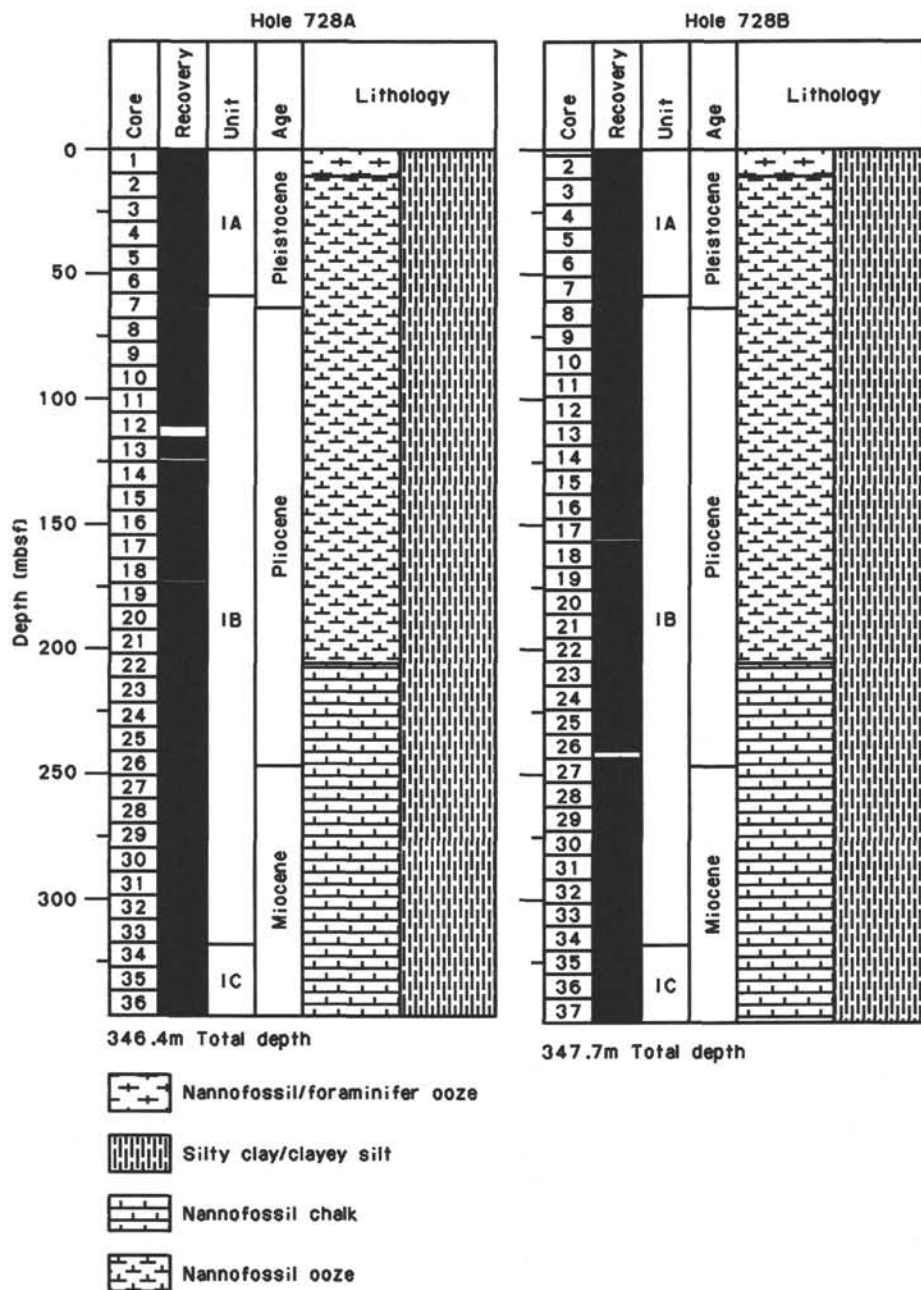


Figure 5. Lithologic summary for Site 728.

and which occurred at approximately 7 Ma (see "Lithostratigraphy" section, Site 722 chapter, this volume).

Significant amounts of quartz are observed in Miocene sediments below 250 mbsf. The increase may be related to increased supply of terrigenous sediment, or to a change in the depositional environment, which increases the flux of quartz. The shallow sites nearer the continent today have the highest fraction of quartz. Site 728 may have been located in shallower water during the late Miocene (see "Biostratigraphy" section, this chapter), and the abundance of quartz is consistent with this observation. The decrease in quartz in the uppermost Miocene suggests that the site subsided below the shallow-water depositional environment at that time.

BIOSTRATIGRAPHY

Introduction

Site 728 is located in a deep slope basin in 1428 m of water. The age of the sediments ranges from late Miocene to Holocene (Fig. 7). A plot of faunal datum levels and paleomagnetic reversals vs. depth below the seafloor is presented in Figure 8; for a detailed listing of these events, see Table 3. Benthic and planktonic foraminifers are common to abundant, and preservation is good down to approximately 50 mbsf. Below 66.5 mbsf, planktonic foraminifers are few to rare, with moderate to poor preservation. Benthic foraminifers remain common down to 160 mbsf, but preservation is moderate to poor. Below this level, preserva-

Table 2. Calcium carbonate and organic carbon determinations.

Core, section, interval (cm)	Depth (mbsf)	Total carbon (%)	Inorganic carbon (%)	Organic carbon (%)	CaCO ₃ (%)
117-728A-					
1H-2, 100-102	2.50	8.74	7.21	1.53	60.1
2H-2, 80-82	11.90	8.13	7.44	0.69	62.0
3H-2, 80-82	21.40	9.27	7.49	1.78	62.4
3H-4, 119-120	24.79	7.90	6.86	1.04	57.1
4H-2, 80-82	30.80	7.79	6.60	1.19	55.0
5H-2, 80-82	40.30	8.95	7.77	1.18	64.7
6H-2, 80-82	49.80	7.92	6.11	1.81	50.9
6H-4, 80-82	52.80	8.82	6.45	2.37	53.7
6H-4, 119-120	53.19	8.51	6.24	2.27	52.0
6H-6, 80-82	55.80	6.67	5.99	0.68	49.9
7H-2, 80-82	59.30	7.96	5.91	2.05	49.2
7H-4, 80-82	62.30	7.78	5.52	2.26	46.0
7H-6, 80-82	65.30	10.01	7.98	2.03	66.5
8H-2, 80-82	68.80	9.13	7.18	1.95	59.8
8H-4, 80-82	71.80	9.45	4.11	5.34	34.2
8H-6, 80-82	74.80	8.05	4.97	3.08	41.4
9H-2, 80-82	78.40	11.22	7.54	3.68	62.8
9H-4, 80-82	81.40	10.67	5.86	4.81	48.8
9H-4, 119-120	81.79	11.11	6.14	4.97	51.2
9H-6, 80-82	84.40	9.68	6.45	3.23	53.7
10X-2, 80-82	88.00	10.09	6.84	3.25	57.0
10X-4, 80-82	91.00	10.98	7.95	3.03	66.2
10X-6, 80-82	94.00	10.11	7.26	2.85	60.5
11X-2, 80-82	97.60	8.05	5.57	2.48	46.4
11X-4, 78-80	100.58	9.00	6.51	2.49	54.2
11X-6, 80-82	103.60	8.20	6.77	1.43	56.4
12X-1, 70-72	105.60	8.50	5.75	2.75	47.9
12X-2, 119-120	107.59	8.88	5.93	2.95	49.4
13X-1, 80-82	115.30	10.48	7.27	3.21	60.6
14X-2, 80-82	126.50	9.63	7.22	2.41	60.1
15X-2, 72-74	136.12	10.18	6.41	3.77	53.4
15X-4, 119-120	139.59	10.18	6.78	3.40	56.5
16X-2, 80-82	145.80	8.32	5.29	3.03	44.1
17X-2, 73-75	155.33	9.57	6.46	3.11	53.8
18X-2, 135-137	165.65	10.63	7.87	2.76	65.6
18X-4, 119-120	168.49	11.36	8.60	2.76	71.6
19X-2, 93-95	174.93	11.15	8.12	3.03	67.6
20X-2, 118-120	184.88	9.62	7.11	2.51	59.2
21X-2, 56-58	193.86	8.06	5.17	2.89	43.1
21X-5, 0-1	197.80	9.06	5.95	3.11	49.6
22X-2, 79-81	203.79	7.94	5.02	2.92	41.8
23X-2, 80-82	213.40	9.98	7.11	2.87	59.2
24X-2, 69-71	222.99	9.70	7.43	2.27	61.9
25X-2, 85-87	232.85	8.37	6.43	1.94	53.6
26X-2, 21-23	241.81	10.32	8.63	1.69	71.9
27X-2, 116-118	252.46	8.68	6.81	1.87	56.7
28X-3, 7-9	262.57	10.74	7.41	3.33	61.7
29X-2, 51-53	271.11	8.04	5.78	2.26	48.2
30X-2, 134-136	281.64	7.64	5.94	1.70	49.5
31X-2, 126-128	291.26	6.45	4.74	1.71	39.5
32X-4, 77-79	303.37	5.49	4.47	1.02	37.2
33X-4, 94-96	313.24	8.09	6.81	1.28	56.7
34X-3, 77-79	321.27	6.68	4.78	1.90	39.8
35X-2, 104-106	329.74	4.93	3.45	1.48	28.7
36X-3, 32-35	340.12	7.97	6.41	1.56	53.4
1H-2, 100-102	2.50	8.74	7.21	1.53	60.1
1H-4, 100-102	5.50		7.26		60.5
1H-6, 100-102	8.50		6.12		51.0
2H-2, 80-82	11.90	8.13	7.44	0.69	62.0
2H-4, 80-82	14.90		7.68		64.0
2H-6, 80-82	17.90		7.50		62.5
3H-2, 80-82	21.40	9.27	7.49	1.78	62.4
3H-4, 80-82	24.40		6.95		57.9
3H-4, 119-120	24.79	7.90	6.86	1.04	57.1
3H-6, 28-30	26.88		6.76		56.3
4H-2, 80-82	30.80	7.79	6.60	1.19	55.0
4H-4, 80-82	33.80		6.47		53.9
4H-6, 80-82	36.80		8.48		70.6
5H-2, 80-82	40.30	8.95	7.77	1.18	64.7
5H-4, 80-82	43.30		7.36		61.3
5H-6, 80-82	46.30		6.39		53.2
6H-2, 80-82	49.80	7.92	6.11	1.81	50.9
6H-4, 80-82	52.80	8.82	6.45	2.37	53.7
6H-4, 119-120	53.19	8.51	6.24	2.27	52.0
6H-6, 80-82	55.80	6.67	5.99	0.68	49.9
7H-2, 80-82	59.30	7.96	5.91	2.05	49.2
7H-4, 80-82	62.30	7.78	5.52	2.26	46.0

Table 2 (continued).

Core, section, interval (cm)	Depth (mbsf)	Total carbon (%)	Inorganic carbon (%)	Organic carbon (%)	CaCO ₃ (%)
117-728A- (Cont.)					
7H-6, 80-82	65.30	10.01	7.98	2.03	66.5
8H-2, 80-82	68.80	9.13	7.18	1.95	59.8
8H-4, 80-82	71.80	9.45	4.11	5.34	34.2
8H-6, 80-82	74.80	8.05	4.97	3.08	41.4
9H-2, 80-82	78.40	11.22	7.54	3.68	62.8
9H-4, 80-82	81.40	10.67	5.86	4.81	48.8
9H-4, 119-120	81.79	11.11	6.14	4.97	51.2
9H-6, 80-82	84.40	9.68	6.45	3.23	53.7
10X-2, 80-82	88.00	10.09	6.84	3.25	57.0
10X-4, 80-82	91.00	10.98	7.95	3.03	66.2
10X-6, 80-82	94.00	10.11	7.26	2.85	60.5
11X-2, 80-82	97.60	8.05	5.57	2.48	46.4
11X-4, 78-80	100.58	9.00	6.51	2.49	54.2
11X-6, 80-82	103.60	8.20	6.77	1.43	56.4
12X-1, 70-72	105.60	8.50	5.75	2.75	47.9
12X-2, 119-120	107.59	8.88	5.93	2.95	49.4
13X-1, 80-82	115.30	10.48	7.27	3.21	60.6
13X-3, 80-82	118.30		6.90		57.5
13X-5, 80-82	121.30		7.01		58.4
14X-2, 80-82	126.50	9.63	7.22	2.41	60.1
14X-4, 80-82	129.50		6.99		58.2
14X-6, 80-82	132.50		7.17		59.7
15X-2, 72-74	136.12	10.18	6.41	3.77	53.4
15X-4, 73-75	139.13		6.51		54.2
15X-4, 119-120	139.59	10.18	6.78	3.40	56.5
15X-6, 94-96	142.34		5.74		47.8
16X-2, 80-82	145.80	8.32	5.29	3.03	44.1
16X-4, 92-94	148.92		6.70		55.8
16X-6, 80-82	151.80		5.23		43.6
17X-2, 73-75	155.33	9.57	6.46	3.11	53.8
17X-4, 69-71	158.29		8.14		67.8
17X-6, 75-77	161.35		6.61		55.1
18X-2, 135-137	165.65	10.63	7.87	2.76	65.6
18X-4, 101-103	168.31		7.11		59.2
18X-4, 119-120	168.49	11.36	8.60	2.76	71.6
18X-6, 61-63	170.91		8.10		67.5
19X-2, 93-95	174.93	11.15	8.12	3.03	67.6
19X-4, 98-100	177.98		6.91		57.6
19X-7, 31-33	181.81		6.97		58.1
20X-2, 118-120	184.88	9.62	7.11	2.51	59.2
20X-4, 106-108	187.76		4.64		38.7
20X-6, 122-124	190.92		6.61		55.1
21X-2, 56-58	193.86	8.06	5.17	2.89	43.1
21X-4, 72-74	197.02		7.15		59.6
21X-5, 0-1	197.80	9.06	5.95	3.11	49.6
21X-6, 103-105	200.33		5.95		49.6
22X-2, 79-81	203.79	7.94	5.02	2.92	41.8
22X-4, 80-82	206.80		6.26		52.2
22X-6, 76-78	209.76		5.21		43.4
23X-2, 80-82	213.40	9.98	7.11	2.87	59.2
23X-4, 80-82	216.40		7.45		62.1
23X-6, 80-82	219.40		6.77		56.4
24X-2, 69-71	222.99	9.79	7.43	2.27	61.9
24X-4, 69-71	225.99		5.83		48.6
24X-4, 138-140	226.68		6.97		58.1
24X-6, 79-81	229.09		8.59		71.6
25X-2, 85-87	232.85	8.37	6.43	1.94	53.6
25X-4, 48-50	235.48		7.50		62.5
25X-6, 147-149	239.47		5.69		47.4
26X-2, 21-23	241.81	8.60	8.63	0.00	71.9
26X-5, 72-74	246.82		7.31		60.9
27X-2, 116-118	252.46	8.68	8.81	1.87	56.7
27X-4, 17-19	254.47		4.26		35.5
27X-6, 107-109	258.37		7.03		58.6
28X-3, 7-9	262.57	10.74	7.41	3.33	61.7
28X-6, 137-139	268.37		6.74		56.1
28X-7, 41-43	268.91		7.07		58.9
29X-2, 51-53	271.11	8.04	5.78	2.26	48.2
29X-5, 67-69	275.77		7.68		64.0
30X-2, 134-136	281.64	7.64	5.94	1.70	49.5
30X-4, 115-117	284.45		5.00		41.7
31X-2, 126-128	291.26	6.45	4.74	1.71	39.5
31X-CC, 30-32	298.23		5.19		43.2
32X-4, 77-79	303.37	5.49	4.47	1.02	37.2
32X-6, 93-95	306.53		5.66		47.2

Table 2 (continued).

Core, section, interval (cm)	Depth (mbsf)	Total carbon (%)	Inorganic carbon (%)	Organic carbon (%)	CaCO ₃ (%)
117-728A- (Cont.)					
33X-4, 94-96	313.24	8.09	6.81	1.28	56.7
33X-5, 96-98	314.76		5.32		44.3
34X-3, 77-79	321.27	6.68	4.78	1.90	39.8
34X-CC, 33-35	327.28		3.47		28.9
35X-2, 104-106	329.74	4.93	3.45	1.48	28.7
35X-6, 64-66	335.34		8.55		71.2
36X-3, 32-35	340.12	7.97	6.41	1.56	53.4
36X-6, 103-106	345.33		4.34		36.2

tion is good, but benthic foraminifers are rare. Calcareous nanofossils are abundant throughout the cored sequence. Preservation is moderate in Hole 728A down to 269.1 mbsf. From 269.1 to 346.4 mbsf, preservation is moderate to poor. Preservation throughout Hole 728B is moderate. Siliceous microfossils are not present in the upper 38 m. Only a few radiolarians are found between 38 and 76.1 mbsf, but below this level to the bottom of the hole, radiolarians are common and well preserved.

Planktonic Foraminifers

The planktonic foraminiferal fauna in the core-catcher samples of Hole 728A is abundant, and preservation of the tests is

good in the upper part of the sequence (Samples 117-728A-1H, CC, through 117-728A-6H, CC; 9.6-57.0 mbsf), which is composed mainly of Pleistocene marly nannofossil oozes. Sample 117-728A-7H, CC (66.5 mbsf) and underlying sediments contain few to rare planktonic foraminifers; preservation ranges from moderate to poor. These sediments are Pliocene and late Miocene in age.

The uppermost six core-catcher samples contain *Globigerinella calida calida* and/or *Globorotalia truncatulinoides*. Both species indicate a Pleistocene age. The Pleistocene/Pliocene boundary tentatively was placed between Samples 117-728A-6H, CC and 117-728A-7H, CC (57.0-66.5 mbsf), based on the last appearances of *Globorotalia limbata* and *Globigerinoides obliquus extremus* in the latter sample. The *Globorotalia tosaensis*-*G. truncatulinoides* lineage could not be used to discern this boundary because only a few specimens could be found. For the same reason, Zone N21 could not be distinguished from Zones N19a and N20. Pliocene sediments were found in Samples 117-728A-7H, CC, through 117-728A-25X, CC (66.5-240.1 mbsf). The fact that thick-walled *Globorotalia tumida tumida* specimens dominate the assemblages indicates that dissolution processes have affected the shells.

The lower part of the section (117-728A-26X, CC, through 117-728A-36X, CC; 249.8-346.4 mbsf) was assigned to the upper Miocene, based on rare specimens of *Globorotalia tumida plesiotumida* and *Globorotalia tumida merotumida*.

Benthic Foraminifers

The benthic foraminiferal fauna was studied at Site 728 in the core-catcher samples of Hole 728A. Abundances range from common in the upper part (above 160 mbsf) to rare in the lower part (below 160 mbsf) of the recovered sequence. Preservation is good in the upper 50 m, but becomes moderate to poor downhole to about 160 mbsf; preservation in the remainder of the sequence (below 160 mbsf) is good.

The planktonic/benthic (P/B) ratio is about 100% in the upper 60 m, but gradually decreases to below 10% at approximately 160 mbsf. This ratio remains below 10% in most of the samples downhole, and increases slightly in the lowermost five samples (approximately 305-345 mbsf).

The benthic foraminiferal fauna at Site 728 can be divided into three assemblages that intergrade. Thus, sharp boundaries between these assemblages are difficult to define. However, one can define the intervals of transition from one assemblage to another. The transition from Assemblage I to Assemblage II occurs between approximately 143 and 163 mbsf, and the transition from Assemblage II to Assemblage III occurs between approximately 230 and 250 mbsf.

Assemblage I is characterized by the presence of abundant *Cassidulina carinata* and *Bulimina aculeata*, which occur solely in this assemblage. Other species that are found exclusively in Assemblage I, but in lower relative abundance, are *Ehrenbergina trigona*, *Globocassidulina subglobosa*, *Pullenia subcarinata*, and *Quadrinorhina laevigata*. These species are found together with those also found in Assemblage III: *Cibicidoides wuellerstorfi*, *Melonis barleeianum*, *Pullenia bulloides*, and *Uvigerina spinicostata*. However, *M. barleeianum* and *P. bulloides* are found only in the lower part of Assemblage I.

Species characterizing Assemblage II are *Ammonia beccarii* and *Melonis pompiolides*. In Assemblage II, those species common in Assemblage I are absent or occur in low relative abundance.

Assemblage III is characterized by the high abundance of *Melonis barleeianum*, *Pullenia bulloides*, and *Uvigerina spinicostata*. Other species found in Assemblage III are *Cibicidoides wuellerstorfi* and *Uvigerina peregrina*.

Data from the previous sites drilled during Leg 117 as well as information from other areas (e.g., Ingle et al., 1980; Pflum

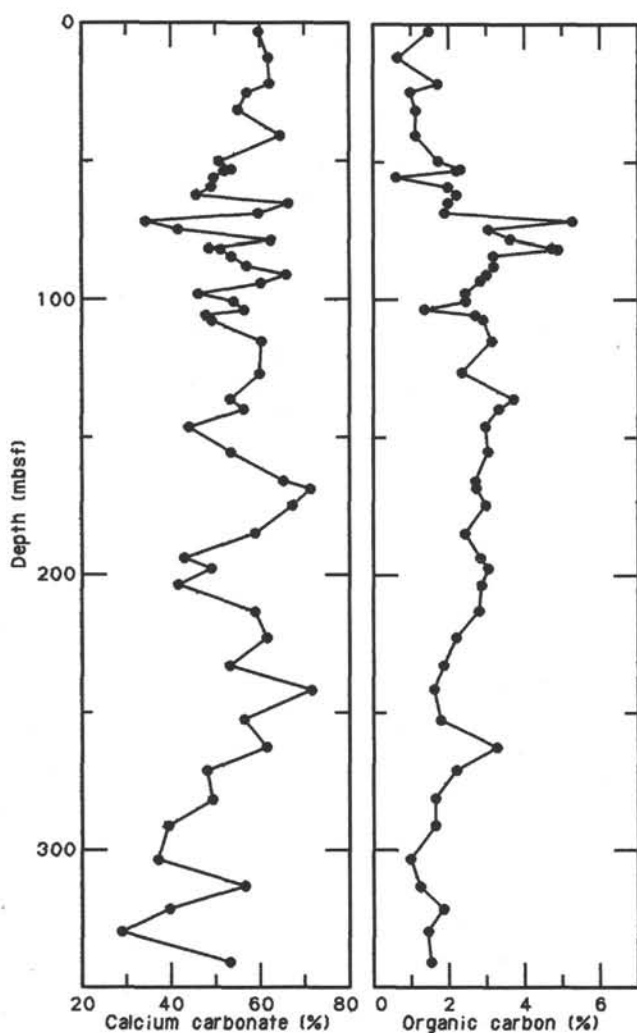


Figure 6. Calcium carbonate and organic carbon content.

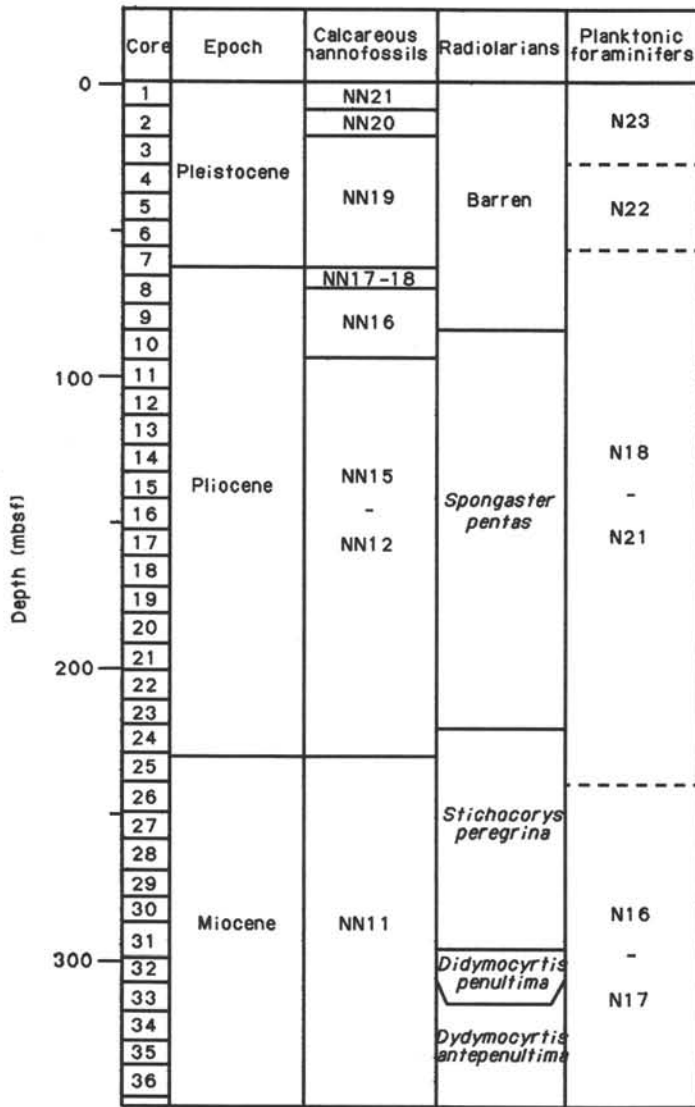


Figure 7. Correlation of planktonic microfossil zones in Hole 728A.

and Frerichs, 1976; van Morkhoven et al., 1986) indicate that these three assemblages include species characteristic of certain water depths. The species in Assemblage I seem to prefer a water depth that exceeds 500 m and can be considered characteristic of the upper middle bathyal zone. Assemblage II contains shallow-water species and accordingly can be regarded as characteristic of the neritic zone (above 150 m), whereas Assemblage III contains species that prefer the depth range between those species occurring in Assemblages I and II. Thus, Assemblage III would indicate an upper bathyal environment. The transition from Assemblage I to the "shallow water" assemblage (II) occurs over the same interval where the P/B ratio reaches less than 10%. These two indicators suggest substantial subsidence of Site 728 through time. The absence of "shallow water" species in Assemblage III indicates a slightly deeper environment during this time.

Calcareous Nannofossils

The holes drilled at Site 728 provide a nearly identical biostratigraphic sequence from the Pleistocene to the upper Mio-

cene (Fig. 9). Calcareous nannofossils are abundant and moderately well preserved in Hole 728A to 269.1 mbsf. From 269.1 to 346.4 mbsf, nannofossils are abundant, but preservation deteriorates and ranges from moderate to poor. Nannofossils are abundant throughout Hole 728B, where preservation ranges from moderate to good.

Quaternary

In Hole 728A, sediments from the mudline to 10.78 mbsf, and in Hole 728B, sediments from the mudline to 1.2 mbsf contain *Emiliania huxleyi* and thus were assigned to Zone NN21 (uppermost Pleistocene to Holocene). Sediments from Samples 117-728A-2H-3, 118-119 cm, down to 177-728A-2H, CC (13.78-19.10 mbsf) and in Sample 117-728B-2H, CC (10.7 mbsf) in Hole 728B contain neither *E. huxleyi* nor *Pseudoemiliania lacunosa* and were assigned to Pleistocene Zone NN20. *P. lacunosa* is present, but *Discoaster brouweri* is absent in Samples 117-728A-3H-1, 118-119 cm, through 117-728A-7H-5, 125-126 cm (20.26-64.25 mbsf), and 117-728B-3H, CC, through 117-728B-7H, CC (20.1-58.1 mbsf); thus, these intervals were assigned to Zone NN19. The following datum levels were recognized in Zone NN19 (see "Explanatory Notes" chapter, this volume, for explanation of datums).

Hole 728B

Datum 1	Uncertain
Datum 2	1.2-10.7 mbsf in Core 117-728B-2H
Datum 3	10.7-20.1 mbsf in Core 117-728B-3H
Datum 4	Uncertain
Datum 5	29.6-39.1 mbsf in Core 117-728B-5H
Datum 6	29.6-39.1 mbsf in Core 117-728B-5H
Datum 7	39.1-48.6 mbsf in Core 117-728B-6H
Datum 8	48.6-58.1 mbsf in Core 117-728B-7H
Datum 9	48.6-58.1 mbsf in Core 117-728B-7H
Datum 10	48.6-58.1 mbsf in Core 117-728B-7H

The Pleistocene/Pliocene boundary can be recognized in Hole 728A between 61.25 and 64.25 mbsf (between Samples 117-728A-7H-3, 125-126 cm, and 117-728A-7H-5, 125-126 cm) and in Hole 728B between 48.6 and 58.1 mbsf (between Samples 117-728-6H, CC, and 117-718B-7H, CC).

Neogene

Zonation of the Neogene sediments is not extremely accurate, as has been true with all other sites of this leg, because some of the tropical zonal markers are absent or are extremely rare.

Sediments in Samples 117-728A-7H, CC (66.5 mbsf) and 117-728B-8H, CC (67.7 mbsf) in Hole 728B contain *Discoaster brouweri*, but not *D. pentaradiatus* and were assigned to upper Pliocene Zone NN18. Samples 117-728A-3H, 118-119 cm, through 117-728A-11X-1, 118-119 cm (76.1-96.48 mbsf), contain *Discoaster surculus*. The top of *D. surculus* is used to distinguish Zone NN16 from Zone NN17. The top of *D. pentaradiatus* was not recognized in Hole 728A, thus Zones NN17 and NN18 cannot be differentiated. Sample 117-728B-9H, CC, belongs to Zone NN17; Samples 117-728B-10X, CC, and -11X, CC (86.9-96.5 mbsf) contain *D. surculus*, but not *Reticulofenestra pseudumbilica*, and were assigned to Zone NN16.

The zonal markers for Zones NN13 and NN14, *Ceratolithus rugosus* and *Amaurolithus tricorniculatus*, are absent and thus, the only possible alternative, although not a very satisfactory

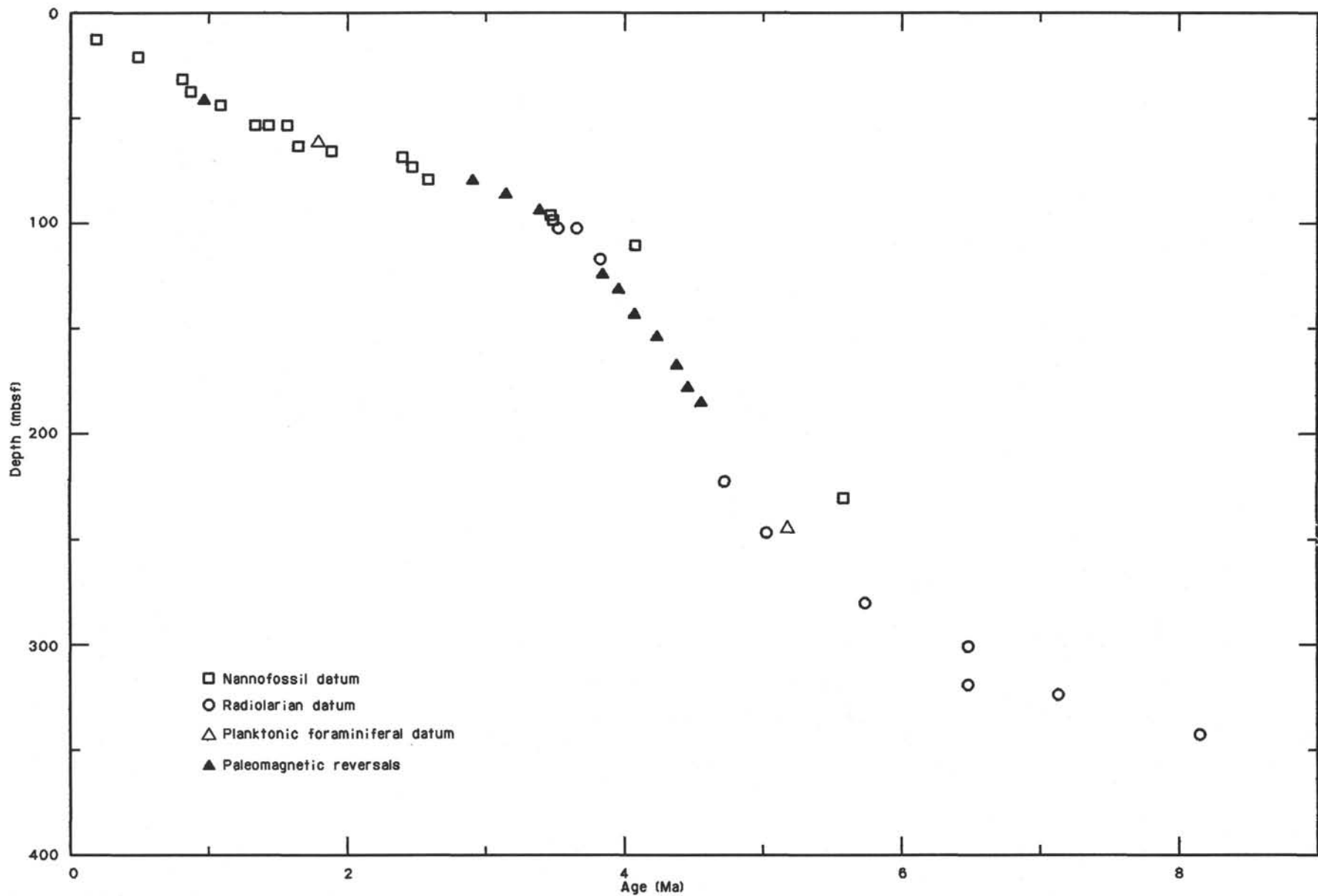


Figure 8. Age-depth plot for Hole 728A. For a detailed listing of events, see Table 3.

Table 3. Stratigraphic list of faunal events and paleomagnetic reversals for Hole 728A.

	Event	Core, section, interval (cm)	Depth (mbsf)	Age (Ma)	Source of age
B	<i>Emiliana huxleyi</i>	2H-1, 118-119	10.78	0.19	3
T	<i>Pseudoemiliana lacunosa</i>	2H-3, 118-119	13.78		
T	<i>Reticulofenestra</i> sp. A	2H, CC	19.10	0.49	3
B	<i>Gephyrocapsa parallela</i>	3H-1, 118-119	20.28		
B	Jaramillo	4H-1, 118-119	29.68	0.82	3
		4H-3, 118-119	32.68		
		4H-5, 118-119	35.68	^a 0.89	4
		4H, CC	38.00		
		5H-2, 120-122	40.70	0.98	5
		5H-3, 120-122	42.20		
^b T	<i>Gephyrocapsa</i> "large"	5H-3, 118-119	42.18	^a 1.10	4
		5H-5, 118-119	45.19		
^c T	<i>Helicosphaera sellii</i>	6H-1, 118-119	48.68		
		6H-2, 118-119	51.68		
^b B	<i>Gephyrocapsa</i> "large"	6H-3, 118-119	51.68	^a 1.36	4
		6H-5, 118-119	54.69		
T	<i>Calcidiscus macintyreii</i>	6H-3, 118-119	51.68	1.45	5
B	<i>Gephyrocapsa oceanica</i>	6H-5, 118-119	54.68	^a 1.57	4
T	<i>Globigerinoides extremus</i>	6H, CC	57.00	^d 1.8	5
		7H, CC	66.50		
B	<i>Gephyrocapsa caribbeanica</i>	7H-3, 125-126	61.25	^c 1.66	6
		7H-5, 125-126	64.25		
T	<i>Discoaster brouweri</i>	7H-5, 125-126	64.25	1.9	5
		7H, CC	66.50		
T	<i>Discoaster surculus</i>	8H-1, 118-119	67.68	2.4	5
		8H-3, 118-119	70.68		
		8H-4, 120-122	72.20	2.47	5
		8H-5, 120-122	73.70		
T	<i>Discoaster tamalis</i>	9H-1, 118-119	77.28	^f 2.6	5
		9H-3, 118-119	80.28		
T	Kaena	9H-2, 120-122	78.80	2.92	5
		9H-3, 120-122	80.30		
B	Mammoth	9H-6, 120-122	84.80	3.18	5
		10X-1, 120-122	86.90		
		10X-5, 120-122	92.90	3.40	5
		10X-6, 120-122	94.40		
T	<i>Sphenolithus abies</i>	10X, CC	95.30	3.47	5
		11X-1, 118-119	96.48		
T	<i>Reticulofenestra pseudoumbilica</i>	11X-1, 118-119	96.48	3.5	5
		11X-3, 118-119	99.48		
T	<i>Phormostichoartus doliolum</i>	11X-4, 85-87	100.65	3.53-3.55	1
		11X, CC	104.90		
B	<i>Amphirhopalum ypsilon</i>	11X-4, 85-87	100.65	3.77-3.79	1
		11X, CC	104.90		
B	<i>Discoaster asymmetricus</i>	12X-3, 118-119	109.08	^g 4.1	5
		12X, CC	114.50		
B	<i>Spongaster tetras tetras</i>	12X, CC	114.40	3.83-3.85	1
T	Cochiti	13X-4, 85-87	120.95		
		13X-5, 120-122	121.70	3.88	5
		14X-1, 115-117	125.35		
B	Cochiti	14X-5, 120-122	131.40	3.97	5
		14X-6, 119-121	132.89		
T	Nunivak	15X-6, 120-122	142.60	4.10	5
		16X-1, 120-122	144.70		
^h T	<i>Spongodiscus ambus</i>	15X-4, 85-87	139.25		
		15X, CC	143.50		
T	<i>Didymocyrtis penultima</i>	16X-4, 85-87	148.85		
		16X, CC	153.10		
B	Nunivak	16X-6, 108-110	152.08	4.24	5
		17X-2, 120-122	155.80		
T	Sidufjall	18X-3, 129-130	167.08	4.40	5
		18X-4, 111-113	168.41		
B	Sidufjall	19X-3, 125-127	176.75	4.47	5
		19X-4, 122-124	178.22		
T	Thvera	20X-2, 97-99	184.67	4.57	5
		20X-3, 112-114	186.32		
T	<i>Solenosphaera omnitubus</i>	23X, CC	220.80	4.7-4.8	2
		24X-4, 85-87	226.15		
T	<i>Discoaster quinqueramus</i>	24X, CC	230.50	ⁱ 5.6	5
		25X-1, 116-119	231.68		
B	<i>Globorotalia tumida tumida</i>	25X, CC	240.10	5.2	5
		26X, CC	249.80		
T	<i>Siphostichartus corona</i>	26X-4, 85-87	245.45	5.0-5.1	5
		26X, CC	249.80		

Table 3 (continued).

	Event	Core, section, interval (cm)	Depth (mbsf)	Age (Ma)	Source of age
T	<i>Stichocorys delmontensis</i>	26X-4, 85-87	245.45		
		26X, CC	249.80		
T	<i>Stichocorys johnsoni</i>	29X, CC	278.80	^j 5.7-5.8	2
		30X-4, 85-87	284.15		
B	<i>Spongodiscus ambus</i>	30X, CC	288.50		
		31X-4, 85-87	293.82		
		31X, CC	298.10	6.1-6.7	2
		32X, CC	307.60		
T	<i>Calocyclus caepa</i>	32X-4, 85-87	303.45	^k 6.2-6.6	2
		32X, CC	307.80		
B	<i>Stichocorys peregrina</i>	33X-4, 85-87	313.15		
		33X, CC	317.50		
B	<i>Solenosphaera omnitubus</i>	33X, CC	317.50	6.3-6.5	2
		34X-4, 85-87	322.35		
T	<i>Diartus hughesi</i>	24X-4, 85-87	322.85	7.1-7.2	2
		34X, CC	327.20		
T	<i>Dictyocoryne ontongensis</i>	35X-4, 85-87	332.55		
		35X, CC	336.80		
T	<i>Botryostrobus miralestensis</i>	36X-4, 85-87	342.15	^l 8.1-8.2	2
		36X, CC	346.40		
T	<i>Didymocyrtis laticonus</i>	36X-4, 85-87	342.15		
		36X, CC	346.40		

Note: T = upper limit of event and B = lower limit; "an evolutionary transition." Sources of age are: 1 = Johnson et al., in press; 2 = Johnson and Nigrini, 1985; 3 = oxygen-isotope data for Site 723 (Niitsuma, unpubl. data); 4 = Takayama and Sato, 1987; 5 = Berggren et al., 1985; and 6 = Sato et al., in press.

^a North Atlantic data.

^b Long axis greater than 6 μ m.

^c No good published age; event appears to be diachronous.

^d *G. obliquus extremus* in Berggren et al., 1985.

^e North Atlantic age consistent with Italian-type section.

^f Equatorial region only.

^g Should be lower.

^h ? Reworking or T may be between 11X-4 and 11X, CC.

ⁱ Age appears to be erroneous.

^j *E. cf. diaphanes* in Johnson and Nigrini, 1985.

^k Age in western Pacific.

^l May be reworked.

one, was to combine uppermost Miocene and lower Pliocene Zones NN12 through NN15. Samples 117-728A-11X-3, 118-119 cm, through 117-728A-24X, CC (99.48-230.50 mbsf) and 117-728B-12X, CC, through 117-728B-24X, CC, (106.1-222.2 mbsf) contain *R. pseudoumbilica* and *Discoaster asymmetricus*, but not *Discoaster quinqueramus*.

Discoaster quinqueramus, the marker species for Zone NN11 (upper Miocene), is present from Sample 117-728A-25X-1, 118-119 cm, to the bottom of the hole (231.68-346.4 mbsf) and from 117-728B-25X, CC, to the bottom of the hole (231.8-347.7 mbsf).

Several reworked species include *Chiasmolithus grandis* and *Discoaster barbadiensis* from the Eocene, and *D. exilis*, *D. deflandrei*, *D. quinqueramus*, *Cyclicargolithus floridanus*, and *Sphenolithus moriformis* from the Oligocene-Miocene. *D. variabilis*, *S. abies*, and *R. pseudoumbilica* from the Miocene-Pliocene were encountered throughout both holes. Reworked Cretaceous species found in Hole 728A include *Watznaveria barnesae*, *Arkhangeliskiella* spp., *Eiffelithus eximius*, *Microrhabdulus decoratus*, *Prediscosphaera* spp., *Cribrosphaerella ehrenbergii*, and *Tranolithus phacelosus*.

Radiolarians

The core-catcher samples of Cores 117-728A-1H through 117-728A-4H (9.6-38.0 mbsf) are barren of radiolarians. Between Cores 117-728A-5H and 117-728A-8H (47.5-76.1 mbsf), a few radiolarian fragments were found in the core-catcher sam-

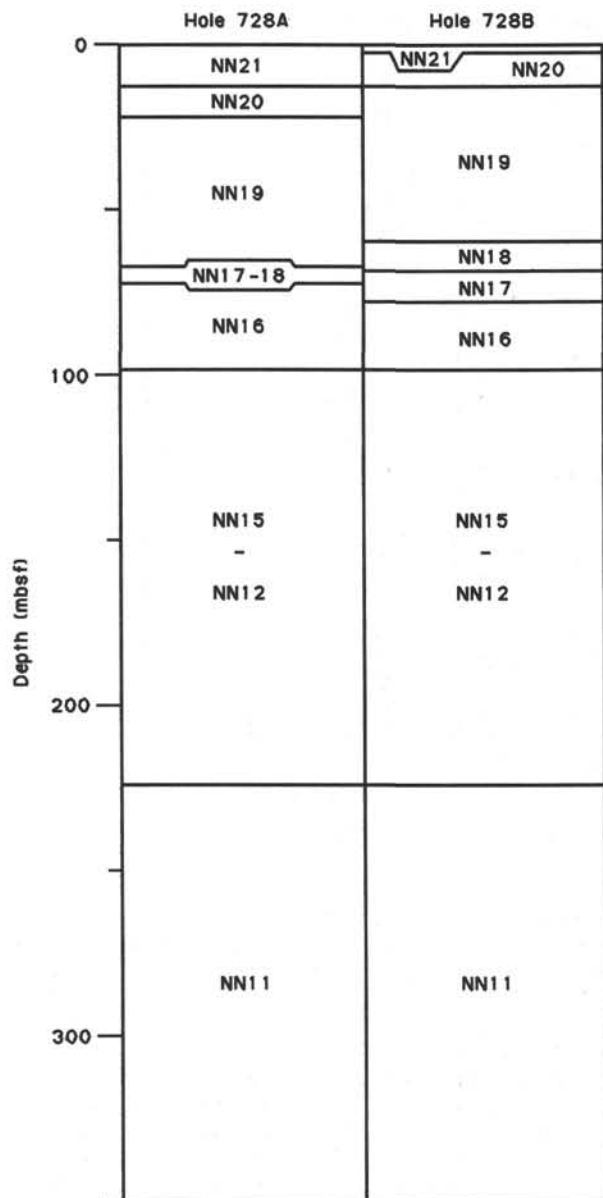


Figure 9. Correlation of calcareous nannofossil zones in Hole 728A and Hole 728B.

ples. However, radiolarians are common and well preserved from Sample 117-728A-9H, CC to Sample 117-728A-36X, CC (85.7–346.4 mbsf). The top of this siliceous sequence coincides with a pronounced spike in clay content, as shown by downhole logging (“Downhole Measurements” section, this chapter), and a change in porosity, as shown by the physical properties measurements (see “Physical Properties” section, this chapter). The radiolarians are generally mixed with varying quantities of mineral fragments, sponge spicules, and diatoms. Samples 117-728A-9H, CC through 117-728A-23X (85.7–220.8 mbsf) are in the *Spongaster pentas* Zone. Since *S. pentas* and *S. berminghami* are virtually absent, the *S. pentas/Stichocorys peregrina* boundary has been approximated to the LAD of *Solenosphaera omnitubus*. The *S. peregrina* Zone extends from Samples 117-728A-24X-4, 85–87 cm, to 117-728A-31X-4, 85–87 cm (226.15–293.82 mbsf). Samples 117-728A-31X, CC, and 117-72-32X-4, 85–87 cm (298.10–303.45 mbsf), lie within the *Didymocyrtis penultima* Zone and Samples 117-728A-32X, CC, to 117-728A-

36X, CC (307.80–336.8 mbsf), lie within the *Didymocyrtis antepenultima* Zone.

Environmental Implications

The nannofossil genus, *Helisphaera*, which is thought to prefer areas of upwelling, was found in abundance in Samples 117-7A-4H, CC, through 117-728A-8H, CC (38.0–76 mbsf). *Coccolithus pelagicus*, a cold-water species, was present in unusually high numbers in Samples 117-728A-6H, CC, and 117-728A-7H, CC (48.6–58.1 mbsf).

The three different benthic foraminiferal assemblages found at Site 728 and the variation in the P/B ratio indicate that this site was located in the upper bathyal zone during the late Miocene. The water depth decreased in early Pliocene, and Site 728 was located in the neritic zone. During the late Pliocene, a significant increase occurred in water depth to the modern depth of Site 728 in the upper middle bathyal zone.

The fact that robust, thick-walled *Globorotalia tumida* subspecies dominate the planktonic foraminiferal assemblages in the Pliocene and upper Miocene may be caused by dissolution. These processes may have been enhanced in an extended or intensified oxygen-minimum zone during these time intervals.

PALEOMAGNETISM

Magnetic Measurements

At Site 728, we used the pass-through cryogenic magnetometer for all measurements in Cores 117-728A-1H through 117-728A-13X after pass-through alternating field (AF) demagnetization at 5 mT. Unfortunately, we were again frustrated by a combination of high scatter and incomplete removal of steep overprints, probably induced by coring or retrieval through the drill string.

Therefore, as at previous sites, paleomagnetic information at Site 728 was obtained using the Minispin fluxgate magnetometer and the Schonstedt AF demagnetizer. These efforts were successful; Figure 10 shows one of the better paleomagnetic records obtained during Leg 117. Our record covers sub-bottom depths of 0 to 200 m; below this interval, the sediments were too weakly magnetized to provide reliable data. An arithmetic mean intensity of 0.96 mA/m was obtained after AF demagnetization at 10 mT. Figure 11 indicates that inclination values for this interval correspond well to the expected axial dipole values.

Magnetostratigraphy

Table 4 lists the sub-bottom depths, depths within the cores, and ages (after Berggren et al., 1985) of the inferred polarity transitions. The main points of interest are (1) the absence of a Chron C1/C1r (Brunhes/Matuyama Chronozone) boundary—again after reference to the nannofossil stratigraphy (see “Biostratigraphy” section, this chapter), we interpret the first normal-to-reverse transition as the lower boundary of Subchron C1r-1 (Jaramillo Subchronozone); (2) the absence of Chron C2 (Olduvai Subchronozone), again as inferred from the nannofossil stratigraphy; and (3) the relatively high degree of detail with which Chrons C2Ar and C3 (upper and middle Gilbert Chronozone) are recorded: the Cochiti, Nunivak, and Sidufjall subchronozones appear to be present, together with the upper part of the Thvera Subchronozone. Figure 12 shows an age vs. depth curve based on the correlations with the polarity time scale.

Magnetic Susceptibility

The volume magnetic susceptibility of Site 728 sediments recovered from the Oman margin was measured using Bartington Instruments’ whole-core sensor at 0.1 sensitivity and low-frequency (0.47 kHz) settings. Short intervals of pipe rust contamination in the XCB core tops appear as regular ~10-m spikes in

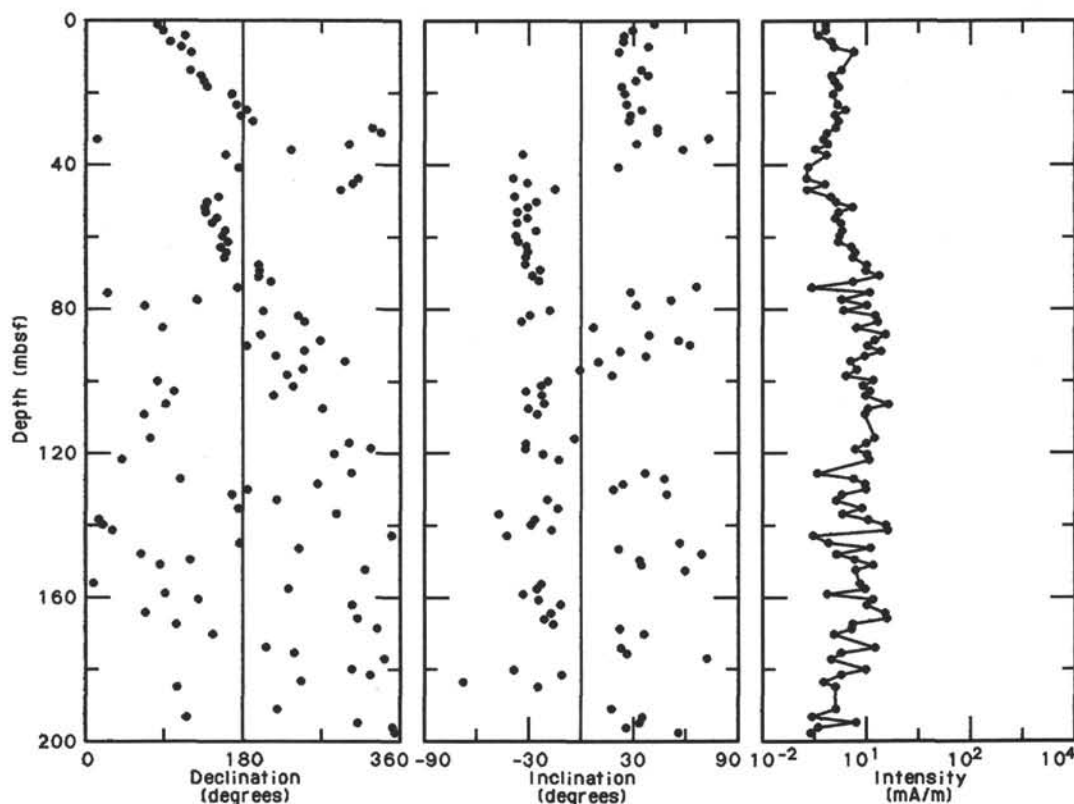


Figure 10. Declination, inclination and intensity for discrete samples from Hole 728A, obtained by shipboard measurements.

the susceptibility data. Susceptibilities were measured at 8 cm intervals, which resulted in approximately 4000 measurements each for Holes 728A and 728B. Recovery and core quality were excellent at both holes.

The susceptibility records of Holes 728A and 728B show well-defined variations that extend to the base of each hole (Fig. 13). The average amplitude of the Site 728 susceptibility variability is 30 to 100×10^{-6} volume SI units. These fluctuations can be correlated between holes over most of the recovered sequence with an accuracy of approximately 8 cm. A composite susceptibility record will be constructed for this site (and all others) as part of our shore-based research. Interhole correlations based on these data and lithologic marker layers are presented in the "Interhole Correlation" section of this chapter.

The high-quality susceptibility records obtained for Holes 728A and 728B can be correlated to other Oman margin and Owen Ridge sites. An example of the Brunhes Chronozone correlations possible between Holes 728A and 723B (Oman margin) and Hole 722B (Owen Ridge) is shown in Figure 14. Although the susceptibility record of each hole has a unique character, major and minor relative features are apparent. Since the susceptibility data of Site 728 show well-defined variations over most of the recovered sequence, detailed correlations between the margin and ridge sites should be possible to at least the Matuyama/Gauss Chronozone boundary (2.47 Ma).

ACCUMULATION RATES

Sedimentation rates for Site 728 are based on magnetostratigraphic and biostratigraphic datum levels identified in Hole 728A (Table 3). Rates for the last 2.4 m.y. were determined between nannofossil datums that were assigned ages based on oxygen-isotope stratigraphy (N. Niitsuma, unpubl. data) or from Berggren et al. (1985). Over the last 1.9 m.y., average sedimentation

rates varied from 15 to 65 m/m.y., with an overall mean of 34 m/m.y. (Fig. 15 and Table 5). This mean rate is low compared with those at other margin sites and reflects differences in depositional setting. Site 728, in the lower slope basin, receives mostly a pelagic influx, compared to the dominance of hemipelagic sedimentation in the upper slope basin (see "Lithostratigraphy" section, this chapter). Because of the low rate of sediment accumulation at Site 728 in this interval, errors in the age model may account for some of the high variability. Mean rates of sedimentation from 8.2 to 2.4 m.y. (23–88 m/m.y.) are based on a best fit to the reliable stratigraphic datums listed in Table 3. The mass accumulation of calcium carbonate, organic carbon, and noncarbonate sediment components are calculated from average values within intervals where the mean sedimentation rate is calculated (Table 5, Fig. 16).

At Site 728, sediments in the late Pliocene are characterized by a low mean sedimentation rate, high organic carbon concentrations (3%–4%), and the accumulation of siliceous microfossils. Similar associations were found at other Oman margin sites (see "Site 724" chapter, this volume), where accumulations occurred at more than twice the rate of Site 728. Upper Miocene to lower Pliocene sediments were deposited rapidly (~88 m/m.y.), with accumulation of organic carbon and abundant siliceous microfossils. These associations are thought to reflect sedimentation in environments of high biological productivity. Benthic foraminifer data from Site 728 (see "Biostratigraphy" section, this chapter) indicate that this site was at a depth near 350 m in the late Miocene and early Pliocene, when rapid deposition occurred, and has since subsided to its present depth of 1400 m. These results suggest that changes in the tectonic setting in addition to surface productivity are responsible for the variations in sediment accumulation at Site 728 during the Neogene.

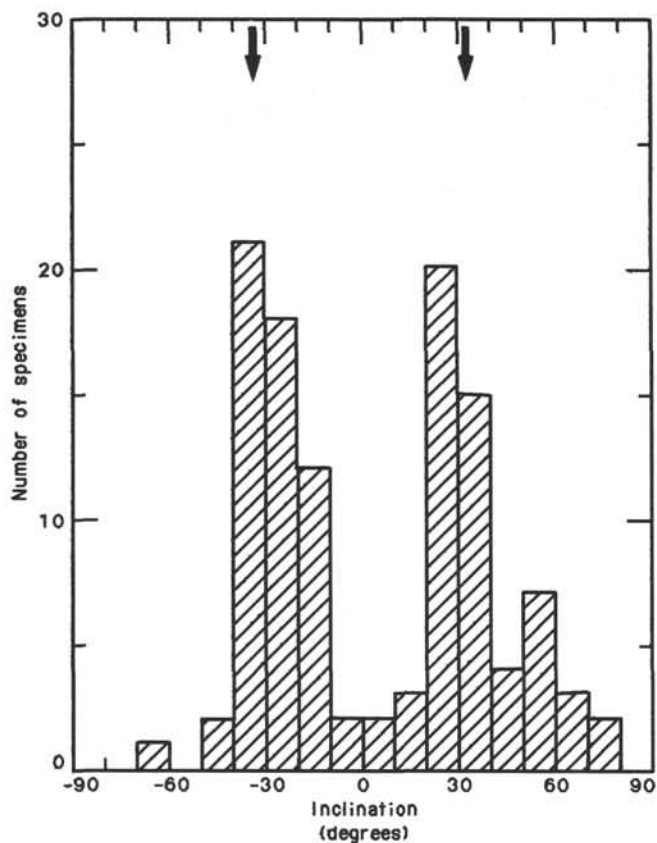


Figure 11. Inclination values grouped into 10° classes. Arrows indicate the expected geocentric axial dipole values for the site latitude.

Table 4. Magnetozone boundaries in Hole 728A.

Boundary	Age (Ma)	Sample interval (cm)	Depth (mbsf)
Bottom of Jaramillo (C1r-1/C1r)	0.98	5H-2, 120/5H-3, 120	40.70/42.20
Matuyama/Gauss (C2r/C2A)	2.47	8H-4, 120/8H-5, 120	72.20/73.70
Top of Kaena (C2A/C2A-1)	2.92	9H-2, 120/9H-3, 120	78.80/80.30
Bottom of Mammoth (C2A-2/C2A)	3.18	9H-6, 120/10X-1, 120	84.80/86.90
Gauss/Gilbert (C2A/C2Ar)	3.40	10X-5, 120/10X-6, 120	92.90/94.40
Top of Cochiti (C2Ar/C3.1)	3.88	13X-5, 120/14X-1, 115	121.70/125.35
Bottom of Cochiti (C3.1/C3.1r)	3.97	14X-5, 120/14X-6, 119	131.40/132.89
Top of Nunivak (C3.1r/C3.2)	4.10	15X-6, 120/16X-1, 120	142.60/144.70
Bottom of Nunivak (C3.2/C3.2r)	4.24	16X-6, 108/17X-2, 120	152.08/155.80
Top of Sidufjall (C3.2r/C3.2r-1)	4.40	18X-3, 128/18X-4, 111	167.08/168.41
Bottom of Sidufjall (C3.2r-1/C3.2r)	4.47	19X-3, 125/19X-4, 122	176.75/178.22
Top of Thvera (C3.2r/C3.3)	4.57	20X-2, 97/20X-3, 112	184.67/186.32

Note: Ages of chronozone boundaries are after Berggren et al. (1985).

PHYSICAL PROPERTIES

Introduction

Physical properties measured on discrete samples of sediments recovered from Site 728 include index properties (wet-

bulk density, porosity, water content, and grain density), thermal conductivity, vane shear strength, and compressional-wave velocity (Tables 6 and 7). Wet-bulk density was measured on all whole-round cores that were at least 80 cm in length using the GRAPE logging system. Acquisition of compressional-wave velocity data using the *P*-wave logger was limited to the interval between the seafloor and approximately 100 mbsf. All techniques and equipment used are described in the "Explanatory Notes" (this volume).

Index Properties

As observed at the other sites on the Oman margin, the sequences of marly nannofossil ooze at Site 728 show relatively low wet-bulk and grain densities, as well as high porosities and water contents (Fig. 17). This may be a result of fairly high concentrations of organic material at this site, as well as of the common occurrence of radiolarians and diatoms from Core 117-728A-9H to total depth.

Lithologic Subunit IA

Within the marly foraminifer-nannofossil to foraminifer-bearing marly nannofossil oozes of lithologic Subunit IA (0–58 mbsf), porosity and water contents decrease from 60% to 55% and 36% to 33%, respectively, in response to increasing overburden pressure. Within this subunit, the foraminifers are abundant in some intervals and may account for the variability in index properties. Grain density is variable at all depths (ranging from 2.50 to 2.73 g/cm³), but decreases downsection as the organic carbon content increases from 1% to 2%. Wet-bulk density varies widely in this interval, but overall values of bulk density increase from 1.70 to 1.75 g/cm³. An exception to these trends occurs in an interval between 36 and 43 mbsf (Sections 117-728A-4H-6 to 117-728A-5H-4). Here, a maximum porosity of 64% and a minimum wet-bulk density of 1.62 g/cm³ coincide with a local maximum in calcium carbonate (65%–71%), most likely in the form of foraminifers. The wet-bulk density of this interval is correspondingly low (1.62 g/cm³).

Lithologic Subunit IB

Several distinct trends in physical properties can be identified within the marly nannofossil ooze and chalk of lithologic Subunit IB (58–320 mbsf) that are related to the presence of siliceous microfossils in the sequences below Section 117-728A-8H, CC (76 mbsf) and to variations in the abundance of organic carbon throughout the section (see "Lithostratigraphy" section, Fig. 6, this chapter). Index properties in Cores 117-728A-7H through 117-728A-9H (58–85 mbsf) display gradients opposite to those expected in a consolidating section because of a rapid increase in organic carbon from 2% at the base of Core 117-728A-6H to maxima of 4.5% and 5.0% at depths of 72 and 82 mbsf. Grain density is markedly lower throughout this interval (2.50 to 2.63 g/cm³) and decreases gradually with depth to 2.55 g/cm³ at 85 mbsf. As observed in the overlying sediments, wet-bulk density shows considerable variation. In this interval, however density decreases with depth (1.75 to 1.65 g/cm³) in response to decreases in grain density. The coincident increases in porosity (55%–62%) and water content (33%–41%) result from the open-fabric framework that is characteristic of organic-rich sediments.

Within the interval of siliceous-bearing, marly nannofossil ooze between 85 mbsf and the base of lithologic Subunit IB, index properties closely track the variation in organic carbon content. Between 85 and 170 mbsf, porosity and water content remain high and increase slightly to maximum values of 65% and 42%, respectively, in an interval between 150 and 170 mbsf. Wet-bulk density is correspondingly low (1.60 g/cm³) in this interval, which, in addition to being high in organic carbon, is especially rich in calcium carbonate (see Fig. 6, "Lithostratigra-

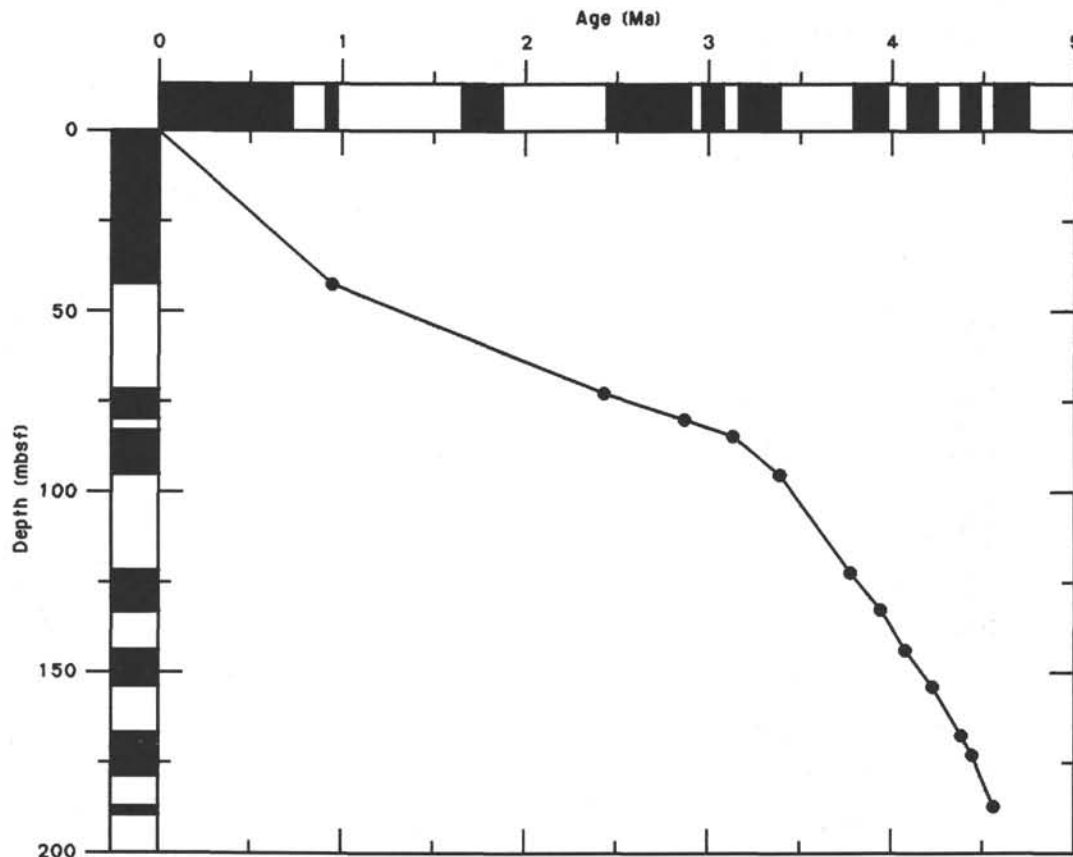


Figure 12. Age-depth curve for the upper 200 mbsf for Hole 728A, using magnetic chronozone boundaries.

phy" section, this chapter). Grain density varies from 2.45 to 2.65 g/cm³ and averages 2.55 g/cm³ between 85 and 170 mbsf.

Below 170 mbsf to the base of lithologic Subunit IB at 320 mbsf, porosity, water content, and wet-bulk density resume normal downsection gradients; porosity decreases from 63% to 59%, water content decreases from 41% to 36%, and wet-bulk density increases from 1.62 to 1.72 g/cm³. Grain density varies throughout this interval at all depths, but generally increases from an average of 2.58 to 2.65 g/cm³ in response to a decrease from 3.0% to 1.3% in organic carbon.

Lithologic Subunit IC

Within lithologic Subunit IC (320–349 mbsf), index properties are found to vary significantly with minor changes in sediment composition. Samples from the layers of marly nannofossil and diatomaceous chinks are distinctly higher in porosity (64%–67%) and water content (41%–43%) and lower in wet-bulk density (1.59 to 1.63 g/cm³) than the more calcareous nannofossil chinks. Grain densities show a less consistent correlation but tend to be lower in the siliceous and clay-rich units (2.50 to 2.60 g/cm³) than in the nannofossil-rich layers (2.51 to 2.65 g/cm³).

Compressional-Wave Velocity

Compressional-wave velocity was measured perpendicular to bedding on discrete samples from all cores in Holes 728A and 728B from which suitable samples could be extracted. Velocities were also measured parallel to bedding on samples that were sufficiently indurated to allow a cubic sample to be cut (Tables 6 and 7; Fig. 18).

Velocities measured in the uppermost 100 m of Hole 728A vary from 1515 to 1594 m/s but correspond well to velocities

measured by the *P*-wave logger (Fig. 19) and reflect the slight decrease in bulk density measured in the discrete samples (Fig. 17) and on the continuous GRAPE density logs (Fig. 20). Velocities could not be successfully measured in the friable and brittle sediments recovered from depths greater than 100 and less than 220 mbsf, with the curious exception of one core from each of the two holes at 180 mbsf (Fig. 18). Compressional-wave velocities in the more indurated nannofossil chinks below 220 mbsf are variable but again reflect the slight downhole decrease in density. Anisotropy in compressional-wave velocity shows no consistent correlation with density or sub-bottom depth. Velocities measured parallel to bedding averaged 3.0% greater than those measured perpendicular to bedding.

Thermal Conductivity

Thermal conductivity, measured on even-numbered cores from Cores 117-728A-1H to 117-728A-26X, decreases consistently with depth from approximately 1.45 W/m K near the seafloor to an average of 1.25 W/m K at 250 mbsf. Below this depth, the sediments were too stiff to allow insertion of the needle probes. The observed downsection decrease at first appeared to be attributed to the friable nature of the sediments below 100 mbsf, but a positive correlation between thermal conductivity and wet-bulk density (Fig. 21) suggests that thermal conductivity decreases in response to the gradual downsection decrease in wet-bulk density.

Vane Shear Strength

Vane shear strength increases from 10 kPa near the seafloor to 135.7 kPa at 70 mbsf. The sharp decrease in shear strength below this level coincides with the change in sediment composition to more siliceous and organic-rich sediments.

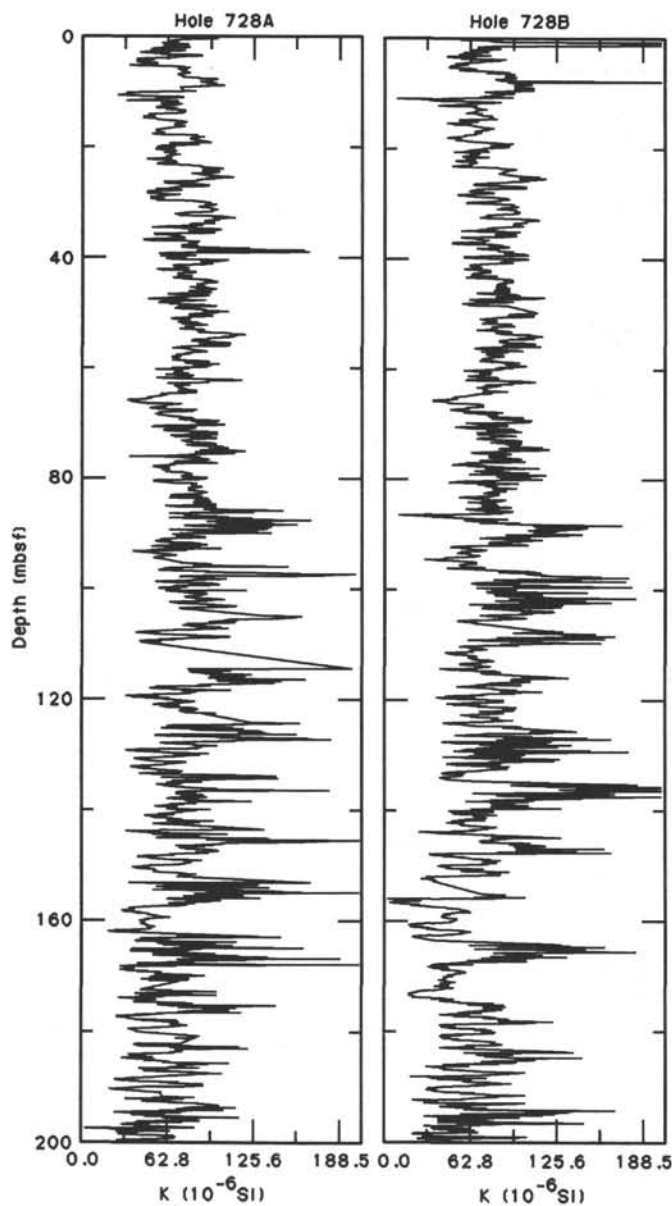


Figure 13. Whole-core magnetic susceptibility data for Holes 728A and 728B. Regular ~10-m susceptibility spikes are caused by pipe rust contamination of the XCB core tops.

GRAPE and *P*-Wave Logs

The quality of data obtained from the GRAPE and *P*-wave logging systems was generally very good at Site 728. Continuous GRAPE data were obtained to total depth in Holes 728A and 728B. The pattern of bulk-density variation determined by the GRAPE records corresponds to that of the discrete samples, although the quality of the match between the two data sets varies with depth. Between 0 and 85 mbsf, the discrete samples display a large variation and are approximately 0.05 to 0.10 g/cm³ lower than the GRAPE values, perhaps as a result of the addition of water to the sediments during coring, splitting, and/or sampling. A reduction in the disturbance of the discrete samples may contribute to the improved match between the two data sets between 85 and 150 mbsf. Below 150 mbsf, the GRAPE and discrete-measurement records overlap, but the GRAPE system consistently underestimated the wet-bulk density because cores did not completely fill the liners.

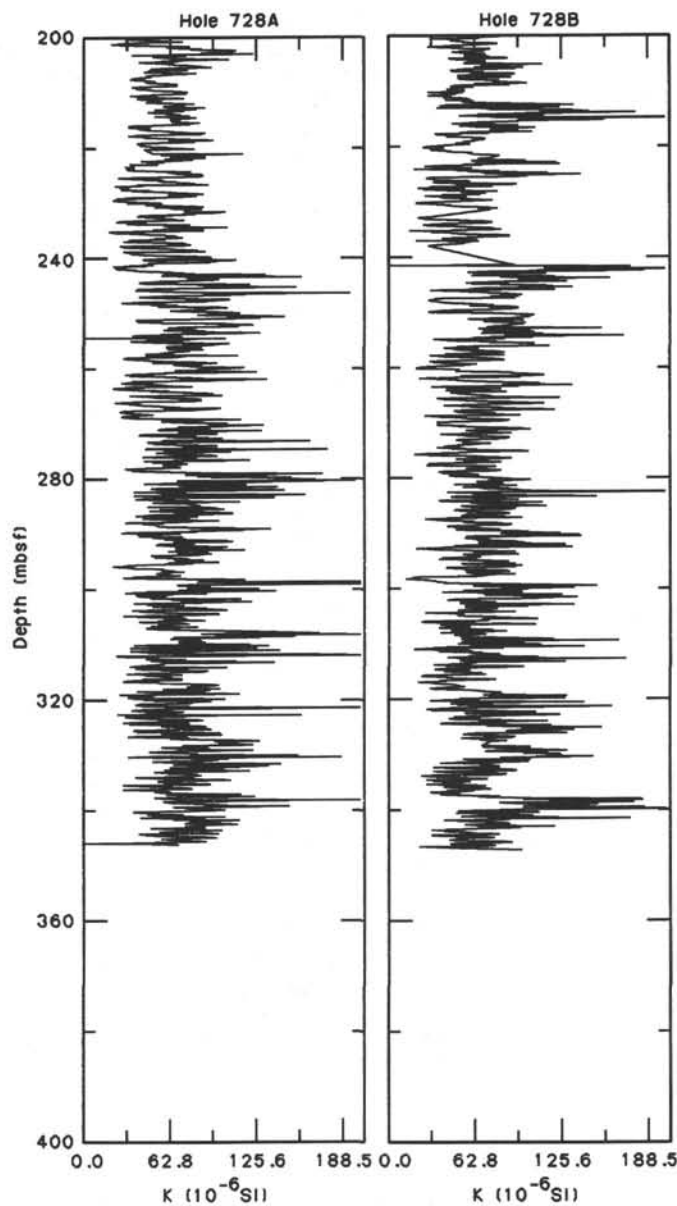


Figure 13 (continued).

P-wave velocity logs were obtained in Cores 117-728A-1H through -10X and Core 117-728B-1H through Section 117-728B-14X-2. These velocities average 1590 m/s to a depth of 30 mbsf. At greater depths, the values decrease gradually to 1550 m/s at 95 mbsf. This negative gradient in part reflects the decrease in wet-bulk density associated with changes in texture and composition of the sediment but may also be accentuated by the increasing thickness of drilling slurry around the sediment cores.

SEISMIC STRATIGRAPHY

Site 728 is located in the distal slope basin of the Oman margin. This basin is separated from an outer basement high by a major normal fault (Fig. 22). The basin is flanked on the northwest by a complexly faulted region that is uplifted in relation to the slope basin. Here, we first examine the relationship between seismic traveltimes and core depth to provide a basis for regional extrapolation across a seismic section from the very detailed information available at Site 728. Next, we provide a preliminary seismic interpretation of the seismic section in Figure 22, keyed to the data from Site 728. Implicit in such a discussion of a sin-

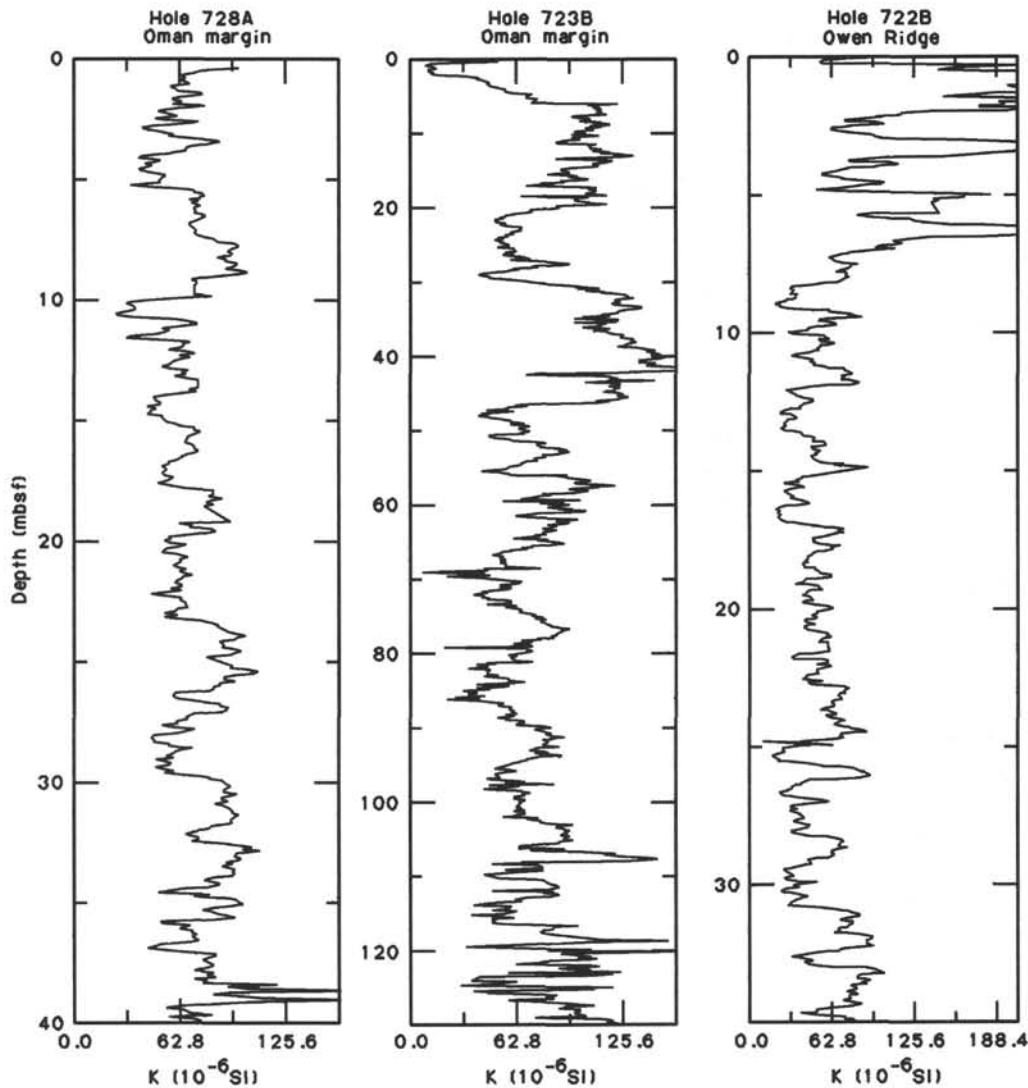


Figure 14. Brunhes Chronozone correlations of Holes 728A, 723B (Oman margin), and 722B (Owen Ridge).

gle seismic line is a lack of knowledge of many three-dimensional aspects of the geology, such as whether apparent normal faults are actually strike-slip faults.

Relationship of Seismic Time to Core Depth

A continuous sonic log is available for the interval of 55.5 to 327.6 mbsf. A resistivity log, which was lower on the tool string than the sonic log, extends to 341.3 mbsf. Based on a regression between velocity and resistivity ($R = 0.71$) for the lowest 23.6 m of overlap between the two logs, a pseudosonic log was generated for the short interval of 327.6 to 341.3 mbsf (see "Down-hole Measurements" section, this chapter). A composite sonic log was used to calculate a synthetic seismogram for Site 728. No density log was available, thus, a constant density was assumed. This assumption probably does not degrade the accuracy of the synthetic seismogram much because a synthetic seismogram calculated for Site 723 using a constant-density assumption was almost identical to that calculated from both sonic and density logs (see "Seismic Stratigraphy" section, Site 723 chapter). The synthetic seismogram was calculated based on a convolutional model with interbed multiples and a wavelet estimate for the *Conrad* (see "Seismic Stratigraphy" section, Site 720 chapter).

Figure 23 compares the synthetic seismogram for Site 728 to a single expanded seismic trace and the portion of Figure 22 that approaches the site. This single seismic trace is a 10-trace mix centered at the site, from the same seismic line as Figure 22. The amplitudes of the synthetic seismogram and seismic trace are individually scaled to the largest peak or trough. Because scaling for the seismic trace is based on the strong seafloor reflection, amplitudes are smaller than for correlative portions of the synthetic seismogram.

A good character match was found between the composite seismic trace and the synthetic seismogram (Fig. 23) down to 2.19 s (267 mbsf), and a tentative match can be extended to 2.23 s (300 mbsf). Below 300 mbsf, the synthetic seismogram indicates much higher amplitudes than the composite seismic trace. Similar high amplitudes were observed on the seismic section adjacent to the site, with the same wavelength between peaks. Furthermore, the strongest seismic reflector intersects the site at 2.28 s, the location of the strongest peak on the synthetic seismogram. The inconsistency of seismic reflector amplitudes between the seismic section and the composite trace from the same section probably results from the substantial dip of these deeper reflectors, which causes averaging of a peak with its adjacent trough across a 10-trace mix. Sonic traveltimes are considered to

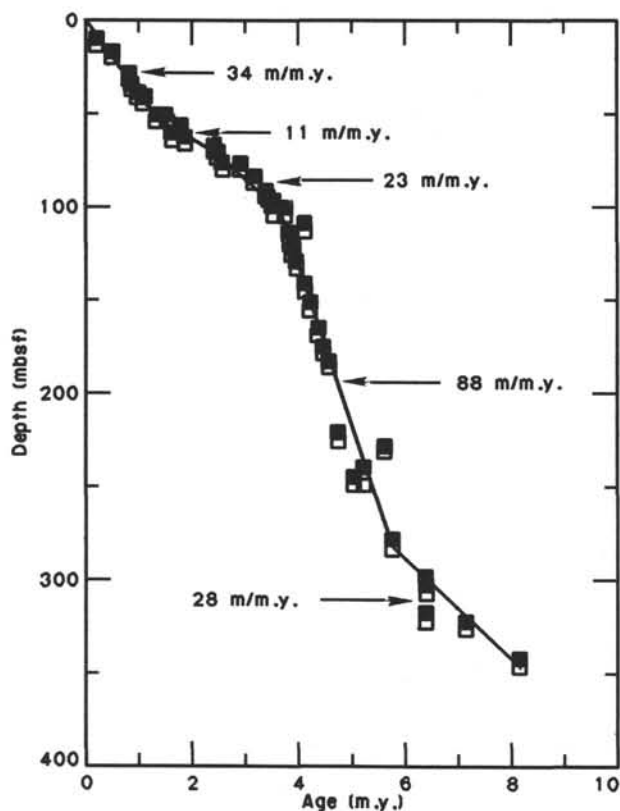


Figure 15. Age-depth plot of stratigraphic datums listed in Table 5. The filled and open boxes are upper and lower depths of each datum level, respectively. Indicated mean sedimentation rates (solid lines) are determined by a best fit to the data. Rates calculated between reliable datums younger than 1.9 m.y. are listed in Table 5.

be reliable in the lower portion of Site 728 down to the lowest sonic log value at 327.6 mbsf (see "Downhole Measurements" section, this chapter), and the deepest seismic reflector on the synthetic seismogram (at 338 mbsf) is caused by velocity contrasts above this level, rather than by the short pseudosonic log. Thus, the match with the seismic peak at 2.28 s is probably correct.

Based on the match of the synthetic seismogram with the seismic section, a continuous match between core depth and seismic reflectors can be made for the depth interval 55.5 to 338 mbsf. We identified three significant seismic reflectors on the seismic section, on the basis of downhole changes in lithostratigraphy and logs.

An impedance rise occurs at 88 mbsf (Fig. 23), immediately below the 63-85 mbsf zone of rapid variations in log responses,

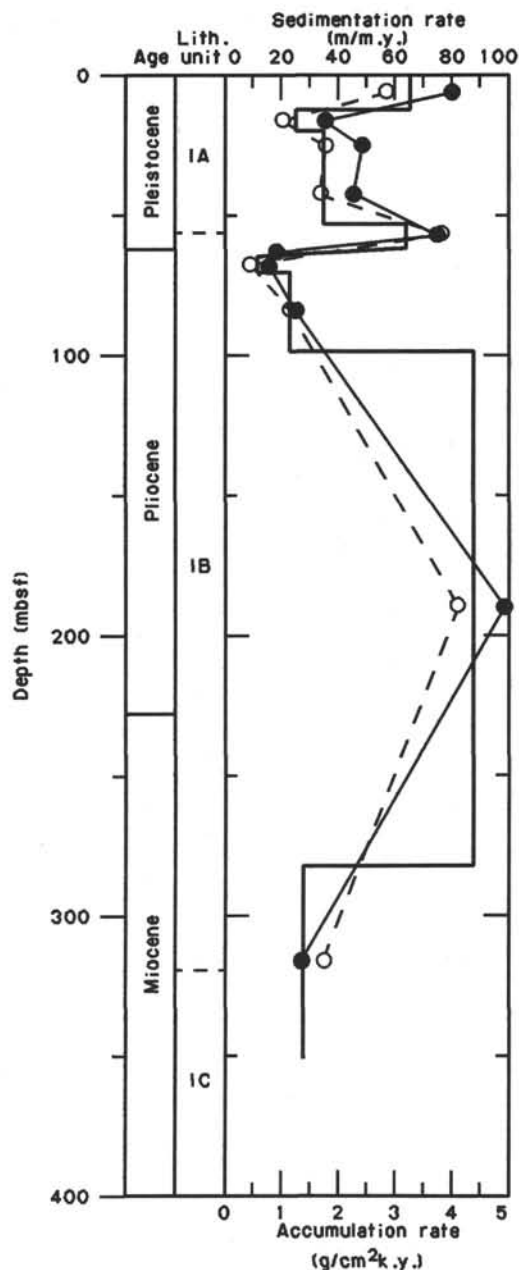


Figure 16. Sedimentation rate (m/m.y.; solid line), calcium carbonate accumulation rate ($\text{g}/\text{cm}^2/\text{k.y.}$; dots), and noncarbonate accumulation rate ($\text{g}/\text{cm}^2/\text{k.y.}$; open circles) vs. depth (mbsf) at Site 728. Accumulation rates are plotted at the midpoint of the respective depth intervals.

Table 5. Sedimentation and accumulation rate data for Site 728.

Depth interval (mbsf)	Age range (m.y.)	CaCO ₃ (\bar{x} %)	C _{org} (\bar{x} %)	Dry-bulk density (\bar{x} g/cm ³)	Sed. rate (\bar{x} m/m.y.)	CaCO ₃ acc. rate ($\text{g}/\text{cm}^2/\text{k.y.}$)	Non-CaCO ₃ acc. rate ($\text{g}/\text{cm}^2/\text{k.y.}$)	C _{org} acc. rate ($\text{mg}/\text{cm}^2/\text{k.y.}$)
0.0-12.3	0-0.19	58.4	1.11	1.05	64.7	3.97	2.83	75.4
12.3-19.7	0.19-0.49	63.3	ND	1.11	24.7	1.74	1.01	ND
19.7-31.2	0.49-0.82	57.7	1.34	1.20	34.8	2.41	1.77	56.0
31.2-53.2	0.82-1.45	57.5	1.91	1.13	34.9	2.27	1.68	75.3
53.2-61.5	1.45-1.66	49.6	1.37	1.18	63.8	3.73	3.79	103.1
61.5-64.5	1.66-1.90	46.0	2.26	1.18	15.0	0.81	0.96	40.0
64.5-70.0	1.90-2.40	63.2	1.99	1.09	11.0	0.76	0.44	23.9
70.0-98.0	2.40-3.6	52.2	3.67	1.04	23.3	1.27	1.16	89.0
98.0-282.0	3.6-5.7	54.4	2.59	1.03	87.6	4.91	4.11	233.7
282.0-350.0	5.7-8.15	43.7	1.49	1.12	27.8	1.36	1.75	46.4

Note: ND = no data for the interval.

Table 6. Physical properties summary for Hole 728A.

Core, section, interval (cm)	Depth (mbsf)	Wet-bulk density (g/cm ³)	Porosity (%)	Water content (%)	Gain density (g/cm ³)	Dry-bulk density (g/cm ³)	Velocity (m/s)	Thermal conductivity (W/mK)	Vane shear strength (kPa)
117-728A-									
1H-2, 100-102	2.50	1.581	64.3	41.7	2.686	0.922			
1H-4, 100-102	5.50	1.671	60.9	37.3	2.701	1.047			
1H-6, 100-102	8.50	1.751	57.3	33.5	2.724	1.164			10.0
2H-2, 80-82	11.90	1.646	56.8	35.4	2.640	1.064		1.36	
2H-4, 80-82	14.90	1.676	57.5	35.1	2.738	1.087		1.35	
2H-6, 80-82	17.90	1.699	56.0	33.8	2.735	1.124		1.54	
3H-2, 80-82	21.40	1.651	58.2	36.1	2.678	1.056			
3H-4, 80-82	24.40	1.797	53.4	30.4	2.667	1.251			
3H-6, 28-30	26.88	1.804	52.4	29.8	2.750	1.267			18.1
4H-2, 80-82	30.80	1.781	54.4	31.3	2.639	1.223		1.53	
4H-4, 80-82	33.80	1.738	53.7	31.6	2.637	1.188		1.43	
4H-5, 57-60	35.77						^a 1594		
4H-6, 80-82	36.80	1.623	64.1	40.5	2.581	0.966		1.31	
5H-2, 80-82	40.30	1.628	59.9	37.7	2.630	1.015			
5H-3, 50-53	41.50						^a 1550		
5H-4, 80-82	43.30	1.759	57.3	33.3	2.677	1.173			
5H-6, 80-82	46.30	1.745	55.9	32.8	2.587	1.172			40.8
6H-2, 80-82	49.80	1.789	53.6	30.7	2.641	1.240		1.44	
6H-4, 75-77	52.75								96.1
6H-4, 80-82	52.80	1.716	57.0	34.0	2.502	1.132		1.36	
6H-6, 75-78	55.75						^a 1555		
6H-6, 80-82	55.80	1.764	56.1	32.6	2.609	1.190		1.44	
7H-2, 80-82	59.30	1.745	55.6	32.6	2.554	1.176			
7H-4, 80-82	62.30	1.747	55.3	32.4	2.522	1.181			78.1
7H-6, 75-78	65.25						^a 1515		
7H-6, 80-82	65.30	1.727	57.7	34.2	2.620	1.136			
8H-2, 80-82	68.80	1.669	60.3	37.0	2.575	1.051		1.30	
8H-4, 80-82	71.80	1.669	61.1	37.5	2.584	1.042		1.19	135.7
8H-6, 75-78	74.75						^a 1564		
8H-6, 80-82	74.80	1.790	55.6	31.8	2.626	1.221		1.48	
9H-2, 80-82	78.40	1.628	63.9	40.2	2.566	0.973			61.3
9H-4, 80-82	81.40	1.672	62.6	38.4	2.604	1.031			
9H-6, 75-78	84.35						^a 1594		
9H-6, 80-82	84.40	1.754	58.9	34.4	2.654	1.150			
10X-2, 80-82	88.00	1.636	63.4	39.7	2.556	0.986		1.17	
10X-4, 80-82	91.00	1.562	65.8	43.2	2.460	0.887		1.17	39.6
10X-6, 80-82	94.00	1.666	60.8	37.4	2.526	1.043		1.26	
11X-2, 80-82	97.60	1.697	61.4	37.0	2.656	1.068			
11X-4, 78-80	100.58	1.714	59.8	35.8	2.610	1.101			75.7
11X-6, 75-78	103.55						^a 1578		
11X-6, 80-82	103.60	1.762	56.8	33.0	2.584	1.181			
12X-1, 70-72	105.60	1.662	63.7	39.3	2.622	1.009		1.23	
12X-3, 70-72	108.60	1.669	61.9	38.0	2.557	1.034		1.19	
13X-1, 80-82	115.30	1.613	63.5	40.3	2.486	0.963			
13X-3, 80-82	118.30	1.624	62.2	39.2	2.473	0.987			
13X-5, 80-82	121.30	1.625	65.7	41.5	2.530	0.961			
14X-2, 80-82	126.50	1.639	63.2	39.5	2.564	0.991		1.25	
14X-4, 80-82	129.50	1.625	65.2	41.1	2.626	0.957		1.19	
14X-6, 80-82	132.50	1.605	65.5	41.8	2.543	0.934		1.26	
15X-2, 72-74	136.12	1.651	63.3	39.3	2.597	1.002			
15X-4, 73-75	139.13	1.527	66.7	44.8	2.432	0.843			
15X-6, 94-96	142.34	1.621	65.3	41.3	2.607	0.952			
16X-2, 80-82	145.80	1.605	65.2	41.6	2.539	0.937		1.13	
16X-4, 80-82	148.80							1.21	
16X-4, 92-94	148.92	1.677	62.8	38.4	2.648	1.034			
16X-6, 80-82	151.80	1.674	62.9	38.5	2.659	1.029		1.23	
17X-2, 73-75	155.33	1.619	62.7	39.7	2.534	0.977			
17X-4, 69-71	158.29	1.644	64.8	40.4	2.629	0.980			
17X-6, 75-77	161.35	1.631	63.3	39.8	2.546	0.963			
18X-2, 80-82	165.10							1.10	
18X-2, 135-137	165.65	1.617	65.7	41.6	2.607	0.944			
18X-4, 80-82	168.10							1.05	
18X-4, 101-103	168.31	1.586	68.2	44.1	2.488	0.887			
18X-6, 50-52	170.80							1.14	
18X-6, 61-63	170.91	1.624	64.7	40.8	2.667	0.961	^a 1669		
19X-2, 93-95	174.93	1.671	62.7	38.4	2.603	1.029			
19X-4, 98-100	177.98	1.616	64.6	41.0	2.548	0.954			
19X-7, 31-33	181.81	1.660	63.6	39.3	2.644	1.008			
20X-2, 80-82	184.50							1.06	
20X-2, 118-120	184.88	1.629	63.9	40.2	2.533	0.974			
20X-4, 80-82	187.50							1.18	
20X-4, 106-108	187.76	1.673	60.1	36.8	2.484	1.057			
20X-6, 80-82	190.50							1.24	
20X-6, 122-124	190.92	1.658	62.9	38.8	2.564	1.014			
21X-2, 56-58	193.86	1.708	60.6	36.3	2.641	1.087			
21X-4, 72-74	197.02	1.681	63.6	38.8	2.609	1.029			
21X-6, 103-105	200.33	1.670	60.5	37.1	2.517	1.050			

Table 6 (continued).

Core, section, interval (cm)	Depth (mbsf)	Wet-bulk density (g/cm ³)	Porosity (%)	Water content (%)	Gain density (g/cm ³)	Dry-bulk density (g/cm ³)	Velocity (m/s)	Thermal conductivity (W/mK)	Vane shear strength (kPa)
117-728A- (Cont.)									
22X-2, 80-82	203.80	1.690	60.8	36.9	2.587	1.067		1.20	
22X-4, 80-82	206.80	1.630	66.1	41.5	2.662	0.953		1.14	
22X-6, 76-78	209.76	1.691	59.6	36.1	2.527	1.081			
22X-6, 80-82	209.80							1.26	
23X-2, 80-82	213.40	1.621	62.5	39.5	2.455	0.981			
23X-4, 80-82	216.40	1.661	62.0	38.2	2.550	1.026			
23X-6, 80-82	219.40	1.676	61.5	37.6	2.555	1.046			
24X-2, 69-71	222.99	1.659	63.4	39.2	2.616	1.009			
24X-2, 80-82	223.00							1.09	
24X-4, 69-71	225.99	1.696	62.0	37.5	2.633	1.060			
24X-4, 80-82								1.19	
24X-4, 138-140	226.68	1.668	64.1	39.4	2.663	1.012	^a 1557		
24X-6, 79-81	229.09	1.733	61.2	36.2	2.663	1.105		1.04	
25X-2, 85-87	232.85	1.737	60.1	35.5	2.629	1.121			
25X-4, 48-50	235.48	1.733	58.1	34.4	2.628	1.138	^a 1616		
25X-6, 147-149	239.47	1.768	57.1	33.1	2.587	1.183			
26X-2, 21-23	241.81	1.664	61.9	38.1	2.528	1.030	^a 1617		
26X-2, 21-23	241.81						^b 1603		
26X-2, 80-82	242.40							1.28	
26X-4, 80-82	245.40							1.19	
26X-5, 72-74	246.82	1.721	57.6	34.3	2.565	1.131	^a 1579		
26X-5, 72-74	246.82						^b 1638		
26X-6, 80-82	248.80							1.23	
27X-2, 116-118	252.46	1.743	58.8	34.6	2.654	1.140	^a 1574		
27X-4, 17-19	254.47	1.776	55.9	32.3	2.620	1.203	^a 1601		
27X-4, 17-19	254.47						^b 1637		
27X-6, 107-109	258.37	1.737	56.6	33.4	2.546	1.157	^a 1611		
27X-6, 107-109	258.37						^b 1648		
28X-3, 7-9	262.57	1.693	62.0	37.5	2.628	1.058			
28X-6, 137-139	268.37	1.679	63.1	38.5	2.659	1.033			
28X-7, 41-43	268.91	1.677	60.5	36.9	2.450	1.057			
29X-2, 51-53	271.11	1.760	59.7	34.7	2.617	1.149			
29X-5, 67-69	275.77	1.718	59.0	35.2	2.511	1.114	^a 1624		
30X-2, 134-136	281.64	1.741	57.7	34.0	2.604	1.150	^a 1575		
30X-2, 134-136	281.64						^b 1614		
30X-4, 114-116	284.44	1.744	56.5	33.2	2.541	1.166	^a 1557		
30X-4, 114-116	284.44						^b 1615		
31X-2, 126-128	291.26	1.727	59.4	35.2	2.546	1.119	^a 1612		
31X, CC, 30-32	298.23	1.834	55.5	31.0	2.659	1.266	^a 1615		
31X, CC, 30-32	298.23						^b 1623		
32X-4, 77-79	303.37	1.727	59.3	35.2	2.618	1.120	^a 1562		
32X-4, 77-79	303.37						^b 1592		
32X-6, 93-95	306.53	1.649	62.5	38.8	2.545	1.009	^a 1534		
32X-6, 93-95	306.53						^b 1585		
33X-4, 94-96	313.24	1.751	59.6	34.9	2.730	1.140	^a 1567		
33X-4, 94-96	313.24						^b 1601		
33X-5, 96-98	314.76	1.736	57.5	33.9	2.573	1.147	^a 1573		
33X-5, 96-98	314.76						^b 1625		
34X-3, 77-80	321.27	1.591	67.0	43.1	2.564	0.905			
34X, CC, 30-33	327.25	1.778	58.3	33.6	2.646	1.181	^a 1599		
34X, CC, 30-33	327.25						^b 1554		
35X-2, 104-107	329.74	1.608	64.0	40.8	2.501	0.952			
35X-6, 63-66	335.33	1.704	60.8	36.6	2.594	1.081	^a 1573		
36X-3, 32-35	340.12	1.632	65.0	40.8	2.605	0.966			
36X-6, 103-106	345.33	1.654	61.0	37.8	2.506	1.029	^a 1556		

^a Velocity measurement perpendicular to bedding.

^b Velocity measurement parallel to bedding.

associated partly with very organic-rich horizons and perhaps also partly with phosphorite horizons (see "Downhole Measurements" and "Organic Geochemistry" sections, this chapter). Little lithologic change can be found between 88 and 314 mbsf, near the bottom of Site 728. This approximately 88-mbsf base of the highly variable zone corresponds to a trough at 1.97 s on the seismic section, which is traced laterally in Figure 22, based on the fact that the peak at 1.99 s is from a later part of the wavelet that intersects the same horizon. For convenience in subsequent discussions, this seismic horizon is called reflector A and the seismic sequence between this reflector and the seafloor is called sequence SF-A.

An even larger impedance rise at 226 mbsf is caused by a porosity decrease downhole, rather than a mineralogical change

(see "Downhole Measurements" section, this chapter). This horizon may be significant for two reasons. First, it occurs within a short depth interval (about 219-229 mbsf) of very slow sedimentation rates or possibly a hiatus, bracketed by long depth intervals of much higher sedimentation rates (see "Accumulation Rates" section, this chapter). Second, it is the approximate lower boundary of an interval thought to represent deposition in a neritic environment; this interval extends from about 143-163 to 230-250 mbsf (see "Biostratigraphy" section, this chapter). The 226-mbsf impedance change is associated with a seismic trough at 2.14 s, which is correlated away from Site 728 with the aid of the immediately underlying peak. This seismic horizon is referred to as reflector B, and the seismic sequence between reflectors B and A is sequence A-B.

Table 7. Physical properties summary for Hole 728B.

Core, section, interval (cm)	Depth (mbsf)	Wet-bulk density (g/cm ³)	Porosity (%)	Water content (%)	Gain density (g/cm ³)	Dry-bulk density (g/cm ³)	Velocity (m/s)
1H-1, 92-94	0.92	1.706	59.8	35.9	2.682	1.094	
2H-2, 89-90	3.58	1.736	58.4	34.5	2.645	1.138	
3H-2, 90-92	13.10	1.708	61.1	36.6	2.718	1.082	
4H-2, 90-92	22.50	1.729	58.4	34.6	2.634	1.131	
5H-2, 90-92	32.00	1.793	56.6	32.3	2.707	1.213	
6H-2, 90-92	41.50	1.727	58.6	34.8	2.603	1.127	
7H-2, 90-92	51.00	1.688	58.1	35.3	2.399	1.093	
8H-2, 90-92	60.50	1.731	57.5	34.0	2.527	1.142	
9H-2, 90-92	70.10	1.689	59.9	36.3	2.619	1.076	
10X-2, 91-93	79.71	1.650	62.4	38.7	2.519	1.011	
11X-2, 90-92	89.30	1.608	66.2	42.2	2.404	0.930	
12X-2, 90-92	98.90	1.624	62.2	39.3	2.570	0.986	
13X-2, 90-92	108.50	1.618	65.3	41.4	2.657	0.949	
14X-2, 90-92	118.20	1.600	64.3	41.1	2.521	0.942	
16X-2, 94-96	137.54	1.620	64.1	40.5	2.516	0.963	
17X-6, 90-92	153.10	1.648	67.3	41.8	2.604	0.959	
18X-2, 99-101	156.89	1.623	63.9	40.3	2.520	0.969	
19X-4, 71-73	169.31	1.690	62.4	37.8	2.624	1.051	^a 1646
20X-6, 95-97	182.25	1.627	61.8	38.9	2.467	0.994	
21X-3, 100-102	187.50	1.651	59.8	37.1	2.476	1.038	
22X-2, 78-80	195.48	1.638	61.8	38.6	2.512	1.005	
23X-3, 70-72	206.50	1.639	62.6	39.1	2.543	0.998	
24X-3, 56-58	216.06	1.673	62.4	38.2	2.569	1.033	
25X-5, 70-72	228.90	1.734	59.1	34.9	2.623	1.128	
26X, CC, 40-42	238.53	1.663	61.1	37.6	2.504	1.037	
27X-6, 131-133	250.31	1.687	58.1	35.3	2.475	1.092	
28X-4, 115-117	256.85	1.716	58.9	35.2	2.653	1.112	^a 1594
28X-4, 115-117	256.85						^b 1593
29X-4, 144-146	266.74	1.801	53.3	30.3	2.632	1.254	^a 1634
29X-4, 144-146	266.74						^b 1700
30X-4, 77-79	275.77	1.624	60.8	38.3	2.480	1.001	^a 1598
30X-4, 77-79	275.77						^b 1638
31X-4, 118-120	285.88	1.717	59.5	35.5	2.651	1.107	^a 1581
31X-4, 118-120	285.88						^b 1627
32X-4, 124-126	295.54	1.788	56.1	32.3	2.667	1.208	^a 1567
32X-4, 124-126	295.54						^b 1619
33X-4, 116-118	305.16	1.687	58.6	35.6	2.527	1.086	
34X-5, 16-18	315.36	1.685	61.5	37.4	2.583	1.055	
35X-4, 106-108	324.36	1.796	59.5	34.0	2.739	1.186	^a 1557
35X-4, 106-108	324.36						^b 1622
36X-4, 109-111	334.09	1.695	59.6	36.0	2.586	1.084	^a 1599
36X-4, 109-111	334.09						^b 1603
37X-5, 80-82	344.90	1.689	61.8	37.5	2.567	1.056	^a 1549
37X-5, 80-82	344.90						^b 1656

^a Velocity measurement perpendicular to bedding.

^b Velocity measurement parallel to bedding.

Two beds having very low velocities at 314-319 and 322-327 mbsf (Fig. 22), thought to be highly siliceous (see "Downhole Measurements" section, this chapter), cause the large-amplitude reflectors at the bottom of the synthetic seismogram (Fig. 23). A trough at 2.25 s lies between these two beds (320 mbsf) and is easily correlated across the section with the aid of bracketing high-amplitude peaks. This seismic horizon is referred to as reflector C; sequence B-C immediately overlies it.

Seismic Interpretation

Depositional patterns in the distal slope basin penetrated by Site 728 occur in two seismically distinctive styles, with the boundary between the two styles occurring near reflector C.

Below seismic reflector C, seismic sequences are of relatively uniform thickness throughout the portion of Figure 22 in which they can be identified. No significant onlapping is evident. The sequences are bounded on the southeast by a major normal fault that has dropped the slope basin with respect to the adjacent basement high. Pronounced drag folding is associated with this normal faulting. This folding is responsible for most of the synclinal structure of the sequence between reflector C and a deeper reflector referred to as reflector D; differential sedimentation rates within sequences overlying reflector C also contrib-

ute to the synclinal structure. In the section shown in Figure 22, all of sequence C-D southeast of the fault has been eroded away, and channeling in the fault zone has eroded a small part of sequence C-D northwest of the fault. Horizons deeper than reflector C extend at least as far to the northwest as the buried channel near the left margin of Figure 22. Most reflectors cannot be traced with confidence farther to the northwest because of at least two normal faults, but bedding attitudes clearly continue upslope without significant change.

No convincing seismic evidence can be seen of any influence of faulting on the deposition of units older than seismic reflector C. A small normal fault 1.5 km northwest of the main normal fault appears to end at reflector D, but the seismic reflector pattern here is barely coherent enough to identify the fault. This fault may represent a deep accommodation of strain buildup associated with post-C movement of the major fault, rather than a faulting event that ended at reflector D time. Within the uncertainties implicit in seismic interpretation of a single line, we hypothesize that deposition of sequences older than reflector C is a relatively uniform sedimentation upon an originally flat or gently sloping seafloor (e.g., continental shelf). We have seen no evidence on the Oman margin of pelagic drape that resulted in thicknesses as uniform as those below reflector C.

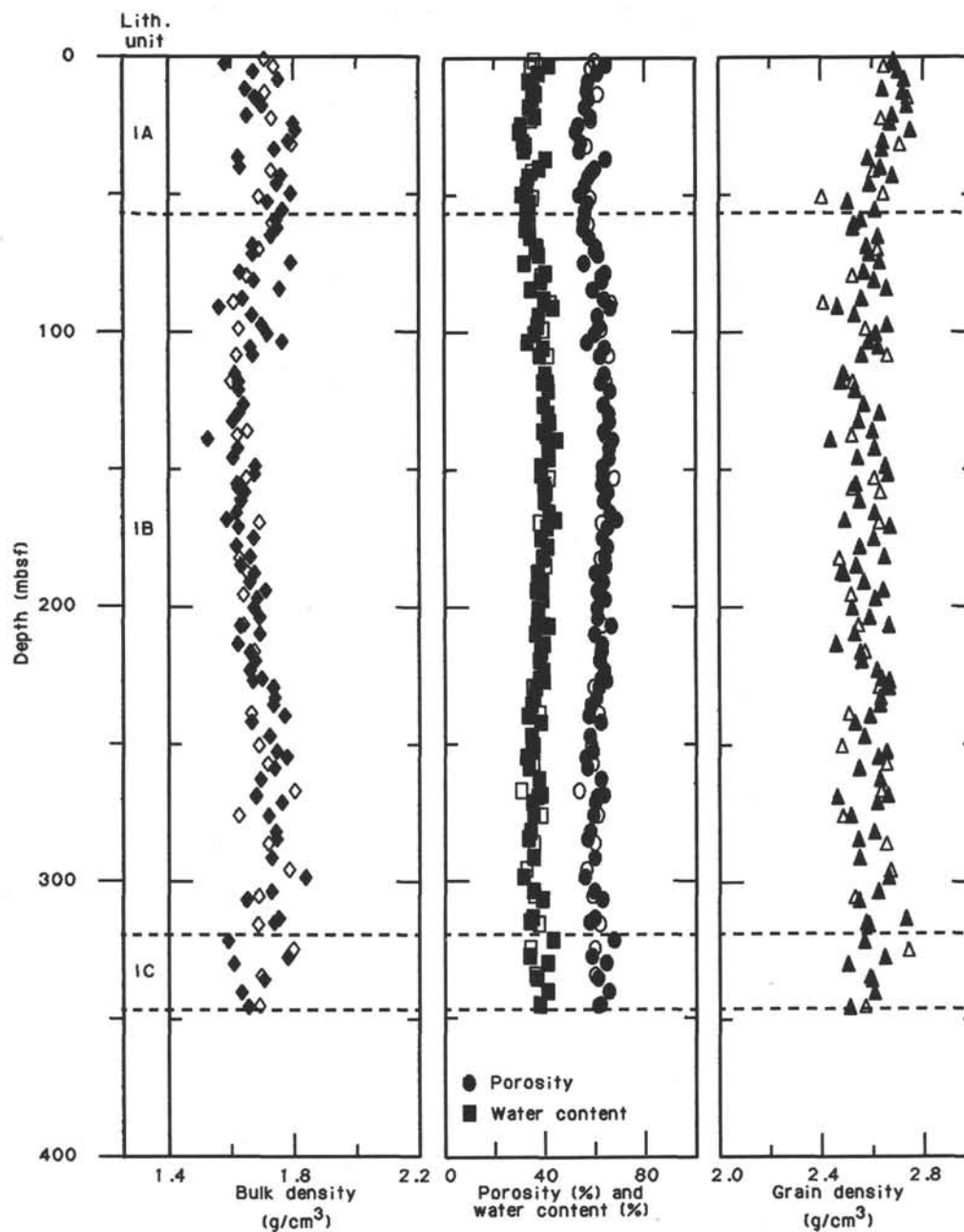


Figure 17. Index properties (wet-bulk density, porosity, water content, and grain density) measured on discrete samples from Holes 728A (solid symbols) and 728B (open symbols).

Above reflector C, seismic sequences exhibit a pronounced thickening in the central portion of the basin, with onlapping obvious toward the northwest topographic high and less certain toward the southeast. This thickening is proportionally greatest for sequence B-C, and least for the youngest sequence SF-A. Channel and levee systems were active during deposition of the three sequences SF-A, A-B, and B-C. The buried channel for sequences B-C and A-B is indicated by dashed lines near the left margin of Figure 22. The modern channel is evident on the seafloor in Figure 22. These two channels probably are primarily erosional. The deeper channel appears to cut down into sequence C-D, and farther to the northeast the erosional relief on the modern channel is more than 180 m. Existence of both modern and buried levees indicates that some spillover of portions of the turbidites occurs. However, no turbidites were iden-

tified at Site 728 (see "Lithostratigraphy" and "Downhole Measurements" sections, this chapter), presumably indicating that the turbidite component at Site 728 is minor in comparison to the pelagic component.

Sequences SF-A, A-B, and B-C are bounded on the southeast by seismic reflector C or a horizon very near it. Onlapping onto this reflector is evident only in the lower portion of sequence SF-A and uppermost portion of A-B. The strong seafloor wavelet pattern precludes determination of whether the upper part of sequence SF-A onlaps reflector C. Continuity of seismic reflectors within most of sequence A-B and all of sequence B-C suddenly becomes poor 1.2 km southeast of Site 728 (Fig. 22). The somewhat chaotic reflector pattern within this region (bounded by a dashed line and reflector C in Fig. 22) is suggestive of a slump. However, the lateral movement of this

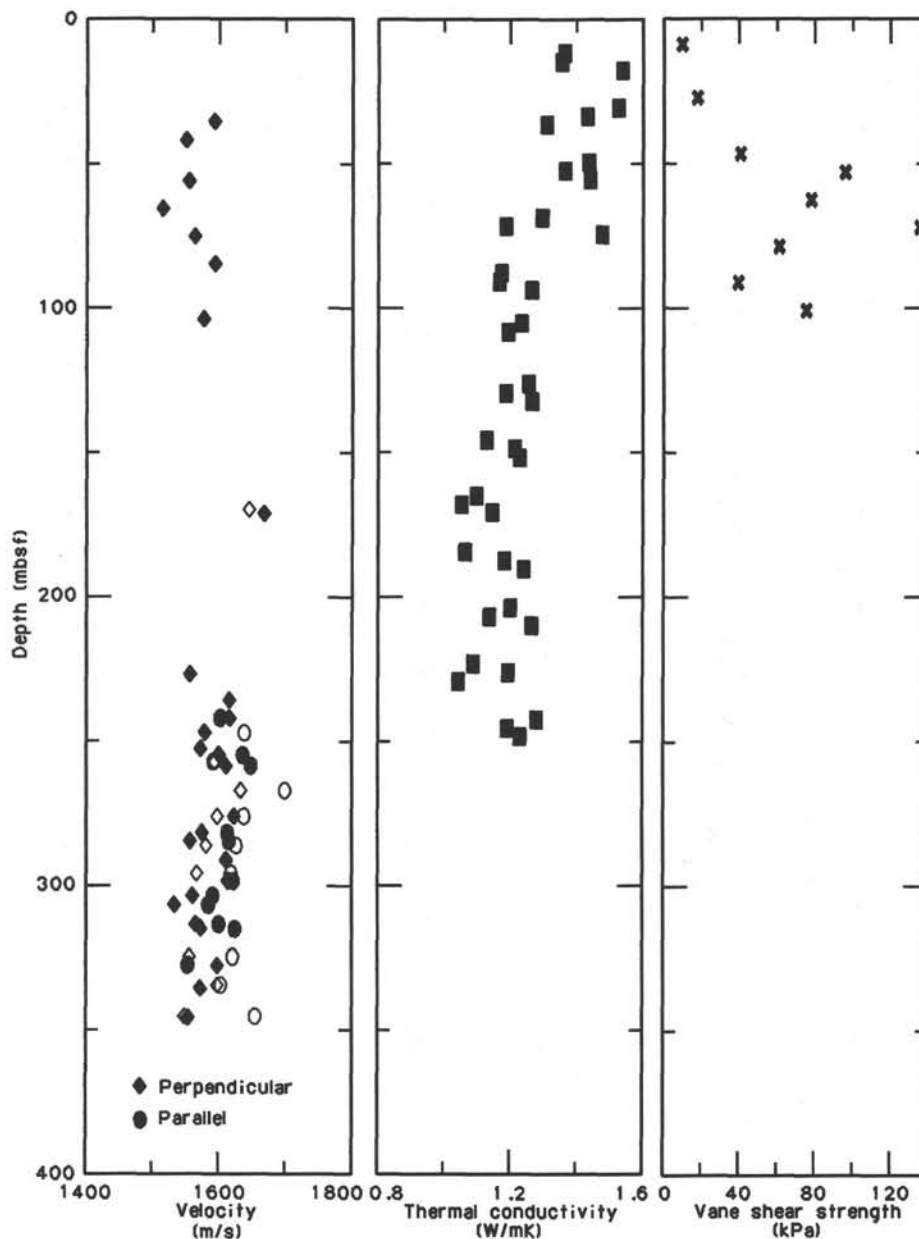


Figure 18. Compressional-wave velocity, thermal conductivity, and vane shear strength measured on discrete samples from Holes 728A (solid symbols) and 728B (open symbols). The designations perpendicular and parallel refer to the orientation of propagation of the compressional wave relative to bedding.

possibly slumped region must have been minor in the plane of Figure 22, because its northwest boundary is too close to vertical for the slump to have preceded deposition of sequences A-B and B-C. This small slump probably has an origin similar to that observed at Site 721 (see "Seismic Stratigraphy" section, Site 721 chapter): gravitational instability of pelagic sediments deposited on an initial slope, with a basal slump plane composed of weak diatomaceous sediments (in this case, the siliceous beds found at 314–319 and 322–327 mbsf at Site 728).

The morphology of sequences SF-A, A-B, and B-C suggests that the depositional environment is somewhat similar to that occurring today in this slope basin and inferred throughout the penetrated section at Site 723 (see "Seismic Stratigraphy" section, Site 723 chapter). Pelagic deposition occurred along a sea-floor sloping gently to the southeast, with highest accumulation

rates in the most rapidly subsiding central portion of the slope basin. However, unlike Site 723, draping of the sequences over the seaward high (in this case, sequence C-D) is almost completely absent. Therefore, seismic horizon C must have been a topographic high that precluded further downslope southeastward motion of sediments.

This topographic high created by tilting of C-D and deeper sequences was pronounced at the beginning of deposition of sequence B-C, as indicated by sudden thinning of the reflectors immediately overlying reflector C at Site 728. A small hiatus there above reflector C is thus possible, but none was detected. The seaward thinning of sequence A-B is substantially less than that of B-C, and the thinning of sequence SF-A is even smaller. Thus, the topographic relief established at reflector C time (about 7.7 Ma; see "Accumulation Rates" section, this chapter) must

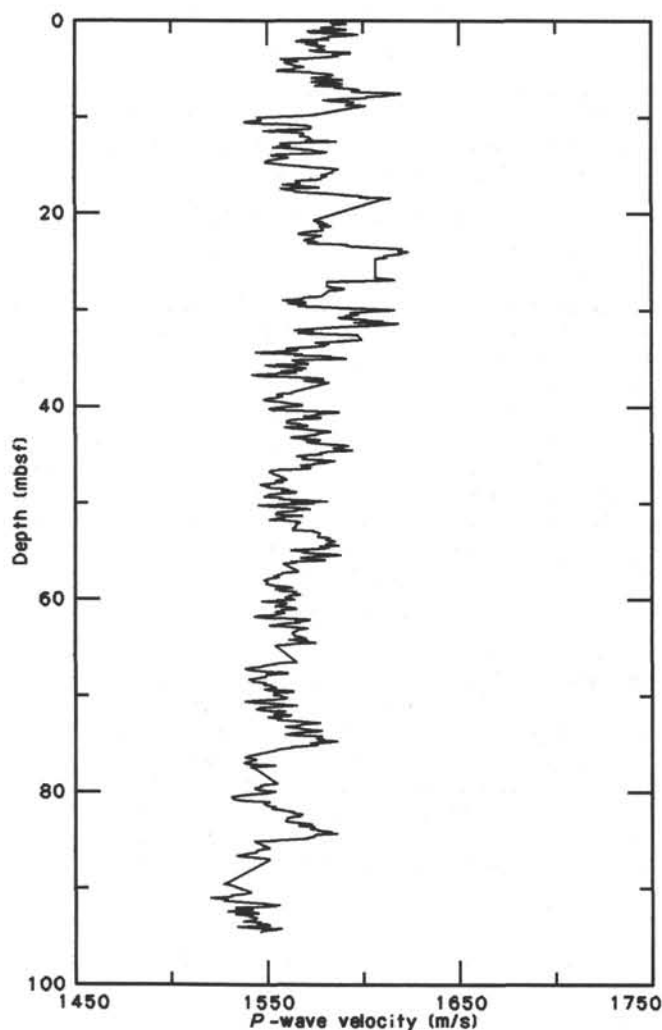


Figure 19. Compressional-wave velocity as measured by the *P*-wave logger in Cores 117-728A-1H through 117-728A-10X. The profile is based on 10-cm-block averages of the data.

have gradually diminished since then. Finally, within the last 0.5 Ma, sediments have overtopped sequence C-D and spilled into the adjacent channel (dashed lines in Fig. 22). Channel building undoubtedly preceded this spillover, probably fed partially from the topographically higher southwest and from the adjacent basement high. Channel cutting preferentially developed on the updip extension of the major normal fault that bounds the basement high.

In summary, our preferred seismic interpretation of the sequences below and penetrated by Site 728 involves a substantial change in depositional environment, which occurred approximately at the base of Site 728. This distal slope basin may have been part of a rather uniform shelf or slope environment until reflector C time (about 7.7 Ma). At that time, the basin was initiated through normal faulting on the northwest flank of the present basement high, and this basin has been filling almost to the present day.

This seismic interpretation is in conflict with one important observation from Site 728: benthic foraminifers from the interval 143–163 to 230–250 mbsf indicate deposition in the neritic zone, shallower than 150 m below sea level (see “Biostratigraphy” section, this chapter). This interval corresponds to the

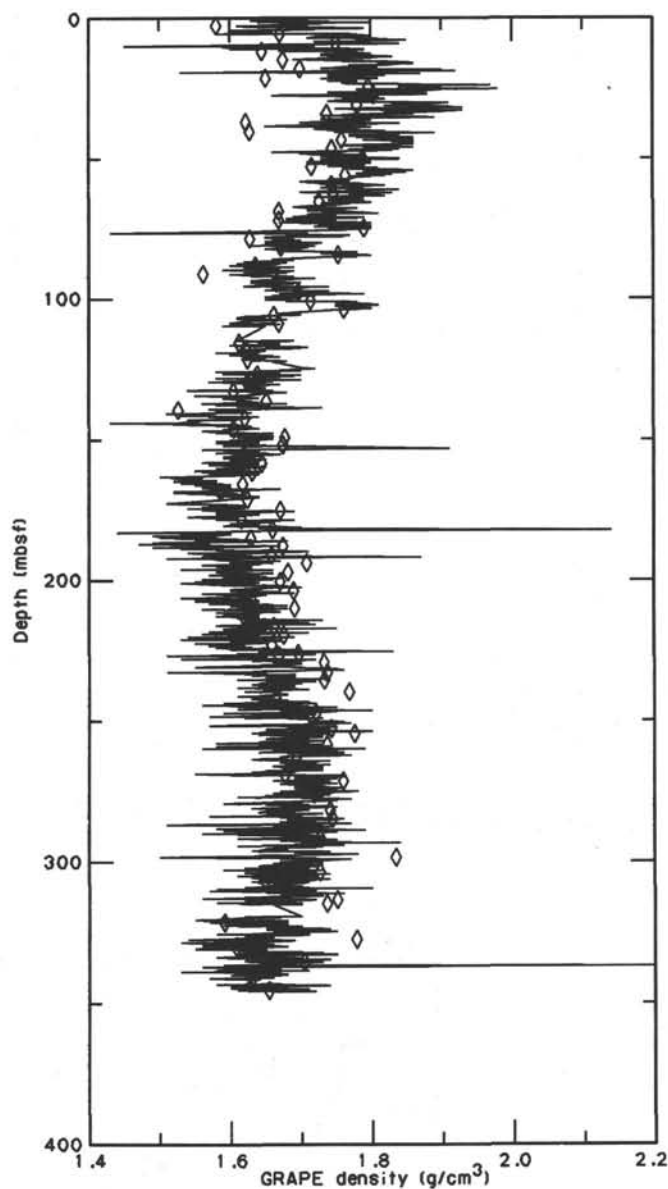


Figure 20. GRAPE wet-bulk density for Hole 728A. The profile is based on 10-cm-block averages of the data. Triangle = discrete sample measurement.

lower half of sequence A-B, a sequence that shows clear updip onlapping toward a channel that was active during the time that this sequence was deposited. Based on the seismic stratigraphic pattern, a depth of less than 150 m for Site 728 would probably have made the channel subaerial, and would certainly have made the two highs flanking the slope basin subaerial, as faulting preceded deposition of sequence A-B. However, both sedimentological and log evidence indicates a remarkably uniform sediment composition between 85 and 320 mbsf (see “Lithostratigraphy” and “Downhole Measurements” sections, this chapter), a period that encompasses benthic foraminiferal evidence of a transition from upper bathyal to neritic to upper middle bathyal zones (see “Biostratigraphy” section, this chapter). Post-cruise studies will investigate both alternative seismic interpretations and the possibility that the foraminifers were reworked and deposited at the site by channel spillover.

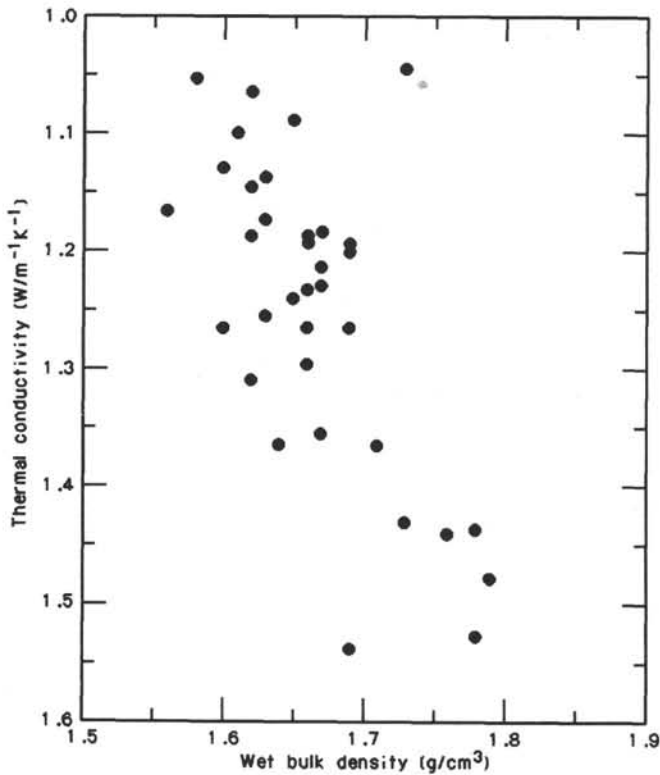


Figure 21. Cross plot of thermal conductivity and wet-bulk density measured on discrete samples from Hole 728A.

INORGANIC CHEMISTRY

Introduction

Twenty-one interstitial water samples were collected at Site 728, 17 by squeezing (Holes 728A and 728B), and the remaining four with the Barnes *in-situ* sampler (Hole 728B only). All data are listed in Table 8 and presented in Figure 24.

Salinity, Chloride, and pH

The distributions of several of the pore-water constituents measured at this site, including salinity, are similar to those seen elsewhere on the Oman margin. The decrease in salinity between ~25 and ~100 mbsf (Fig. 24) is clearly a result of the depletion of sulfate over this interval.

Little variation is seen in the chloride profile. The chloride data give no indication that fresher water is present below the cored section at this site. The pH profile shows a maximum in the upper 100 m. However, a significant difference between pH values measured in Holes 728A and 728B occurs at approximately the same depths (Fig. 24 and Table 8). This variation may be an analytical artifact, rather than being real, and it suggests that the pH data should be viewed with caution.

Alkalinity and Sulfate

Alkalinity increases from the top of the cored section to a maximum of ~15 mmol/L near 100 mbsf, before decreasing linearly to about 5 mmol/L at ~350 mbsf (Fig. 24). The steep positive slope between ~10 and ~100 mbsf reflects sulfate reduction in this zone, but as has often been observed on the margin, the maximum concentration is about 30 to 35 mmol/L, less than would be predicted from the sulfate profile. This deficiency can be explained by the precipitation of authigenic carbonates, possibly both calcite and dolomite, as discussed next.

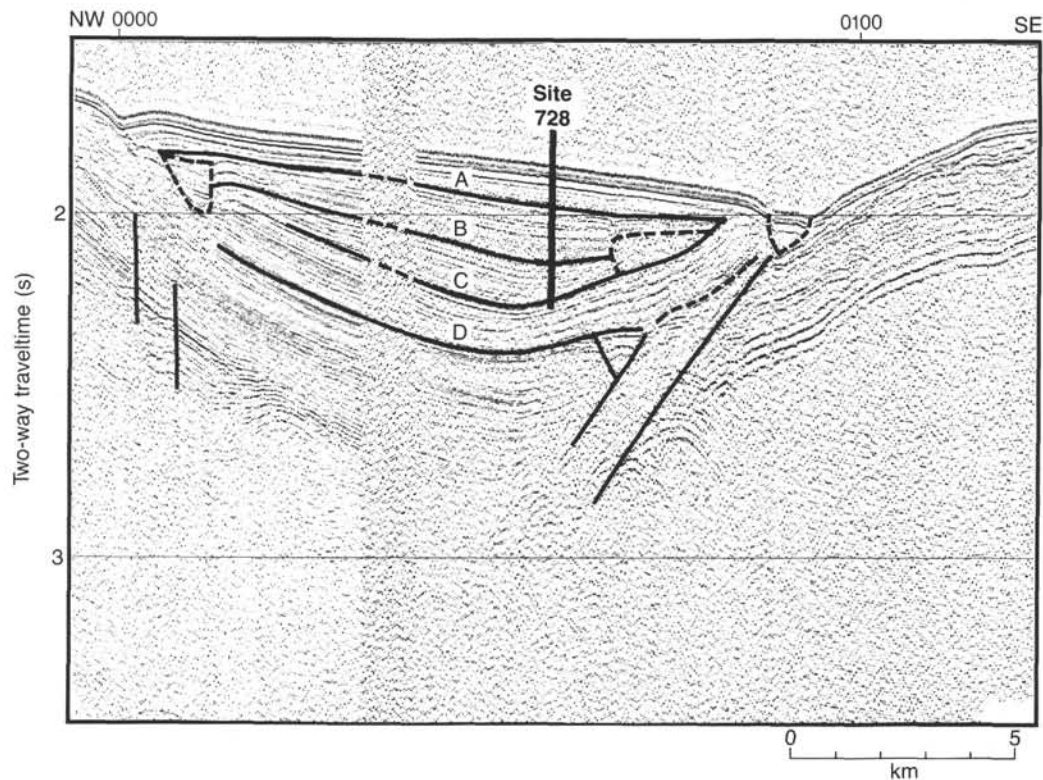


Figure 22. Seismic line 20 of *Robert Conrad* site survey cruise RC2704 across Site 728. Highlights indicate inferred locations of significant seismic reflectors (light lines, dashed where uncertain), faults (heavy lines), and slump and channels (short, dashed lines).

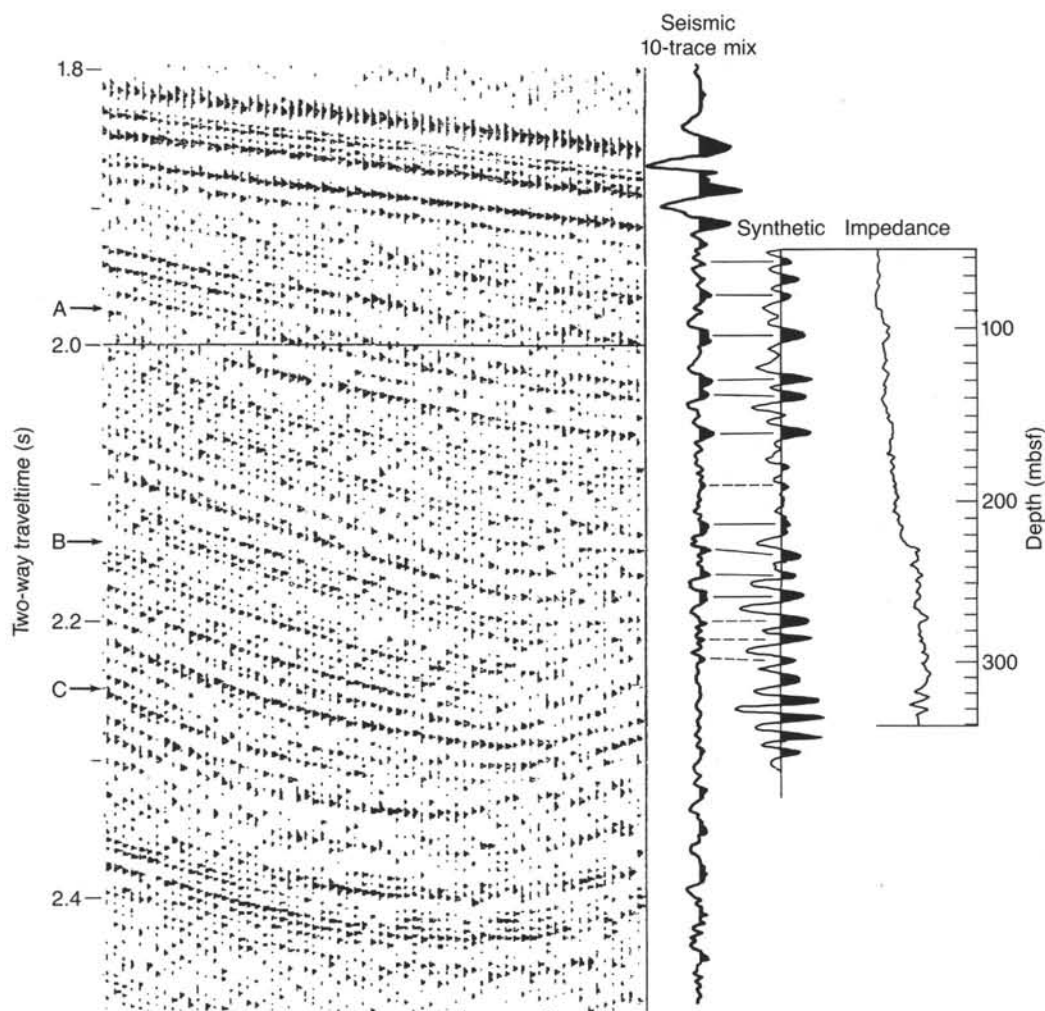


Figure 23. Comparison of a synthetic seismogram for Site 728 with a composite seismic trace (10-trace mix) at the site and with the seismic line of Figure 22. All three are plotted as a function of two-way time; a corresponding depth scale for Site 728 is shown at right.

Sulfate reduction is pronounced between ~ 25 and ~ 80 mbsf. The concentration decreases almost linearly in this interval, with a gradient of ~ -0.5 mmol/L/m; dissolved sulfate is absent from interstitial water below about 80 mbsf. There is no indication from the data that a sulfate source exists at depth, as was observed at Sites 723 and 724. This observation is consistent with the chloride distribution.

Calcium and Magnesium

Both calcium and magnesium concentrations decrease over the top 80 m at this site (Fig. 24). Below this zone, calcium increases steadily, while the magnesium concentration continues to decrease. The curvature in the profiles strongly implies that the major zone of precipitation of authigenic carbonates lies between about 70 and 100 mbsf. This interval is marked by a pronounced increase in the organic carbon concentration (see "Organic Geochemistry" section, this chapter), a maximum in the dissolved organic carbon profile (see below), a high uranium content (see "Downhole Measurements" section, this chapter), and an alkalinity maximum. Joint consideration of all these data suggests that the organic carbon-rich zone is supporting very active, bacterially mediated diagenesis. The reaction zone is estimated as 20 to 30 m thick.

Ammonia, Phosphate, Silica, and Dissolved Organic Carbon

The ammonia concentration increases with depth to ~ 200 mbsf (Fig. 24); below this zone, the concentration does not vary. Maximum curvature in the profile is observed between ~ 50 and ~ 150 mbsf, which is consistent with the extensive suite of data (described above) that indicates a maximum in diagenetic reactivity centered on the organic carbon maximum.

Dissolved phosphate concentrations are low at Site 728, as is the case at all other margin sites. Apatite precipitation is believed to be responsible for the lack of phosphate in the pore waters.

The dissolved silica concentration increases with depth to a maximum of ~ 1200 $\mu\text{mol/L}$ at about 200 mbsf. This profile is similar to those observed previously on both the Owen Ridge (Sites 720 and 721) and the margin, and reflects dissolution of opal. There are two subtle maxima at ~ 100 and ~ 225 mbsf in the profile shown in Figure 24, which suggests that the sedimentary opal concentration is higher at these depths. This interpretation agrees with biostratigraphic observations (see "Biostratigraphy" section, this chapter).

The relative concentration of dissolved organic carbon (Fig. 25) shows a distinct broad maximum between ~ 60 and ~ 130

Table 8. Summary of interstitial water geochemical data for Site 728.

Core, section, interval (cm)	Depth (mbsf)	Vol. (mL)	pH	Alk. (mmol/L)	Sal. (g/kg)	Mg (mmol/L)	Ca (mmol/L)	Cl (mmol/L)	SO ₄ (mmol/L)	PO ₄ (μmol/L)	NH ₄ (mmol/L)	SiO ₂ (μmol/L)	Mg/Ca	DOC (a.u.)
728A-1H-4, 145-150	5.95	33	7.50	3.83	33.0	52.36	10.27	558	25.4	6.1	0.22	293	5.10	0.141
728B-2H-4, 145-150	7.15	50	7.30	3.73	35.5	52.32	10.23	559	24.0	6.2	0.17	305	5.11	0.113
728A-3H-4, 145-150	25.05	38	7.90	4.13	35.4	52.14	9.54	565	24.4	6.2	0.40	394	5.47	0.294
728B-4H-4, 145-150	26.05	50	7.70	4.78	35.8	56.05	9.84	556	26.1	5.3	—	—	5.70	0.260
728B-7I-1, 0-1	48.60	10	8.20	9.19	34.7	48.05	9.02	570	16.3	4.0	2.52	775	5.33	2.059
728A-6H-4, 145-150	53.45	45	8.10	9.35	35.0	46.45	8.15	568	12.7	10.6	1.89	929	5.70	0.987
728B-7H-4, 145-150	54.55	45	7.70	10.15	35.5	43.54	8.20	569	12.7	7.2	1.51	995	5.31	0.898
728A-9H-4, 145-150	82.05	35	8.00	13.63	32.6	33.91	6.65	565	0.0	8.2	3.43	1046	5.10	1.328
728B-10X-4, 145-150	83.25	50	7.20	17.49	33.2	33.30	6.60	565	0.0	11.4	1.19	1038	5.05	1.535
728B-13I-1, 0-1	106.10	10	7.40	18.19	32.8	31.90	8.95	565	0.5	10.2	3.36	1016	3.56	1.225
728A-12X-2, 145-150	107.85	60	8.00	15.56	32.5	32.81	8.04	565	0.0	6.4	4.14	1127	4.08	1.360
728A-15X-4, 145-150	139.85	48	7.70	13.30	32.2	28.10	8.06	565	0.0	12.0	4.89	1098	3.49	1.172
728B-18I-1, 0-1	154.40	10	7.70	16.11	32.4	28.53	9.62	560	0.0	19.7	4.54	1081	2.97	1.168
728A-18X-4, 145-150	168.75	42	7.60	12.57	32.3	28.34	8.54	564	1.3	10.9	5.21	1053	3.32	0.980
728A-21X-4, 145-150	197.75	30	7.20	12.02	32.2	25.14	9.59	564	0.0	12.6	5.75	1225	3.12	0.891
728A-24X-3, 145-150	225.25	35	7.20	10.58	32.1	24.35	9.99	563	0.0	9.8	5.84	1233	2.44	0.795
728B-26I-1, 0-1	231.80	10	7.60	11.91	32.4	23.83	10.98	560	0.0	8.4	6.01	1143	2.17	0.735
728A-27X-4, 145-150	255.75	30	7.20	8.99	32.0	23.09	10.37	563	0.0	12.7	5.90	1235	2.23	0.685
728A-30X-4, 145-150	284.75	30	7.30	7.75	32.0	22.35	11.35	562	0.0	9.9	5.75	1153	1.97	0.557
728A-33X-4, 145-150	313.75	33	7.40	6.18	32.2	22.86	11.40	561	0.3	8.8	5.71	1129	2.01	0.470
728A-36X-4, 145-150	342.75	45	7.40	5.57	32.0	22.35	12.09	560	0.0	9.3	5.69	1227	1.84	0.396

Note: DOC = dissolved organic carbon; a.u. = absorption units.

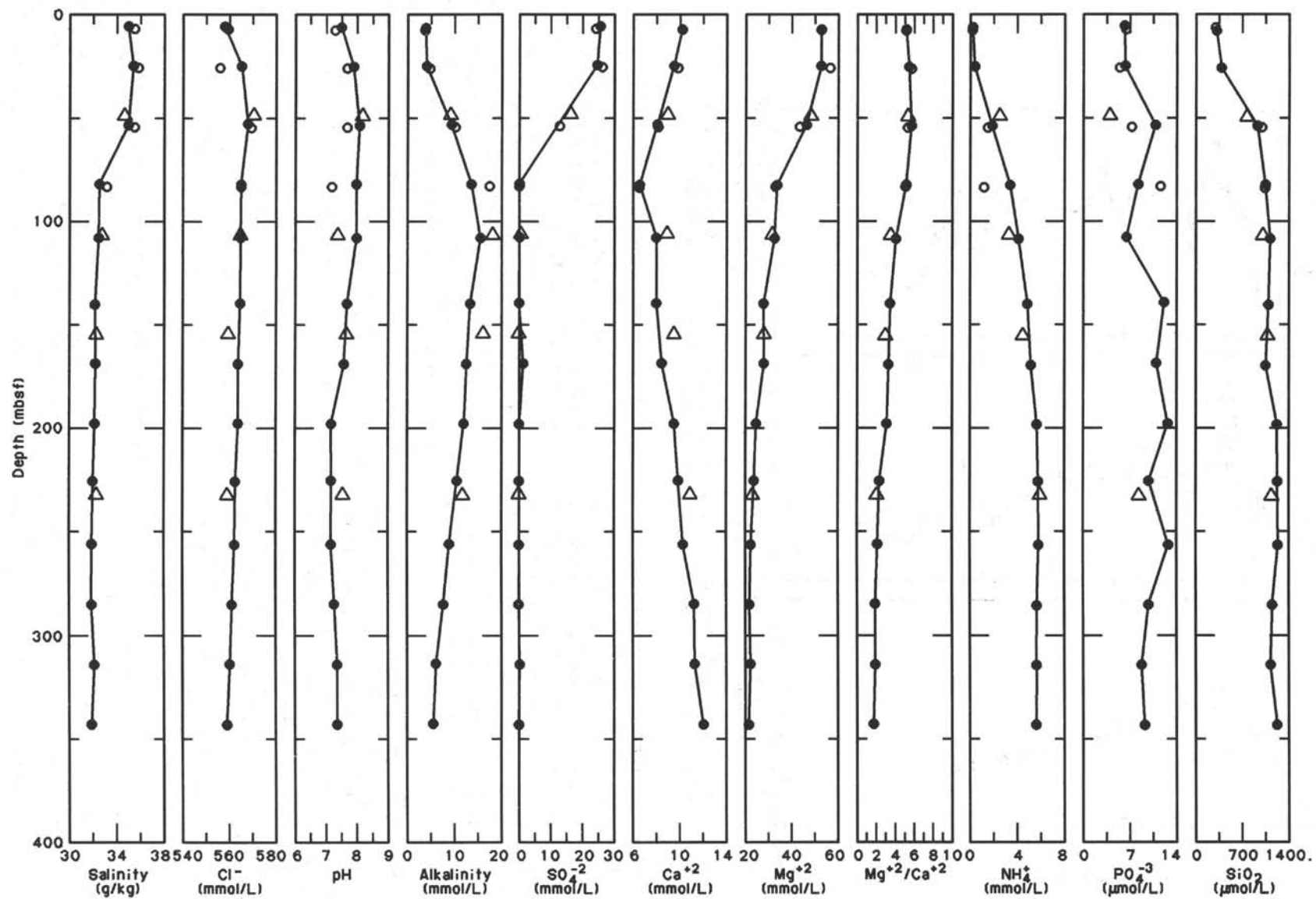


Figure 24. Salinity, chloride, pH profiles, alkalinity, sulfate, calcium, magnesium, Mg/Ca ratio, ammonia, phosphate, and silica profiles for Site 728. Data from Hole 728A are joined by the solid line; open circles represent samples from Hole 728B and triangles represent the *in-situ* samples (all from Hole 728B).

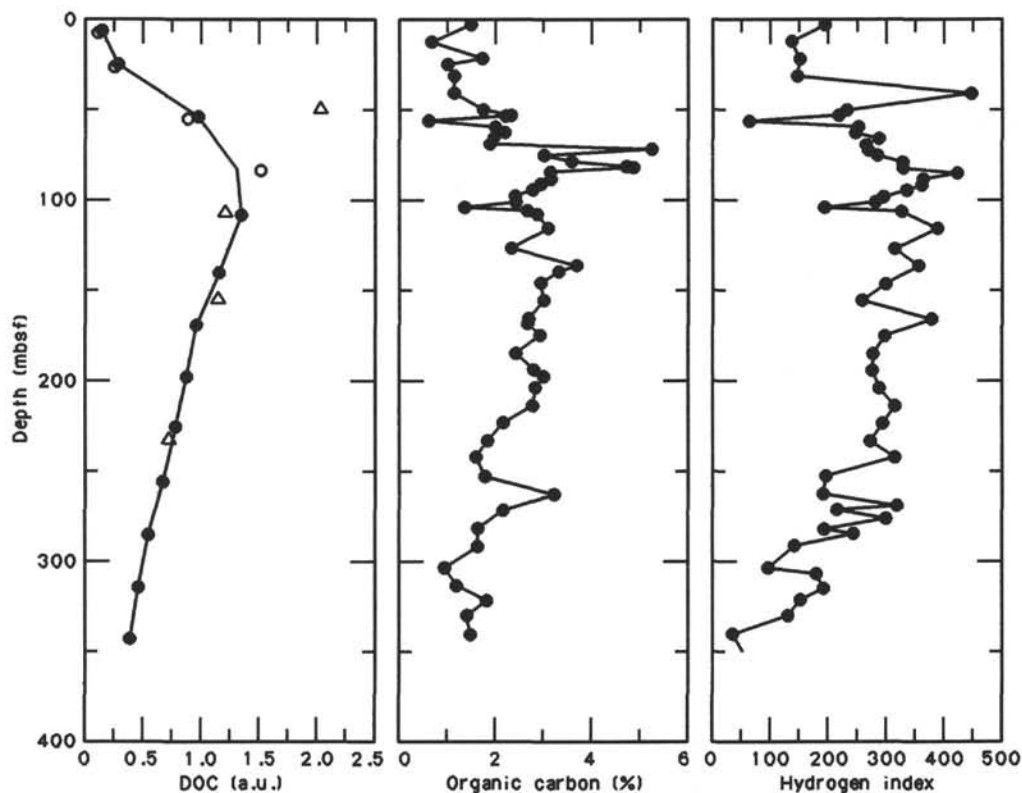


Figure 25. A. Dissolved organic carbon distribution at Site 728 symbols as in Figure 24. B. Downhole plot of organic carbon. C. The ratio of hydrogen-index values from pyrolysis for samples of Hole 728A.

mbsf, which correlates well with the sedimentary organic carbon enrichment in the same depth interval. We presume that this correlation reflects the partial solution of degraded organic matter produced during diagenesis in the organic carbon-rich zone. Because the diffusion coefficient is so low for the high molecular weight humic acids that probably make up most of the dissolved organic carbon (DOC), the DOC profile is less damped by diffusion than the profiles of most other pore-water constituents. For this reason, the DOC profile is a reasonably faithful proxy for the general distribution of reactive organic matter at this site.

In-Situ Pore-Water Samples

As can be seen in Figure 24, the analytical results for the four *in-situ* pore-water samples agree reasonably well with measurements made on the samples extracted by squeezing. Some discrepancy exists between the respective sets of calcium and alkalinity data, with the *in-situ* samples having slightly higher concentrations of both. This may reflect precipitation of calcite induced by decreasing pressure during core recovery. There is no indication that magnesium is affected in a similar way. The high relative DOC concentration measured in the *in-situ* sample collected from Core 117-728B-7I (Table 8) probably signifies contamination by an unknown organic compound.

ORGANIC GEOCHEMISTRY

Character and Abundance of Organic Matter

Fifty-five samples of physical properties and headspace residues from Hole 728A were analyzed for organic carbon and carbonate content (Table 2), and most were analyzed further by Rock-Eval pyrolysis (Table 9).

Organic carbon values are fairly constant in the upper 70 m and average 1.6%, after which a sharp increase occurs (Fig. 25)

to an average value of approximately 2.5% (70–225 mbsf interval). The organic carbon values slowly level out with depth and decline at about 225 mbsf to values similar to those measured in the top of the section. Note the sharp organic carbon spikes between 70 and 82 mbsf (Fig. 25), which appear to correlate with uranium, as measured with the geochemical logging tool (see “Downhole Measurements” section, this chapter).

The hydrogen and oxygen indexes, plotted in a “van Krevelen”-type diagram (Fig. 26), exhibit the same scatter as was observed for samples from other sites. When compared to samples from the Owen Ridge (Site 722; dots in Fig. 26), the samples from Site 728 (open circles in Fig. 26) seem to be characterized by slightly lower oxygen indexes. These appear to be more comparable to values obtained from coeval sediments of Site 727 (triangles in Fig. 26), which were deposited in the center of the oxygen-minimum zone at a water depth of approximately 910 m.

Hydrocarbon Gases

Because of the lack of crimp caps, only seven headspace samples were collected from Hole 728A. In addition, several samples from the Hole 728B were collected and sealed in tin cans for shore-based gas analysis. Results of the headspace gas analyses from Hole 728A are given in Table 10. In these data, we observed a trend of increasing gas concentrations with depth in both biogenic methane and thermogenic ethane and propane. The sharp decline in gas concentrations between the headspace samples of Cores 117-728A-18X and 117-728A-21X is not corroborated by the gas analysis of vacutainer samples (Table 11). The results from Sample 117-728A-21X-5, 0–1 cm (Table 10), seem to be unreliable for lack of correlation with the vacutainer samples, possibly because of a sample-handling artifact. Gas analyses of vacutainer samples were severely hampered by gas pockets often filling with water and because moisture entered the vacutainer under high pressure. The results of those analyses,

Table 9. Results of Rock-Eval pyrolysis of samples from Hole 728A.

Core, section, interval (cm)	Depth (mbsf)	T _{max} (°C)	S ₁	S ₂	S ₃	PI	S ₂ /S ₃	PC	TOC	HI	OI
117-728A-											
1H-2, 100-102	2.50	420	0.48	2.99	2.05	0.14	1.45	0.28	1.53	195	133
2H-2, 80-82	11.90	412	0.21	0.96	1.16	0.18	0.82	0.09	0.69	139	168
3H-2, 80-82	21.40	416	0.39	2.79	1.52	0.12	1.83	0.26	1.78	156	85
4H-2, 80-82	30.80	423	0.23	1.79	1.58	0.11	1.13	0.16	1.19	150	132
5H-2, 80-82	40.30	417	0.55	5.30	2.52	0.09	2.10	0.48	1.18	449	213
6H-2, 80-82	49.80	415	0.50	4.27	1.72	0.11	2.48	0.39	1.81	235	95
6H-4, 80-82	52.80	418	0.47	5.26	2.58	0.08	2.03	0.47	2.37	221	108
6H-6, 80-82	55.80	415	0.09	0.46	1.25	0.17	0.36	0.04	0.68	67	183
7H-2, 80-82	59.30	420	0.43	5.23	2.50	0.08	2.09	0.47	2.05	255	121
7H-4, 80-82	62.30	413	0.75	5.65	2.35	0.12	2.40	0.53	2.26	250	103
7H-6, 80-82	65.30	413	0.61	5.90	2.04	0.09	2.89	0.54	2.03	290	100
8H-2, 80-82	68.80	419	0.60	5.24	2.50	0.10	2.09	0.48	1.95	268	128
8H-4, 80-82	71.80	417	1.77	14.56	3.60	0.11	4.04	1.36	5.34	272	67
8H-6, 80-82	74.80	416	1.02	8.90	2.91	0.10	3.05	0.82	3.08	288	94
9H-2, 80-82	78.40	414	1.68	12.15	3.64	0.12	3.33	1.15	3.68	330	98
9H-4, 80-82	81.40	414	2.04	15.94	3.87	0.11	4.11	1.49	4.18	331	80
9H-6, 80-82	84.40	416	1.86	13.76	3.41	0.12	4.03	1.30	3.23	426	105
10X-2, 80-82	88.00	413	1.50	11.94	2.69	0.11	4.43	1.12	3.25	367	82
10X-4, 80-82	91.00	416	1.30	11.05	3.85	0.11	2.87	1.02	3.03	364	127
10X-6, 80-82	94.00	413	1.22	9.66	3.56	0.11	2.71	0.90	2.85	338	124
11X-2, 80-82	97.60	412	0.83	7.40	2.75	0.10	2.69	0.68	2.48	298	110
11X-4, 78-80	100.58	416	1.05	7.08	1.84	0.13	3.84	0.67	2.49	284	73
11X-6, 80-82	103.60	418	0.41	2.81	1.77	0.13	1.58	0.26	1.43	196	123
12X-1, 70-72	105.60	412	0.92	9.05	2.66	0.09	3.40	0.83	2.75	329	96
13X-1, 80-82	115.30	412	1.68	12.62	2.62	0.12	4.81	1.19	3.21	393	81
14X-2, 80-82	126.50	414	0.77	6.88	3.50	0.10	1.96	0.63	2.41	267	145
15X-2, 72-74	136.20	415	1.41	12.11	3.66	0.10	3.30	1.12	3.77	321	97
16X-2, 80-82	145.80	408	1.19	9.17	2.84	0.11	3.22	0.86	3.03	302	93
17X-2, 73-75	155.33	406	1.36	8.21	2.34	0.14	3.50	0.79	3.11	263	75
18X-2, 135-137	165.65	408	1.63	10.57	2.79	0.13	3.78	1.01	2.76	382	101
19X-2, 93-95	174.93	412	1.15	9.14	2.59	0.11	3.52	0.85	3.03	301	85
20X-2, 118-120	184.88	410	0.95	7.05	2.26	0.12	3.11	0.66	2.51	280	90
21X-2, 56-58	193.86	413	0.88	8.12	2.51	0.10	3.23	0.75	2.89	280	85
22X-2, 79-81	203.79	412	0.81	8.50	2.53	0.09	3.35	0.77	2.92	291	86
23X-2, 80-82	213.40	408	1.51	9.15	2.60	0.14	3.51	0.88	2.87	318	90
24X-2, 69-71	222.99	414	0.70	6.76	2.53	0.09	2.67	0.62	2.27	297	111
25X-2, 85-87	232.85	410	0.70	5.34	3.63	0.12	1.47	0.50	1.94	275	187
26X-2, 21-23	241.81	417	0.74	5.35	3.21	0.12	1.66	0.50	1.69	316	189
27X-2, 116-118	252.46	419	0.41	3.77	2.56	0.10	1.47	0.34	1.87	201	136
28X-3, 7-9	262.57	413	0.86	6.52	3.66	0.12	1.78	0.61	3.33	195	109
28X-7, 41-43	268.91	411	0.83	5.13	3.41	0.14	1.50	0.49	1.60	320	213
29X-2, 51-53	271.11	412	0.67	4.96	3.33	0.12	1.48	0.46	2.26	219	147
29X-5, 67-69	275.77	413	0.49	3.53	2.52	0.12	1.40	0.33	1.17	301	^a 215
30X-2, 134-136	281.64	413	0.49	3.36	2.74	0.13	1.22	0.32	1.70	197	161
30X-4, 115-117	284.45	411	0.77	5.17	2.46	0.13	2.10	0.49	2.10	246	^a 117
31X-2, 126-128	291.26	412	0.42	2.53	2.65	0.14	0.95	0.24	1.71	147	154
31X, CC, 30-32	298.31	415	0.41	3.57	2.51	0.12	1.42	0.33	1.69	211	^a 148
32X-4, 77-79	303.37	411	0.25	1.01	1.93	0.20	0.52	0.10	1.02	99	189
32X-6, 93-95	306.53	407	0.42	1.86	2.37	0.18	0.78	0.19	1.02	182	^a 232
33X-5, 96-98	314.76	413	0.39	2.80	2.25	0.12	1.24	0.26	1.43	195	^a 157
34X-3, 77-79	321.27	413	0.45	2.97	2.42	0.13	1.22	0.28	1.90	156	127
34X, CC, 33-35	327.21	414	0.44	2.19	2.05	0.16	1.06	0.21	1.23	178	^a 166
35X-2, 104-106	329.74	412	0.42	1.97	2.31	0.18	0.85	0.19	1.48	133	156
36X-3, 33-35	340.13	410	0.16	0.61	1.58	0.21	0.38	0.06	1.56	39	101

Note: For a detailed description of the parameters, see "Explanatory Notes" chapter (this volume).

^a Organic carbon values were measured by the Rock-Eval apparatus, and the HI and OI index were calculated with these values.

which were clearly influenced by moisture, are omitted from Table 11. The first gas pockets occurred at a depth of 170 mbsf, well after the depth where interstitial sulfate is depleted (80 mbsf, see "Inorganic Geochemistry" section, this chapter), and biogenic methane is the dominant gas.

DOWNHOLE MEASUREMENTS

Operations

Two logging runs of Schlumberger tool strings were conducted in Hole 728A. We ran a seismic stratigraphic combination (see "Explanatory Notes," this volume) consisting of sonic (BHC), resistivity (DIT), and gamma ray (GR) tools in the open-hole interval. We obtained downgoing logs from the base of pipe (76 mbsf) to 326.2 mbsf. The pipe was raised during up-

coming logging, so that we obtained upcoming logs from 342.4 to 55.5 mbsf. After lowering pipe to 85.6 mbsf, we ran a modified geochemical combination. The tool string consisted of spectral gamma ray (NGT), neutron porosity (CNT-G), gamma spectrometry (GST), and accelerometer (GPIT) tools. We selected this tool combination instead of the usual second and third Schlumberger strings (see "Explanatory Notes," this volume) because the density tools run at Sites 722 and 723 had encountered bowspring sticking while entering pipe. We obtained downgoing logs using this tool string from just above the seafloor to 323.6 mbsf. No downgoing NGT logs were attempted because irradiation of the formation by this tool might preclude reliable logging of natural gamma rays. We obtained upcoming logs from the entire tool string for the interval from 340.7 mbsf to just above the seafloor, including a repeat pass for a short through-pipe interval.

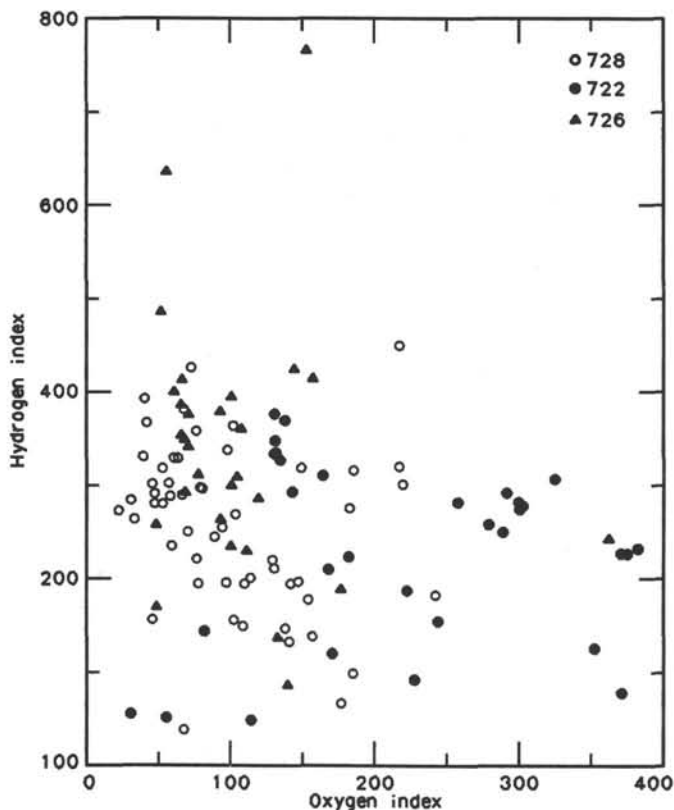


Figure 26. Plot of hydrogen index vs. oxygen index of samples from Site 728 (circles), together with results from Site 722 (dots) and Site 726 (triangles).

Table 10. Results of headspace analysis for interstitial gas at Site 728.

Core, section, interval (cm)	Depth (mbsf)	C ₁ (μL/L)	C ₂ (μL/L)	C ₃ (μL/L)
117-728A-3H-4, 119-120	24.79	51		
6H-4, 119-120	53.19	86	3	
9H-4, 119-120	81.79	49,405	26	6
12X-2, 119-120	107.59	81,635	10	3
15X-4, 119-120	139.59	173,043	38	32
18X-4, 119-120	168.49	227,275	45	40
21X-5, 0-1	197.80	3,500	5	15

Table 11. Results of gas analysis of vacutainer samples from gas pockets at Site 728.

Core, section, interval (cm)	Depth (mbsf)	C ₁ (ppm)	C ₂ (ppm)	C ₃ (ppm)	C ₁ /C ₂
117-728A-18X-6, 10-11	170.40	239,374	30	12	7979
728B-21X-3, 50-51	187.00	899,279	171	82	5259
728B-22X-5, 10-11	199.30	763,225	149	75	5122
728B-23X-3, 145-146	207.25	686,529	122	61	5627
728A-22X-6, 0-1	209.00	262,683	42	20	6254
728B-25X-6, 135-136	231.05	970,184	186	99	5216
728B-27X-1, 30-31	241.80	1,039,019	225	116	4618
728B-29X-6, 140-141	269.70	767,684	188	126	4083
728B-32X-7, 5-6	298.85	459,903	102	65	4508
728A-33X-2, 25-26	309.55	839,872	225	152	3733
728B-34X-7, 10-11	318.30	339,831	76	53	4471
728A-34X-4, 130-131	323.30	813,833	231	164	3523

Very little fill was present in the bottom of the hole, so the bottoms of the two tool strings reached within 2 and 4 m, respectively, of the 346.6 mbsf total drilled depth. The wireline heave compensator was used for only the first run and part of the second run. Seas were extremely flat, and the compensator was observed to be aggravating, rather than reducing, variations in cable tension. We did not encounter bridges during logging of the site. Actual time for logging operations was near the scheduled time: we spent 4.5 hr for hole preparation and 12.5 hr for logging.

Processing and Editing

Log quality was generally good. Based on comparison of downgoing with upcoming logs, reproducibility was excellent. Only upcoming logs are shown here, with the exceptions of the upper GPIT magnetometer data and uppermost NGT data.

GPIT magnetometer data were used for depth shifting of the logs. When expressed as inclination, the magnetometer data show a distinctive pattern of vertical upward and downward magnetizations (Fig. 27), with very sharp transitions at pipe connections that make depth shifting precise and unambiguous. Of relevance to paleomagnetic studies on cores are two observations: (1) cores were exposed to a field of only 0.5 to 1.5 Oe during passage through the pipe (Fig. 27), far less than the magnetization of core barrels; and (2) drill-string magnetization is small at the center of the Monel collar, about 15 m above the base of pipe, where multishot core orientation occurs. Of relevance to downhole magnetometer studies is the observation that drill-string magnetization can be detected to a distance of only about 4 m below the base of pipe. Downhole magnetometer data for the openhole interval were obtained, but are not presented here because the weak sediment magnetization (see "Paleomagnetism" section, this chapter) was dominated by the effect of tool wobbling on the vector sum of tool magnetization and the earth's magnetic field; substantial reprocessing will be needed to eliminate this source of variance.

Data from the NGT tool were reprocessed post-cruise (see "Explanatory Notes" chapter, this volume). The NGT data for the interval from 0 to 85.6 mbsf were obtained through pipe and thus were attenuated (Figs. 28 through 30). To correct for pipe attenuation, we used a gain model (Fig. 31), based on pipe thickness variations, that was nearly identical to the one used at Site 723. The main exception is that the bottom-hole assembly (BHA) was 10 m shorter at Site 728 than at Site 723. To transform from pipe thickness to gain, we used the magnitude of baseline shifts at the top and bottom of the BHA. These shifts imply that pipe attenuation differs for potassium, thorium, and uranium: the maximum gains used were 6 for potassium, 4.5 for thorium, and 3 for uranium (Fig. 31). The gain factor for uranium used at this site is only one-half that estimated for Site 723 (Fig. 31). It is unlikely that both are correct. Even a comparison of downgoing and upcoming logs from Site 728 implies somewhat different gains. Thus, gain-corrected total values for potassium, thorium, and uranium in the interval at 0 to 85.6 mbsf are tentative, but percentage changes in these logs as a function of depth within this interval are not affected.

A total GR log was recomputed from the potassium, thorium, and uranium gain-corrected abundances (Fig. 31). The interval at 54 to 86 mbsf was logged through pipe with the NGT, but through open hole with the GR tool. Comparison of the two runs indicates that gain correction recreated a moderately accurate log. In particular, the peak at 72 mbsf in the GR log is reproduced by the NGT log. The lower flank of this peak is much broader on the GR log than on the NGT log.

Overheating of the data acquisition computer prevented logging of the entire through-pipe interval in a single pass. While the GST was stopped at 45 mbsf, irradiation of the formation

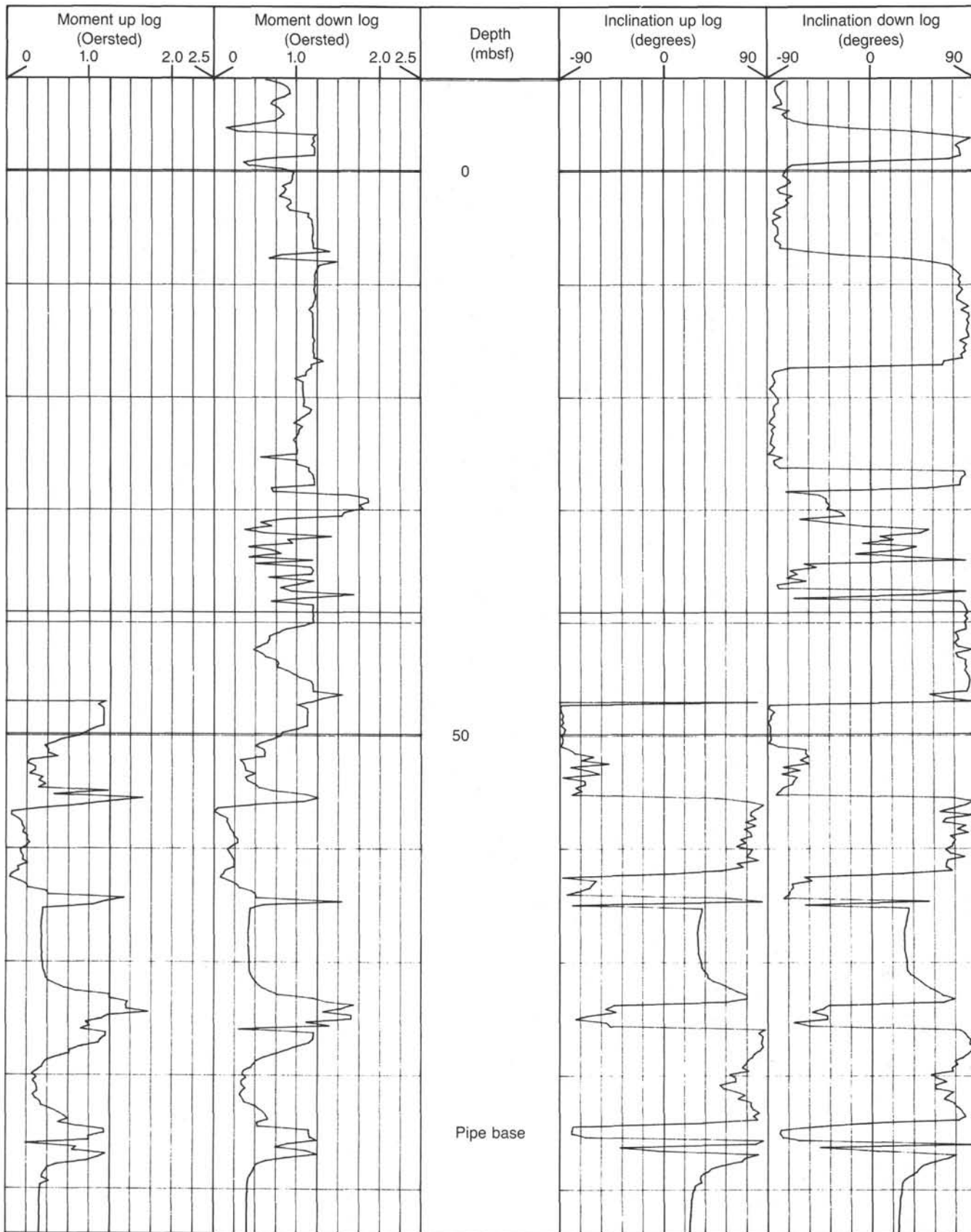


Figure 27. Total magnetic moment (in Oersteds = 0.1 mT) and magnetic inclination (in degrees) measured within the bottom-hole assembly by the GPIT magnetometer. Note the almost identical results from downgoing and upcoming logs. The magnetization changes dramatically at pipe joints, but is everywhere too weak to cause significant isothermal remanent magnetization of ODP cores.

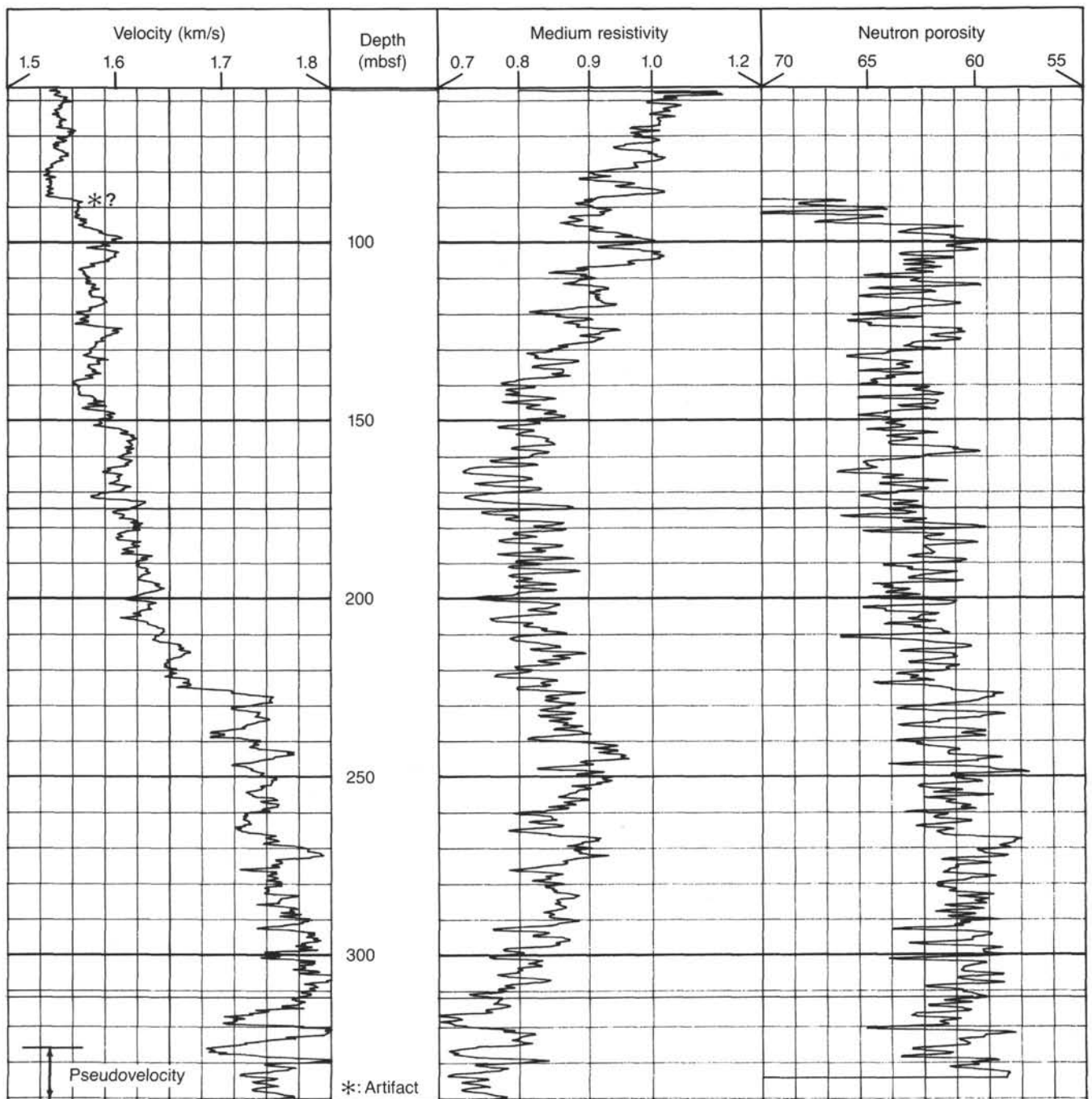


Figure 28. Sound velocity, resistivity, and neutron porosity for the openhole part of Hole 728A.

created an artificial peak in natural GR logs obtained subsequently at this depth (Fig. 31). In addition, subsequent logs above this depth also exhibit an erroneous offset (Fig. 31).

The bottom 30 m of the hole shows gradual increases in potassium and thorium, and a decrease in uranium. These trends are partially artifacts associated with residual gamma radiation caused by irradiation of the bottom of the hole by the GST during the short calibration run. No accurate correction is possible, and the downgoing logs might be more reliable for this interval.

Logs from the GST were reprocessed post-cruise (see "Explanatory Notes" chapter, this volume) to determine relative yields of potassium, titanium, and gadolinium in addition to better yields for silicon, calcium, iron, sulfur, chlorine, and hydrogen (Fig. 32). Significant upward baseline shifts of iron, tita-

nium, and potassium occur as pipe is entered because of high concentrations of these elements in pipe. Based on this offset, a pipe contribution was subtracted from each of these three logs. The shape of the correction model is similar to the model of steel thickness in Figure 35B, except for the low-iron Monel collar evident at 62–72 mbsf on the iron log. Following this pipe correction, GST yields were normalized to 100% total (Fig. 37), as described in the "Explanatory Notes" (this volume).

Sonic logging at Site 728 used a borehole-compensated tool (BHC). This backup tool is less reliable in high-porosity sediments than the normal long-spaced sonic (LSS) tool because of its short source-receiver spacing. At Site 728, the long (1.5 m) source-receiver pairs worked reliably below 87 mbsf, but water arrivals preceded and masked the formation arrival for all of

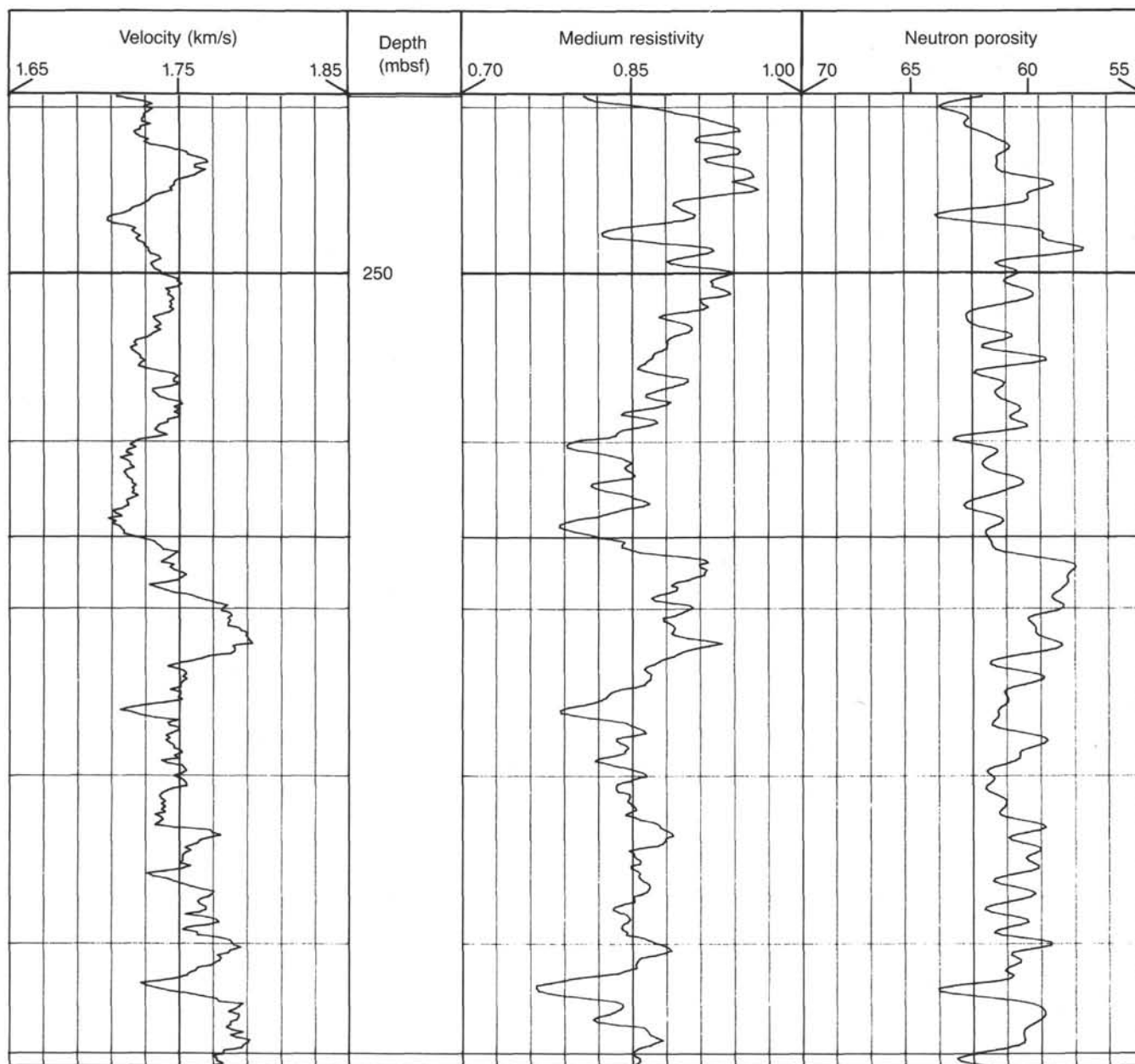


Figure 29. Expanded part of Figure 28, showing the small-scale correlation between velocity, resistivity, and neutron porosity.

one short (0.9 m) source-receiver pair and the upper part (55.5–182.0 mbsf) of the second pair. We replaced the upper part of the second pair with predicted values based on the LSS pair, using a regression ($R = 0.99$) of short-spaced traveltimes on long-spaced traveltimes for the reliable interval 182–243 mbsf. The sonic log was then recalculated, using both long-spaced pairs and the single, partially reconstructed, short-spaced pair. This sonic log (Fig. 28) is considered preliminary and will probably be replaced by a sonic log based on waveform analysis. The velocity increase at 87 mbsf in Figure 28 is probably an artifact, caused by water arrivals preceding formation arrivals, even on the long source-receiver pair.

The resistivity tool obtained data down to a depth 13.6 m nearer the bottom of the hole than the sonic tool because of their relative positions on the seismic stratigraphic tool string. For use in a synthetic seismogram, we generated pseudovelocities for this final 13.6-m interval, based on a regression ($R =$

0.71) of velocity on medium induction resistivity in the overlying 23.6-m interval (Fig. 28).

Mineralogical Variations

The sediments penetrated at Hole 728A were assigned to a single sedimentological unit. These marly nanofossil oozes are dominantly biogenic calcite and clay, with subsidiary opal and organic matter (see "Lithostratigraphy" section, this chapter). Here, we first examine the evidence for variations in clay mineral abundance, then examine that for calcite and organic carbon. Opal abundance is discussed in the next section. The most reliable determination of mineralogical variations is through multi-log inversion. However, clay matrix values for the inversion are unknown at present, so we have postponed log inversion pending availability of results from X-ray diffraction and X-ray fluorescence.

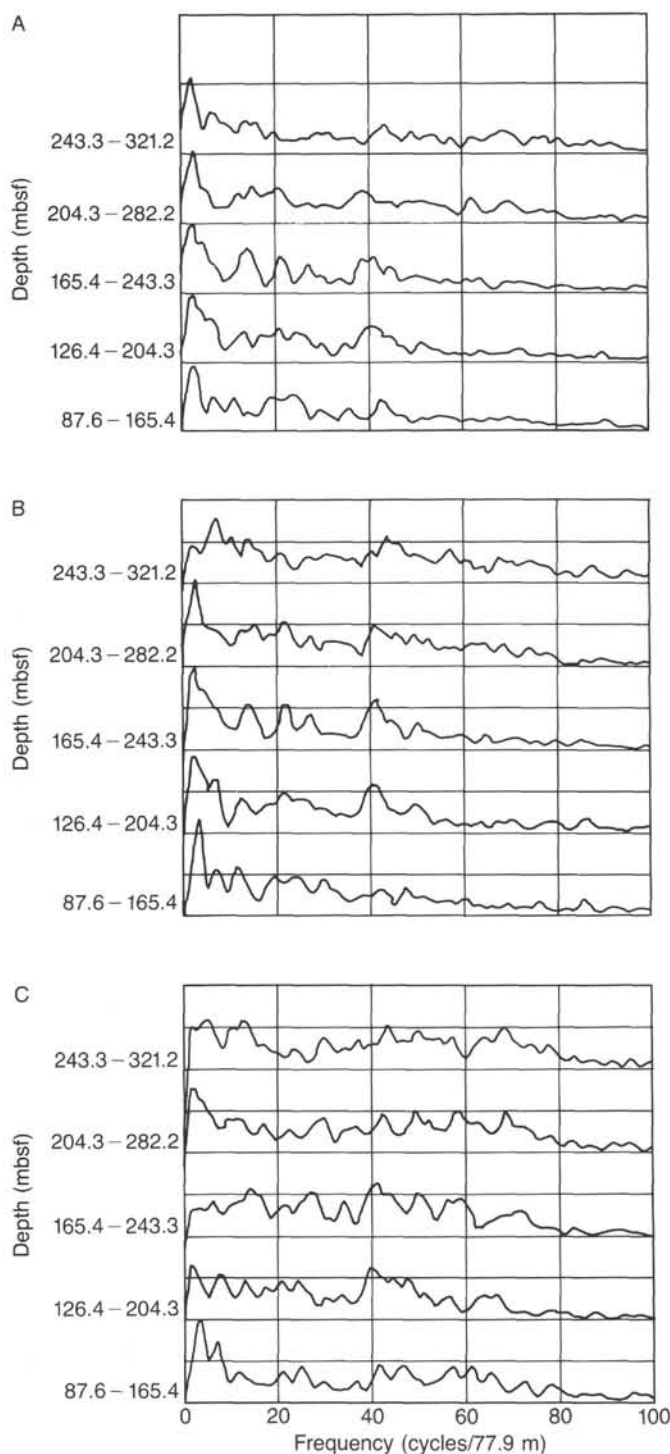


Figure 30. Amplitude spectra for overlapping 77.9-m intervals of the openhole logs for Site 728. **A.** Spectral gamma ray logs. **B.** Gamma ray logs. **C.** Resistivity logs.

The GR log is usually a good indicator of total clay mineral content, because clay minerals contain much higher levels of potassium, thorium, and uranium than do most other minerals. At Site 728, potassium and thorium are strongly correlated (Fig. 31) and thus are present predominantly in the same component. The thorium/potassium ratio is relatively constant at 4 to 6×10^{-4} , suggesting that smectite or palygorskite is the volumetrically dominant clay mineral. Potassium concentrations of 0.5%

to 1.2% below 85 mbsf and up to 2.6% above 85 mbsf are too high for smectite alone (potassium = 0%–0.6%; Fertl, 1979) and imply significant illite (potassium = 3.5%–8.3%; Fertl, 1979), especially in parts of the top 85 m.

Uranium exhibits only a moderate visual correlation with potassium and thorium and thus is not confined to the clay minerals. A concentration of uranium of 3 to 6 ppm (Fig. 31) is too high for any clay mineral except chlorite. The uranium/thorium ratio is about 1 (Fig. 31), whereas uranium/thorium ratios of kaolinite, illite, and smectite are less than 0.3 (Fertl, 1979). The uranium/potassium ratio below 85 mbsf is about 5, which is consistent with smectite, but inconsistent with other clay minerals. Together, uranium, uranium/thorium, and uranium/potassium cannot be reconciled with any clay mineral or mixture of clay minerals.

Two alternative components for the uranium at Site 728 are organic matter and phosphorite. Uranium tends to be precipitated at the redox fronts associated with organic matter, and a high correlation between uranium and abundance of organic matter was found at nearby Site 723 (see Site 723 chapter, this volume). Both organic carbon (see “Organic Geochemistry” section, this chapter) and uranium are present at Site 728 in only about one-half the concentrations found at Site 723. Accordingly, a correlation between organic carbon and uranium is present at Site 728 (Fig. 31), but this correlation is weaker than at Site 723. Probably the uranium log at Site 728 reflects a dominant uranium contribution from organic matter and slightly smaller contribution from clay minerals. Phosphorite has a very high uranium content and may be responsible for at least some of the high-amplitude uranium fluctuations. Phosphorite is present in rare concentrated horizons, rather than as a dilute component throughout the site (see “Lithostratigraphy” section, this chapter). Thus, phosphorite is unlikely to influence most of the uranium log from Site 728.

Based on core descriptions (see “Lithostratigraphy” section, this chapter), biogenic calcite is the dominant nonclay component throughout Site 728. Variations in calcite abundance downhole may be indicated most readily by the potassium and thorium logs (Fig. 31) because calcite dilutes clays that contain potassium and thorium. Both are much more common than other minerals throughout Site 728, except near the very bottom of the hole. However, variations in percentages of different clay mineral components could substantially degrade the accuracy of potassium and thorium logs as indicators of total clay content and, therefore, as an inverse of carbonate content.

The calcium log (Fig. 33) is relatively insensitive to clay mineral variations and responds largely to calcite variations. This log is probably the best indicator of relative calcite abundance. When compared to core analyses of calcite content (see “Organic Geochemistry” section, this chapter), the calcium log shows general similarity.

Sound Velocity and Porosity

Preliminary *P*-wave velocities logged at Site 728 range from 1.54 km/s at 55–81 mbsf to 1.80 km/s in three thin beds below 300 mbsf (Fig. 28). A gradual compaction profile is present, as well as small-scale (10 m) variability and two velocity baseline shifts, at 87 and 226 mbsf. The measured velocity compaction profile at Site 728 is consistently lower than empirical velocity/depth trends, which range from 1.58 km/s at 55 mbsf to 1.87 km/s at 340 mbsf for terrigenous sediments, and from 1.65 to 2.10 km/s for the same depth range in calcareous sediments (Hamilton, 1979).

The 87-mbsf velocity increase may be associated with the major character change observed on potassium, thorium, and uranium logs, from high-frequency, high-amplitude variations

above 85 mbsf to much lower-amplitude variations below. However, as previously discussed, the velocity change may be an artifact.

In contrast, the velocity increase at 226 mbsf is accompanied by a significant neutron porosity decrease and subtle resistivity increase. The porosity change is not evident in pycnometer data (see "Physical Properties" section, this chapter). The qualitatively determined ooze/chalk transition occurs at about 210 mbsf (see "Lithostratigraphy" section, this chapter), and a change in cementation might affect velocity more than it would affect porosity. Geochemical logs (Fig. 33) show a more gradual boundary, with increasing calcium and decreasing titanium over the interval of 215–227 mbsf).

A resistivity log is usually a good indicator of relative porosity, with substantially higher signal-to-noise ratio than neutron porosity logs. Measured formation resistivity depends on both porosity and the resistivity of formation water. The latter decreases at a relatively uniform rate with increasing depth because of increasing temperature, partially masking the overall compaction trend but not affecting the interpretation of porosity fluctuations. A marked long-wavelength variation is present in the resistivity log from Site 728 (Fig. 28). Resistivity decreases from 55 to 163–172 mbsf, then increases down to 245 mbsf, then decreases again below that depth. A similar trend is evident in the potassium and particularly in the thorium logs (Fig. 31). This trend is partially present in the neutron porosity log (Fig. 28), but no trend of increasing neutron porosity below 245 mbsf is evident. Corresponding broad porosity trends are subtle but clearly present in discrete core measurements of porosity and density and are very clear in GRAPE densities (see "Physical Properties" section, this chapter). However, no corresponding broad trends are evident in the velocity log (Fig. 28), for unknown reasons.

The correspondence of long-wavelength trends between thorium, potassium, resistivity, and neutron porosity logs is echoed by a similar correlation of short-wavelength (< 20 m) variations among these logs. Further, although the velocity log lacks the long-wavelength trends of these other logs, it does exhibit a good correlation of short-wavelength variations. For example, Figure 29 focuses on a 58-m interval of Figure 28, illustrating the correlation between velocity, resistivity, and neutron porosity.

Correlation between thorium, potassium, resistivity, porosity, and velocity is very common in deep-sea sediments and arises from the fact that the fibrous, disorganized arrangement of clay minerals at shallow depths causes higher porosity than is associated with most other minerals (e.g., Hamilton and Bachman, 1982). However, this was not the pattern seen at Site 728. Clay content, as indicated by potassium and thorium, is positively correlated with velocity and resistivity and negatively correlated with porosity; this is the opposite of the normal relationship. An additional component must be present that impacts on porosity more than clay. Further, this component must be more common in clay-poor horizons than in clay-rich ones. This component cannot be calcite, as calcite is much faster than clay. It is unlikely to be organic matter (the primary cause of porosity fluctuations at nearby Site 723), because organic matter is more common in clay-rich than clay-poor zones and because uranium is not well-correlated with the porosity logs at this site.

Biogenic opal may be the primary cause of porosity fluctuations at Site 728. Biogenic opal is common below 70 mbsf (see "Biostratigraphy" section, this chapter), reaching levels of greater than 20% in some layers below 320 mbsf (see "Lithostratigraphy" section, this chapter). Two beds with very low velocity and high porosity at 314–319 and 322–327 mbsf (Fig. 28) probably are highly siliceous. A low and variable amount of opal throughout the interval below 70 mbsf may account for the observed interlog correlations and the fact that velocities are lower than em-

pirical models for terrigenous and calcareous sediments. However, high-resolution quantitative determination of opal content will be necessary to test this hypothesis. One observation not obviously accounted for by opal is the absence from the velocity log of the long-wavelength trends seen in resistivity, potassium, and thorium logs.

The correlation between gamma ray and resistivity logs, possibly associated with fluctuations in biogenic opal, can also be examined in the frequency domain. Figure 30 shows normalized amplitude spectra of 77.9 m (512 point) overlapping windows from the gamma ray, spectral gamma ray, and shallow-focused resistivity logs. The frequency spectrum varies somewhat between depth windows, but is very similar for different logs from the same depth window. The similar spectra for the two gamma ray logs indicate that ship heave did not impart spurious frequency to the logs because the logging speed for the GRT was three times as fast as that for the NGT. Similar spectra for the resistivity log, when compared with the two gamma ray logs, indicate that both properties are undergoing similar cyclic variations. This does not identify the cause of these variations, although opal appears likely. A consistent high-frequency component is present in the spectra, at about 38 to 43 cycles per 77.9 m, or a period of 1.8 to 2.0 m. This cyclicity is also obvious in the log plots as a function of depth, although not at the compressed scales of Figures 28 through 33.

INTERHOLE CORRELATIONS

Here, we provide detailed correlations for the upper 30 m of the drilled sediments at Site 728. This upper interval ranges in age from 0 to about 0.5 Ma and is characterized by cyclic changes in the nature of sediments that can be identified by visual observation and by variations of magnetic susceptibility and CaCO₃ content. The coherence and similarity of sediments among these holes provide valuable information about the relative rate of sedimentation, which is necessary information for any high-resolution study of depositional environments. The essence of the interhole-correlation process is described in the "Explanatory Notes" chapter (this volume).

Hole-to-hole correlations were based on visual identification of distinctive layers, as well as on physical and magnetic properties. Magnetic susceptibility was measured at 10-cm intervals on whole-core sections. Photographs of the split cores were taken.

Visual correlation of cores relied primarily on these core photographs. Twenty-six distinct, traceable layers were determined in the correlatable sedimentary sequence at Sites 723 and 724 and were notated as OM-a₁, ..., h₃, and h₅, based on the correlation between the holes at Sites 723 and 724 (see "Lithostratigraphy" sections, Site 723 and Site 724 chapters, this volume). The letter code (i.e., a, b, c, ...) refers to the sequence of cores, and the number code indicates the number of marker layers in each core. For example, the notation "a₂" corresponds to the second marker layer defined in Core 117-723A-1H, and "b₁" denotes the first marker layer in Core 117-723A-2H. The marker layers a₁ through h₄ were defined on the cored sediments of Hole 723A. Three marker layers, c₅, e₃, and h₅, were defined on the sedimentary sequence at Hole 724A, in addition to those noted at Site 723. The criterion for defining a marker layer was that the layer be distinct enough for tracing in the sedimentary sequence of the other holes and that its character not change. Useful criteria for recognizing the marker are color boundaries, distinctly colored layers, shape of bioturbations, and sequence of color change in surrounding sediments. Table 12 lists the depth of the marker layers in two holes of Site 728.

Figure 34 shows the magnetic susceptibility curve and positions of individual, visually correlatable layers. The pattern of the susceptibility and the positions of layers match very well, not only among the two holes, but also between Sites 723 and

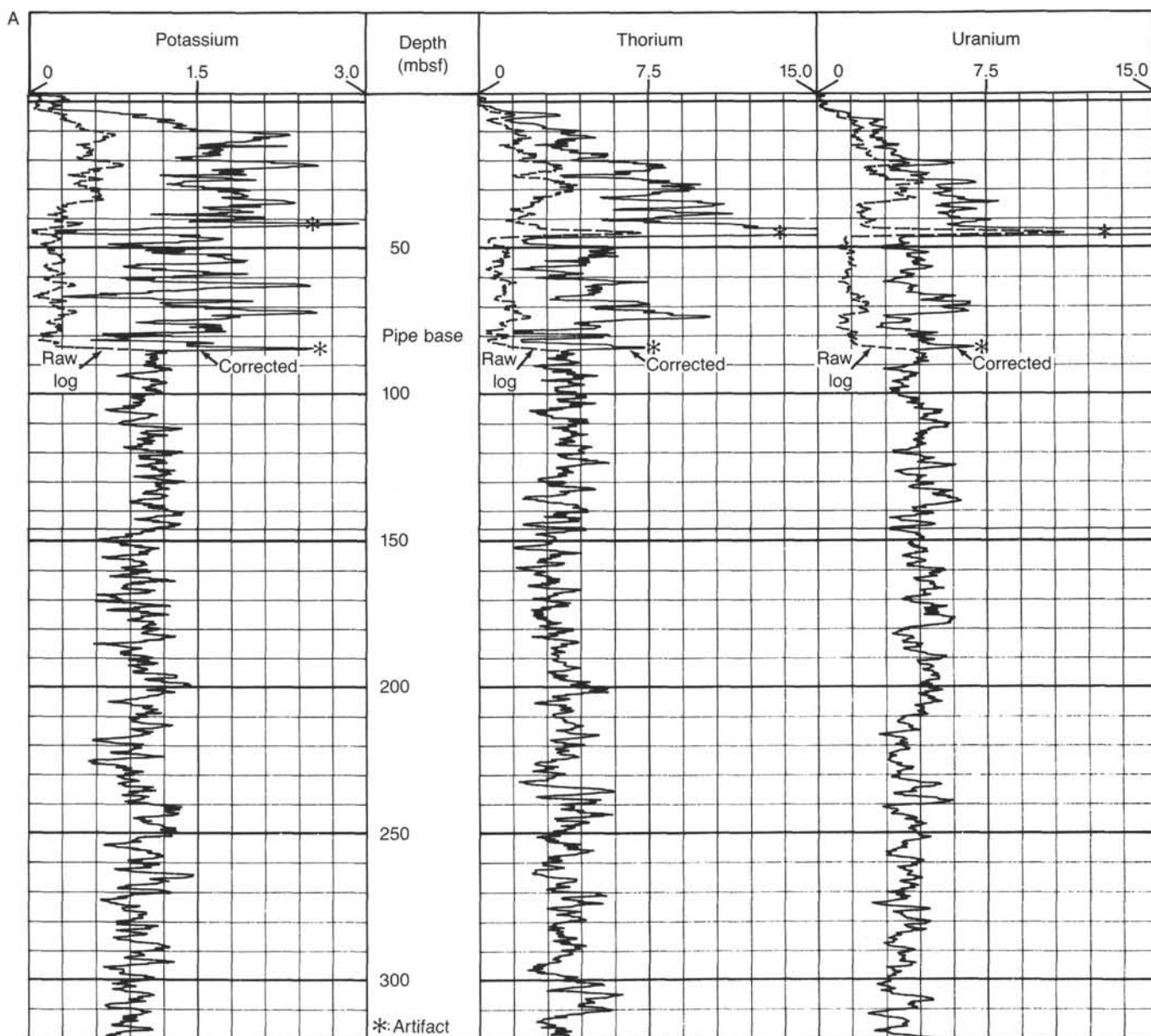


Figure 31. A. Potassium, thorium, and uranium logs, both before (dashed) and after (solid) correction of through-pipe logs for attenuation of signal by pipe. Core measurements of organic carbon percentages are shown for comparison with uranium log. B. Gain factors used for correction of through-pipe logs, spectral gamma ray logs (both before and after applying gain factors), and openhole gamma ray logs.

728 (Fig. 35). The stratigraphy of the magnetic susceptibility data and the visually identified layers is extremely consistent in that a particular visually characteristic layer always coincides in depth with a distinct feature in the magnetic susceptibility curve. In this way, the lithologic correlations could be verified with the magnetic data, which are quantitative and less ambiguous.

The results of this layer-by-layer correlation allowed us to calculate the true thickness of these layers that coincide with and are separated by core boundaries. Occasionally, core tops were expanded by water uptake during drilling. In this case, the apparent thickness of the disturbed sediment layer was observed to be thicker than the original thickness. In some instances, the top part of the core was missing; in this case, apparent thickness was observed to be thinner than the original thickness. Fortunately, the two holes were staggered in depth, so that they have different horizons at core boundaries (Table 12). The original

thickness of layers coinciding with core tops or bottoms can be obtained by comparing thickness of the correlative layer in the continuous section of the other holes. The amount of the difference can be calculated by the differences in the ODP depths of marker layers between the holes ("Holes 728B - 728A" in Table 12). Table 13 gives the differences between the depth (mbsf) calculated by the ODP CORELOG data and the corrected depth (mbsf), calculated by the layer-by-layer correlation method. The mudline was not clearly recognized in Core 117-728A-1H, while according to the layer-by-layer correlation, the top of Core 117-728A-1H obtained the mudline.

The layer-by-layer method on the double-cored sedimentary sequences gives us true stratigraphic thickness after correcting for any core-boundary disturbance. Table 14 shows the stratigraphic thickness at Sites 723 and 724, where the marker layers were defined, and at Holes 728A and 728B. The corrected depths in

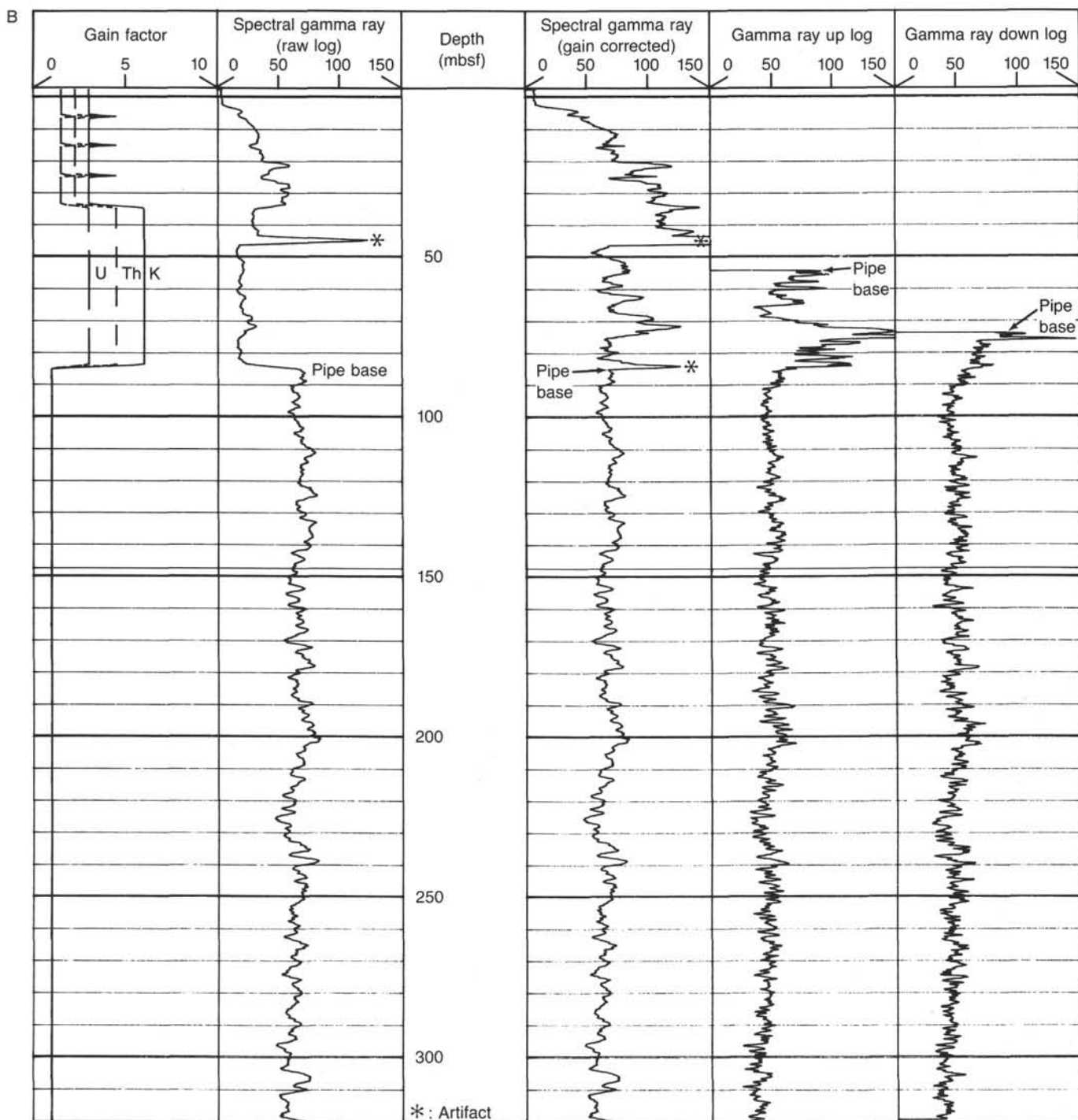


Figure 31 (continued).

Hole 728A and 728B agree well. The intersite correlation of the marker layers clearly shows the differences in sedimentation rate.

SUMMARY AND CONCLUSIONS

Site 728 is located on the Oman margin at a water depth where the lower part of the pronounced mid-water oxygen-minimum zone intersects the continental slope. The location is in a distal slope basin formed by a narrow half-graben in what is presumed to be ophiolitic basement. Biogenic material produced by coastal upwelling and eolian components is deposited here at

high rates (11–88 m/m.y.). The purpose of drilling at Site 728 was to provide a margin site that accumulated dominantly pelagic sediments that could be used to trace the evolution and fluctuation of the oxygen-minimum zone through time. A second intention, in conjunction with drilling at Sites 726, 727, 729, and 730, was to investigate the tectonic movements of adjacent ophiolite blocks by coring the sediments in the two adjacent half-graben basins.

Major findings at Site 728 include:

1. An expanded Pliocene section, which is well constrained by paleomagnetic data;

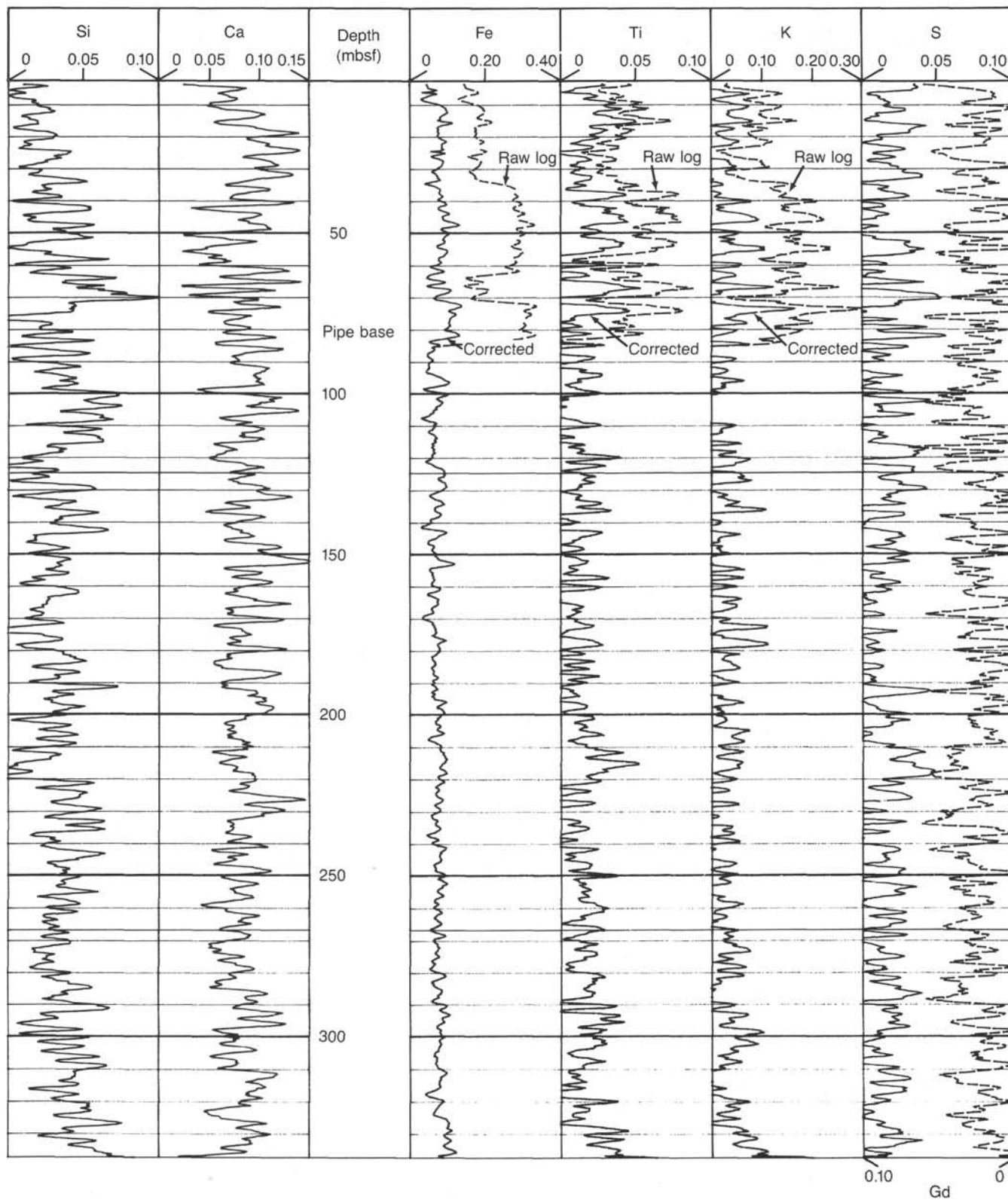


Figure 32. Reprocessed geochemical logs from gamma spectrometry tool. Fe, Ti, and K are shown both before (dashed) and after (solid) correction for pipe contribution.

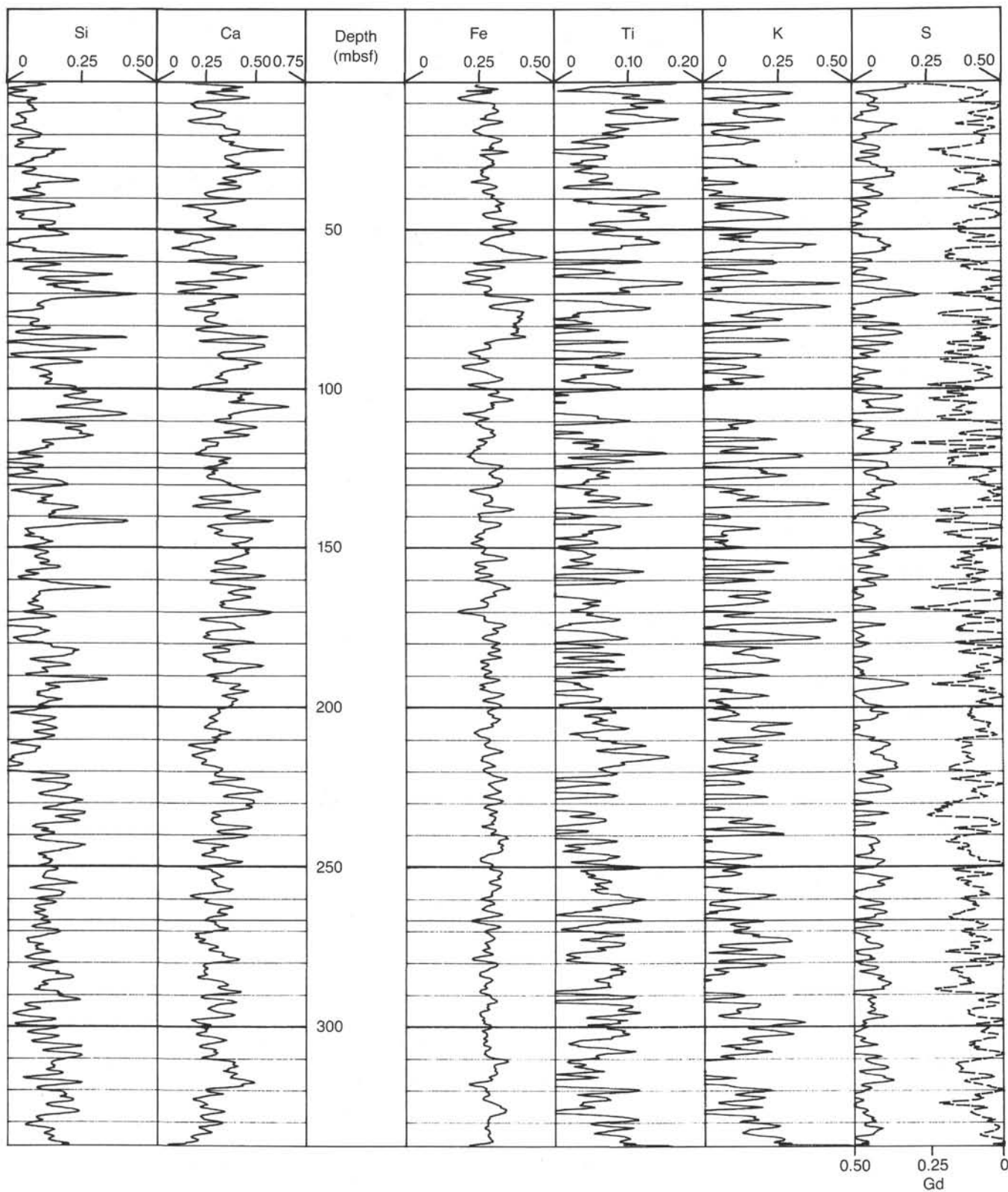


Figure 33. Geochemical logs of Figure 32, after normalization of yields to 100% total.

Table 12. List of marker layers in Site 728.

Layer	Hole 728A		Hole 728B		Holes 728B - 728A
	Core, section, interval (cm)	ODP depth	Core, section, interval (cm)	ODP depth	
OM-					
a ₁			1-1, 65	0.65	
a ₂	1-1, 135	1.35	2-1, 45	1.65	0.35
b ₁	1-2, 90	2.40	2-2, 5	2.75	0.35
b ₂	1-3, 110	4.10	2-3, 30	4.50	0.40
b ₃	1-4, 40	4.90	2-3, 110	5.30	0.40
c ₁	1-5, 70	6.70	2-4, 135	7.05	0.35
c ₂	1-6, 50	8.00	2-5, 115	8.35	0.35
c ₃	1-6, 115	8.65	2-6, 30	9.00	0.35
c ₄	1-7, 40	9.40	2-6, 95	9.65	0.25
c ₅	2-1, 35	9.95			
d ₁	2-2, 5	11.15	3-1, 90	11.60	0.45
d ₂	2-2, 25	11.35	3-1, 110	11.80	0.45
d ₃	2-2, 50	11.60	3-1, 130	12.00	0.40
e ₁	2-2, 95	12.05	3-2, 35	12.55	0.50
e ₂	2-2, 140	12.50	3-2, 80	13.00	0.50
e ₃	2-3, 60	13.20	3-2, 145	13.65	0.45
f ₁	2-4, 20	14.30	3-3, 115	14.85	0.55
f ₂	2-4, 55	14.65	3-4, 5	15.25	0.60
g ₁	2-5, 35	15.95	3-4, 130	16.50	0.55
g ₂	2-5, 105	16.65	3-5, 60	17.30	0.65
h ₁	2-6, 70	17.80	3-6, 35	18.55	0.75
h ₂	2-7, 35	18.95	3-6, 140	19.60	0.65
h ₃	3-1, 90	20.00			
h ₄	3-2, 65	21.25	4-1, 120	21.30	0.05
h ₅	3-2, 150	22.10	4-2, 40	22.00	-0.10

2. The common occurrence of opaline microfossils in the Miocene and Pliocene intervals;

3. Indications of rapid vertical movement of the site, as indicated by benthic foraminifers, from upper bathyal in the late Miocene to neritic in the early Pliocene, and subsiding to middle bathyal depths in the late Pliocene and Pleistocene;

4. The occurrence of an organic-rich interval between 70 and 225 mbsf (Pliocene), with the highest values at the Pliocene/Pleistocene boundary.

One lithologic unit was recognized in the section cored at Site 728, which encompasses sediment deposited since the late Miocene (Fig. 36). Lithologic Unit I was subdivided into three subunits. Subunit IA (0-58 mbsf) is composed of Holocene to upper Pleistocene marly foraminifer-nannofossil ooze with common bivalve and gastropod debris. Subunit IB includes the section from 58 to 320 mbsf, is of late Pleistocene to late Miocene age, and is made up of marly nannofossil ooze grading into chalk at about 200 mbsf. Siliceous microfossils are preserved, but make up less than 10% of the sedimentary components. Subunit IC (320-349.5 mbsf) is composed of nannofossil and marly nannofossil chalks, which are interbedded with dark olive, diatomaceous, marly nannofossil chalks. The age of this subunit is late Miocene.

A significant finding at Site 728 is the presence of siliceous microfossils throughout much of the recovered section. Opal-rich Subunit IC is coeval with opal-rich sediments encountered on the Owen Ridge. Radiolarians are common from 85 to 347 mbsf; they are usually accompanied by diatoms. Planktonic foraminifers are poorly preserved over the same interval. Nannofossil floras are low in diversity, but well preserved. An assemblage with presumed cold-water affinities was recognized in the interval spanning the Pliocene/Pleistocene boundary. Benthic foraminifer assemblages at Site 728 exhibit significant changes in paleowater depth. From 0 to 150 mbsf, benthic foraminifers are abundant, and the ratio of planktonic to benthic foraminifers is high in the uppermost 60 m, whereafter it gradually decreases. The uppermost assemblage reflects upper middle bathyal

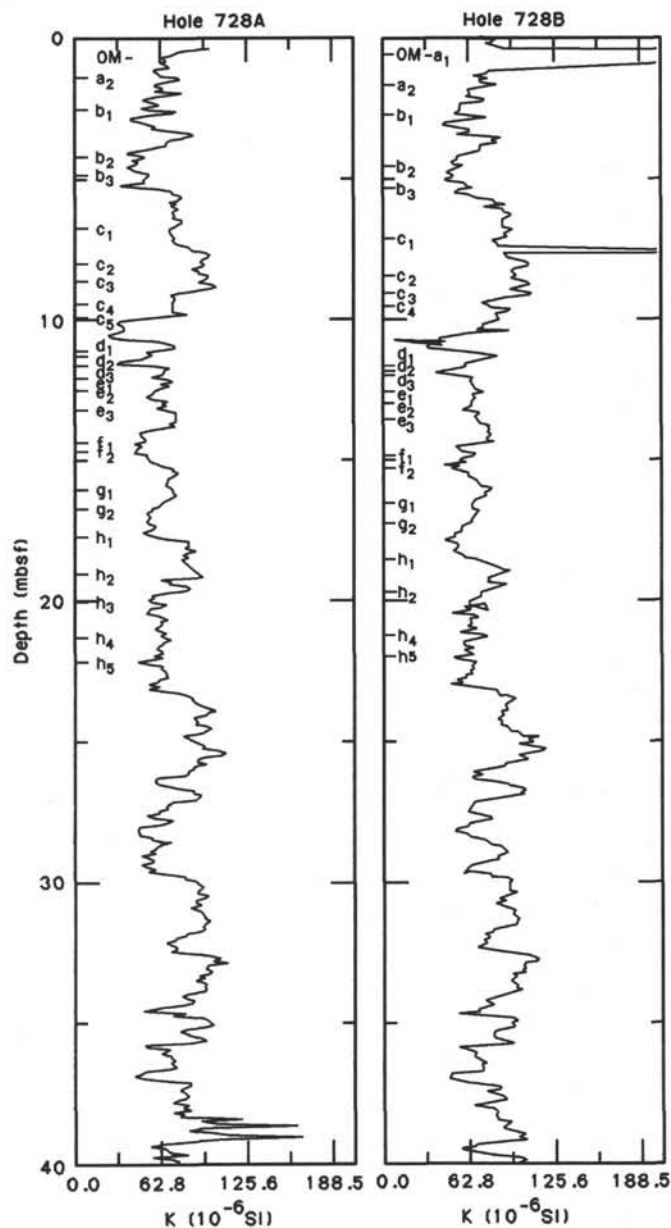


Figure 34. Volume magnetic susceptibility curve and positions of the marker layers in Holes 728A and 728B.

(> 500 m water depth) conditions. In the lower Pliocene and upper Miocene, the interval from approximately 150 to 240 mbsf, an assemblage characteristic of a neritic environment (< 150 m water depth) is present. The upper Miocene section contains rare foraminifers that indicate an upper bathyal environment. Thus, benthic foraminifers suggest that the site was very shallow in the Pliocene and that it rapidly subsided to its modern water depth of 1423 m.

A zone of high organic carbon concentrations that was encountered at 80 to 110 mbsf may reflect a prolonged episode of upwelling or may be associated with the major change in sedimentation rate evident in the late Pliocene (Fig. 36). Detailed logs from this site show maximum concentrations of uranium that correlate well with total organic carbon at this depth, and the zone coincides with maxima in alkalinity in pore waters as well as with the depletion of interstitial sulfate. The elevated organic carbon concentrations (up to 5.3%) appear to foster sig-

Table 13. Corrected depths below seafloor of core top for stratigraphic depth calculation.

Core	Hole 728A			Hole 728B		
	ODP top depth	Difference	Corrected top depth	ODP top depth	Difference	Corrected top depth
1H	0	0.4	0.4	0	0	0
2H	9.6	0.1	10.1	1.2	0	1.2
3H	19.1	0	19.8	10.7	0	10.7
4H				20.1	0.7	20.8

ODP top depth = depth below seafloor of core top calculated using ODP core data. Difference = difference between depth calculated using ODP core data and depth calculated using layer-to-layer correlation method. Corrected top depth = depth below seafloor of core top calculated using layer-to-layer correlation method.

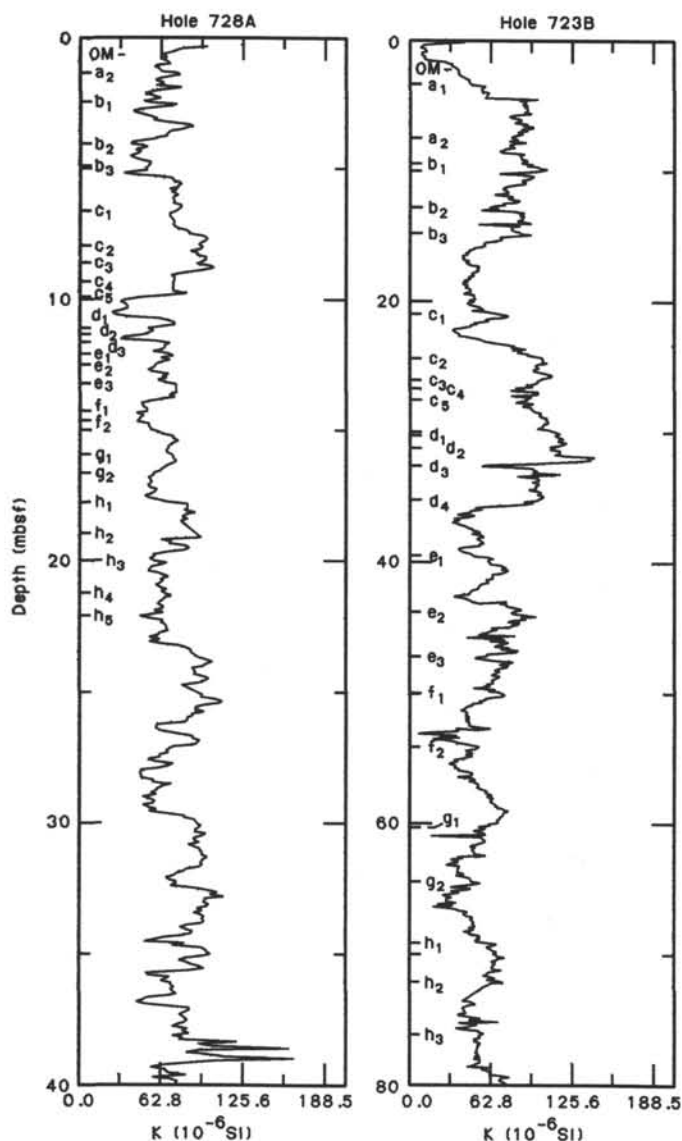


Figure 35. Volume magnetic susceptibility curve and positions of the marker layers in Holes 723B and 728A.

nificant bacterial activity at this depth, which corresponds to the depth of sulfate depletion in interstitial waters. Both Miocene and Pleistocene sediments are low in total organic carbon.

Site 728 provided several important constraints on the environmental and depositional history of the Oman margin. First, we recovered biosiliceous sediments of Miocene to Pliocene age at this site that can be compared to the Owen Ridge sediments. Second, the site provided additional control on the subsidence history of the slope basins. Combined with findings at other sites on the Oman margin, these findings should permit a detailed reconstruction of the history of the Oman margin in post-cruise research.

REFERENCES

- Berggren, W. A., Kent, D. V., Flynn, J. J., and Van Couvering, J. A., 1985. Cenozoic geochronology. *Geol. Soc. Am. Bull.*, 96:1407-1418.
- Berggren, W. A., Kent, D. V., and Van Couvering, J. A., 1985. The Neogene: Part 2, Neogene geochronology and chronostratigraphy. In Snelling N. J. (Ed.), *The Chronology of the Geological Record*. Geol. Soc. Mem. (London), 10:211-259.
- Fertl, H. H., 1979. *Gamma Ray Spectral Data Assists in Complex Formation Evaluation*: Houston (Dresser-Atlas).
- Hamilton, E. L., 1979. Sound velocity gradients in marine sediments. *J. Acoust. Soc. Am.*, 65:909-922.
- Hamilton, E. L., and Bachman, R. T., 1982. Sound velocity and related properties of marine sediments. *J. Acoust. Soc. Am.*, 72:1891-1904.
- Ingle, C. J., Jr., Keller, G., and Kolpack, R. L., 1980. Benthic foraminiferal biofacies, sediments and water masses of the southern Peru-Chile Trench area, southeastern Pacific Ocean. *Micropaleontology*, 26:113-150.
- Johnson, D. A., in press. Pliocene-Pleistocene radiolarian events and magnetostratigraphic calibrations for the tropical Indian Ocean. *Mar. Micropaleontol.*
- Johnson, D. A., and Nigrini, C. A., 1985. Synchronous and time-transgressive Neogene radiolarian datum levels in the equatorial Indian and Pacific oceans. *Mar. Micropaleontol.*, 9:489-523.
- Pflum, C. E., and Frerichs, W. E., 1976. Gulf of Mexico deep-water foraminifers. *Cushman Found. Foram. Res., Spec. Publ.* 14.
- Sato, T., Takayama, T., Kato, M., Kudo, T., and Kameo, K., in press. Calcareous microfossil biostratigraphy of the uppermost Cenozoic formations distributed in the coast of the Japan Sea. Part 4: Conclusion. *Sekiyu Gijutsu Kyokaiishi*.
- Takayama, T., and Sato, T., 1987. Coccolith biostratigraphy of the North Atlantic Ocean, Deep Sea Drilling Project Leg 94. In Ruddiman, W. T., Kidd, R. B., et al., *Init. Repts. DSDP, 94, Pt 2*: Washington (U.S. Govt. Printing Office), 651-702.
- van Morkhoven, F. P., Berggren, W. A., and Edwards, A. S., 1986. Cenozoic cosmopolitan deep-water benthic foraminifera. *Bull. Cent. Rech. Explor.-Prod. Elf-Aquitaine Mem.*, 11.

Table 14. Stratigraphic depths of the marker layers at Sites 723, 724, and 728.

Layer	Hole 723B		Hole 724A		Hole 728A		Hole 728B	
	Core, section, interval (cm)	Corrected depth						
OM-a ₁	1-3, 35	3.35	1-1, 95	0.95			1-1, 65	0.65
a ₂	2-3, 20	7.20	1-2, 115	2.65	1-1, 135	1.75	2-1, 45	1.65
b ₁	2-4, 65	9.15	1-3, 100	4.00	1-2, 90	2.80	2-2, 5	2.75
b ₂	2-6, 110	12.60			1-3, 110	4.50	2-3, 30	4.50
b ₃	3-1, 95	14.75	2-1, 75	7.95	1-4, 40	5.30	2-3, 110	5.30
c ₁	3-5, 110	20.90	2-2, 75	9.45	1-5, 70	7.10	2-4, 135	7.05
c ₂	4-1, 85	24.95	2-3, 130	11.50	1-6, 50	8.40	2-5, 115	8.35
c ₃	4-2, 100	26.60	2-4, 70	12.40	1-6, 115	9.05	2-6, 30	9.00
c ₄	4-3, 15	27.25	2-4, 120	12.90	1-7, 40	9.80	2-6, 95	9.65
c ₅	4-3, 100	28.10	2-5, 35	13.55	2-1, 35	10.45		
d ₁	4-5, 70	30.80	3-1, 40	17.20	2-2, 5	11.65	3-1, 90	11.60
d ₂	4-6, 10	31.70	3-1, 150	18.30	2-2, 25	11.85	3-1, 110	11.80
d ₃	4-7, 5	33.15	3-2, 90	19.20	2-2, 50	12.10	3-1, 130	12.00
d ₄	5-2, 50	35.30	3-3, 85	20.65				
e ₁	5-5, 20	39.50	3-4, 15	21.45	2-2, 95	12.55	3-2, 35	12.55
e ₂	6-1, 90	43.80	3-5, 90	23.70	2-2, 140	13.00	3-2, 80	13.00
e ₃	6-3, 150	47.40	3-6, 95	25.25	2-3, 60	13.70	3-2, 145	13.65
f ₁	6-5, 120	50.10	4-1, 85	27.75	2-4, 20	14.80	3-3, 115	14.85
f ₂	7-2, 15	54.25	4-2, 70	29.10	2-4, 55	15.15	3-4, 5	15.25
g ₁	7-6, 30	60.40	4-4, 120	32.60	2-5, 35	16.45	3-4, 120	16.50
g ₂	8-2, 60	64.40	4-6, 25	34.65	2-5, 105	17.15	3-5, 60	17.30
h ₁	8-5, 90	69.20	4-7, 40	36.30	2-6, 70	18.30	3-6, 35	18.55
h ₂	9-1, 20	72.10	5-1, 80	37.30	2-7, 35	19.45	3-6, 140	19.60
h ₃	9-3, 135	76.25	5-2, 60	38.60	3-1, 90	20.70		
h ₄	9-7, 95	81.85	5-4, 145	42.45	3-2, 65	21.95	4-1, 120	22.00
h ₅			5-5, 145	43.95	3-2, 150	22.80	4-2, 40	22.70

Note: Depths based on the correction factors of Table 13. Corrected depth = corrected depth for stratigraphic thickness.

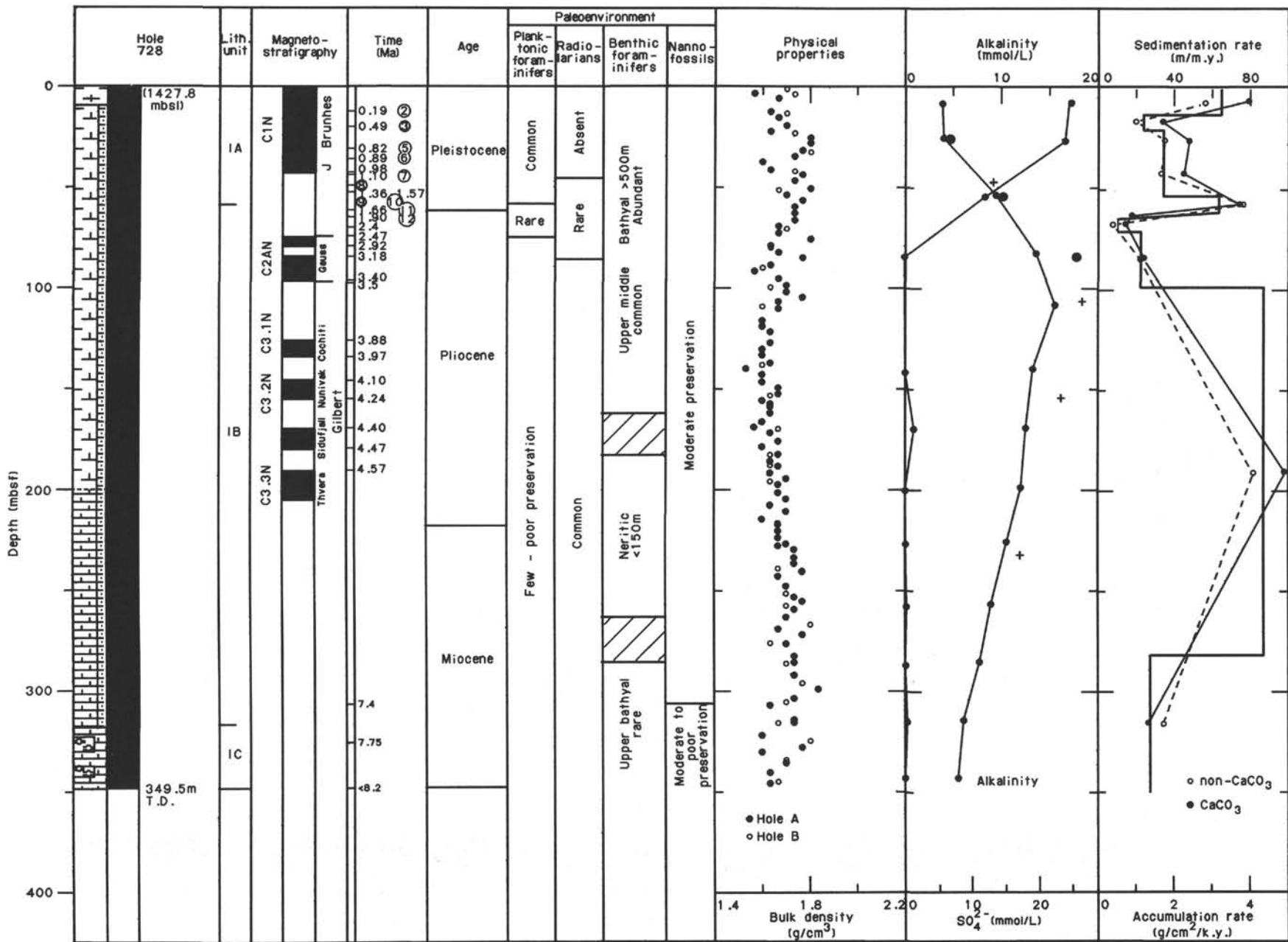
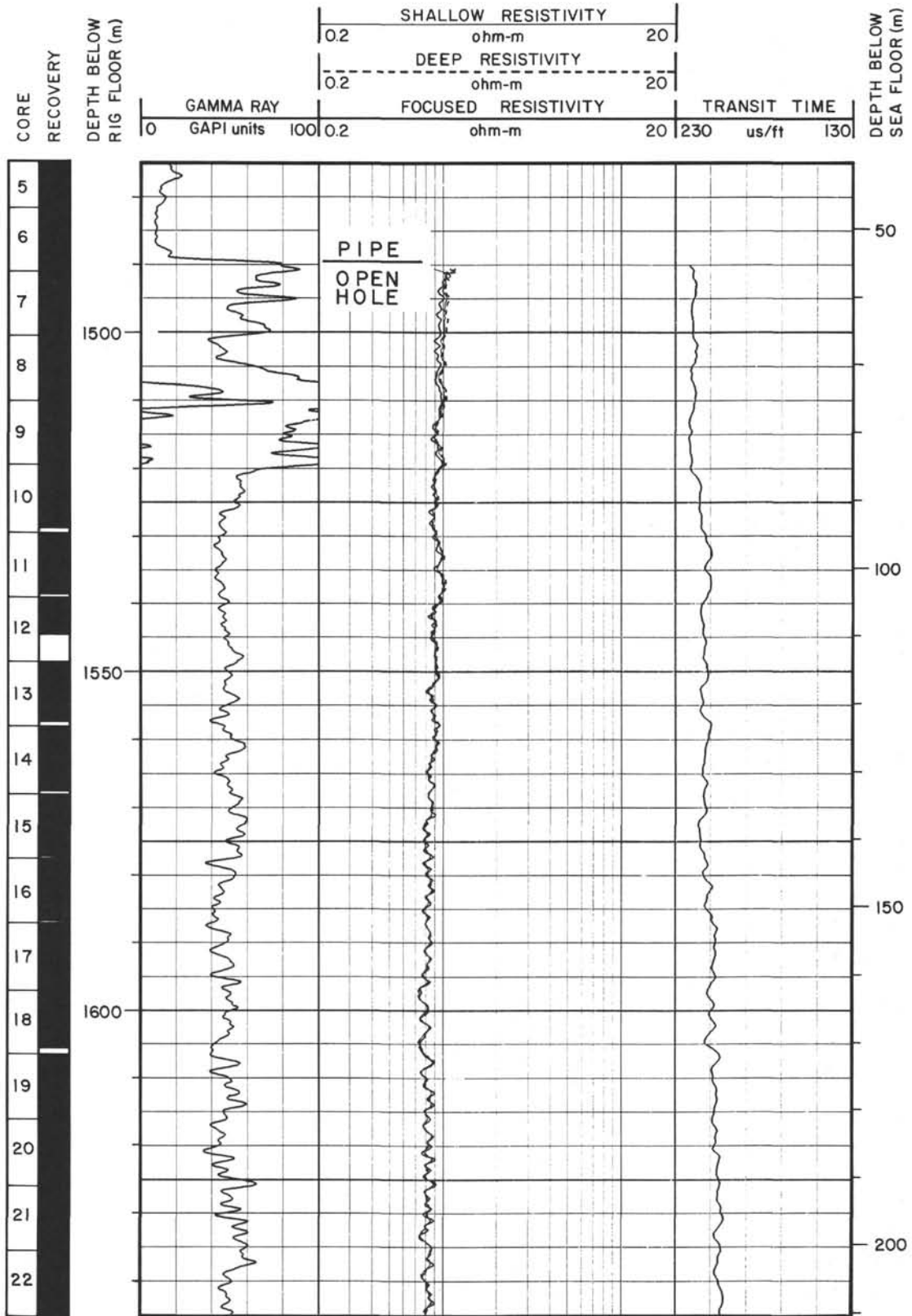
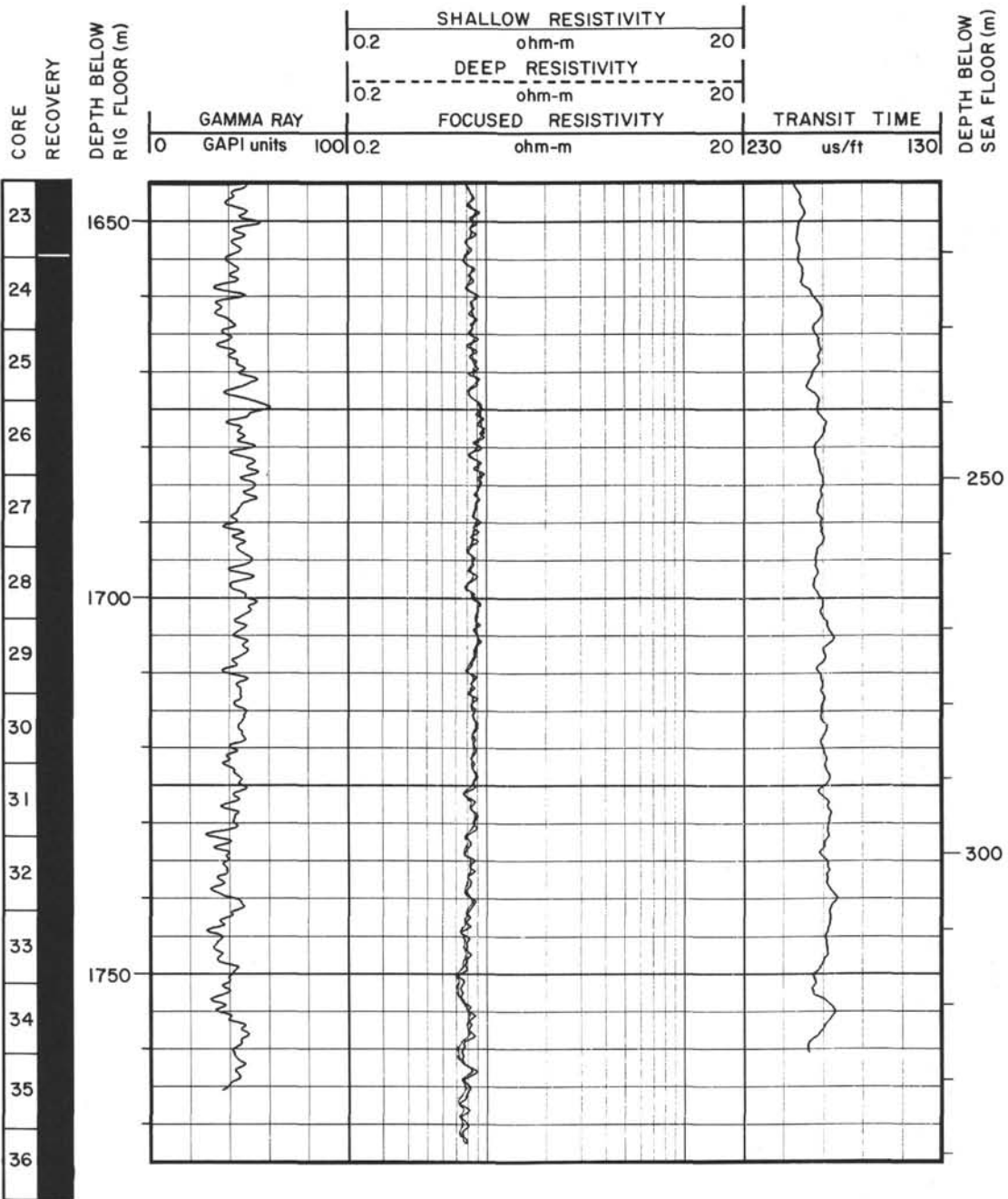


Figure 36. Summary of shipboard results, Site 728. Numbers in circles = nannofossil datum levels.

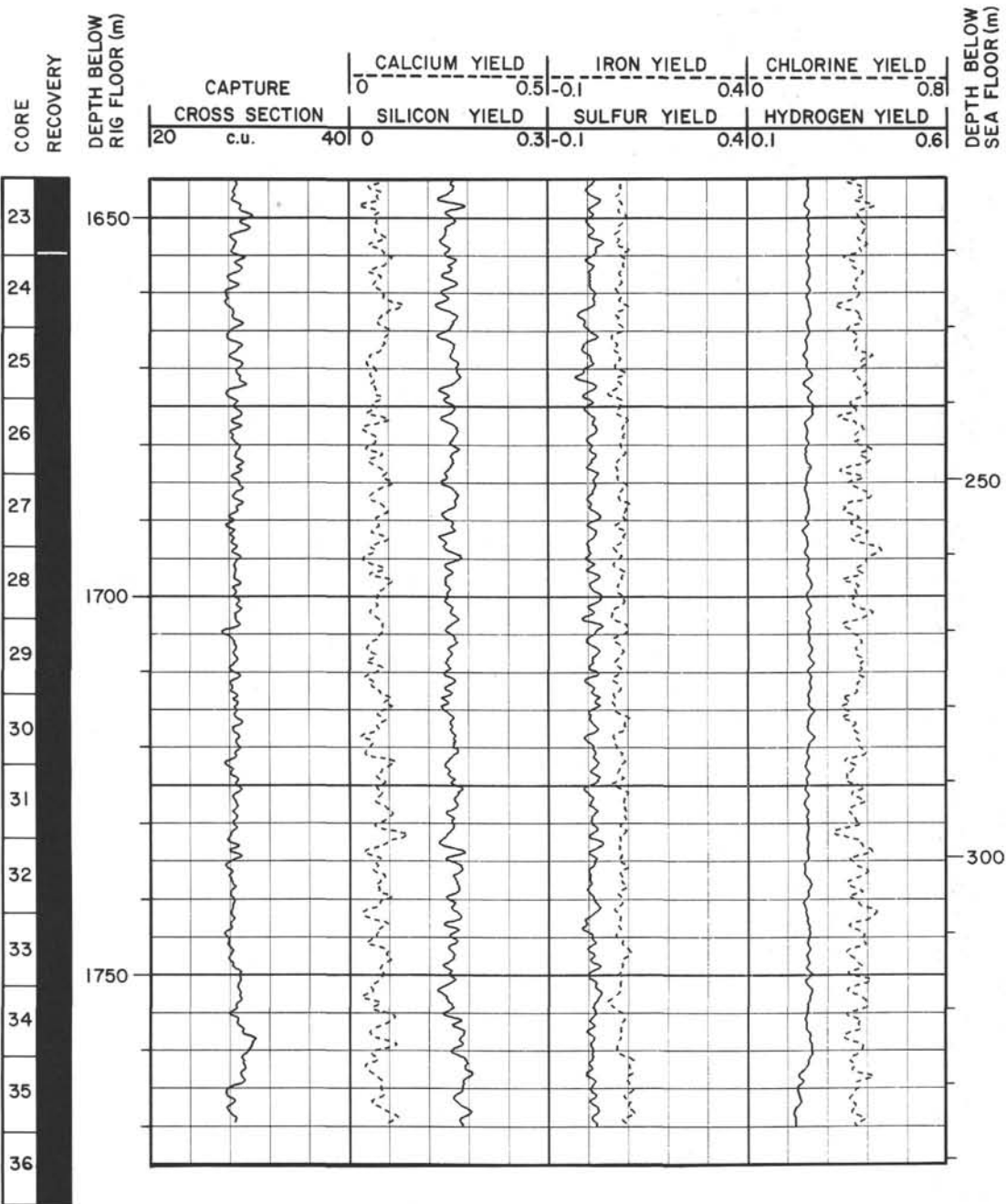
Summary Log for Hole 728A



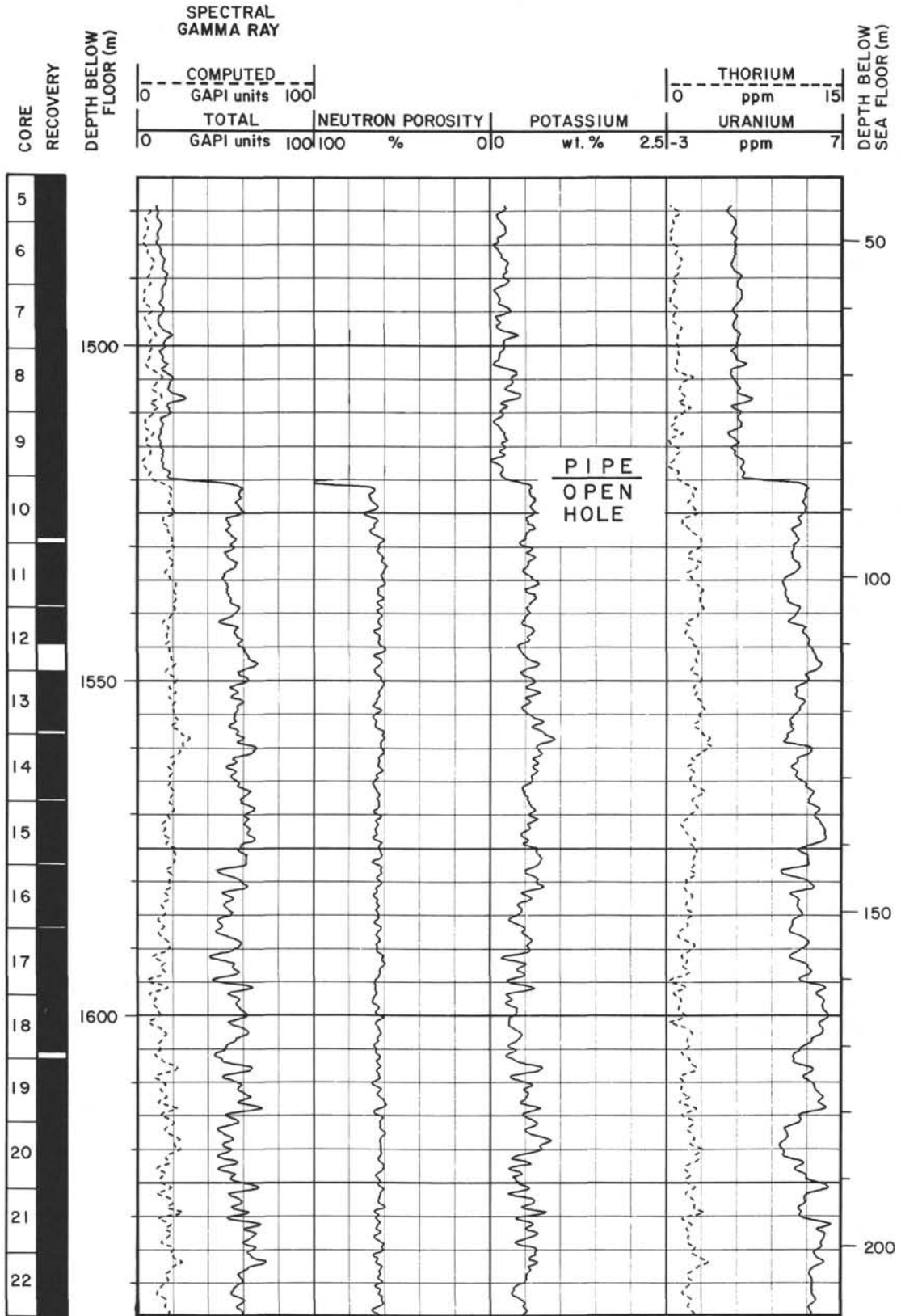
Summary Log for Hole 728A (continued)



Summary Log for Hole 728A (continued)



Summary Log for Hole 728A (continued)



Summary Log for Hole 728A (continued)

